



UNIVERSITEIT VAN PRETORIA
UNIVERSITY OF PRETORIA
YUNIBESITHI YA PRETORIA
Denkleiers • Leading Minds • Dikgopolo tša Dihlalefi

Fakulteit Ingenieurswese, Bou-omgewing & IT
Faculty of Engineering, Built Environment & IT

School of Engineering

**Department of Materials Science and
Metallurgical Engineering**

Recovery of Magnetite from Coal by Dry Beneficiation

By

J. Pieterse 10372742

Supervisor: Prof. N. Naudé

Dissertation submitted in partial fulfilment of the requirements for the degree of Master of Science in Applied Sciences Metallurgy.



UNIVERSITEIT VAN PRETORIA
UNIVERSITY OF PRETORIA
YUNIBESITHI YA PRETORIA

Denkleiers • Leading Minds • Dikgopolo tša Dihlalefi

Abstract

The use of magnetite as a medium in the wet processing of coal has been used since the early days of dense medium separation. The high magnetic susceptibility and density of magnetite make it an ideal medium to use in wet coal beneficiation because it is relatively easily and successfully recoverable. Owing to the need for more sustainable technologies, Coaltech has been investigating alternative dry processing processes: the Bohou process (developed in China) was identified as a possible feasible option. The Bohou process comprises dry dense medium separation using magnetite as the medium. The recovery and re-use of magnetite are, however, problematic. The aim of this investigation was to determine how efficiently magnetite can be recovered and to identify the factors influencing the magnetite losses during this dry processing.

The test work for the project was divided into two phases. The aim of Phase 1 was to identify the magnetite losses to the oversize coal fraction for different moisture conditions of the coal and magnetite. In Phase 2, magnetite and high-titanium magnetite (an alternative source of magnetite) were used to conduct test work to determine which medium could be successfully recovered from fine coal. Magnetite or high-titanium magnetite was mixed with the coal sample as a medium. During Phase 2, the effects of using different screens and different moisture conditions were investigated. For both phases, the samples received were divided into three categories containing different moisture contents: dry coal and dry magnetite, dry coal with wet magnetite (4% to 4.4%), and wet coal (3.5% to 6.5%) with dry magnetite. In Phase 1, the coal samples were screened at 13.2 mm, the oversize mixed with magnetite, and then screened again with a 13.2 mm screen: the magnetite losses were then recorded. For Phase 2, the prepared samples were screened at 3 mm, 13.2 mm, and with a 3 mm high-frequency screen. The undersize was passed through a low-intensity magnetic separator. The recovered magnetite was then passed over a magna chute to recover additional magnetite.

The results for both phases indicated that the highest recovery of magnetite occurred when dry magnetite and dry coal samples were used. The samples with wet magnetite also gave high recovery, but the samples with wet coal were detrimental to recovery and significant losses were observed. It was found that the magnetite stuck to the surface moisture of the coal. The use of a high-frequency screen improved recovery of the magnetite from the wet coal samples from 45.38% to 74.27%. Recovery from the high-frequency screen for both dry and wet magnetite samples was lower than that achieved with a conventional 3 mm screen.

The test results indicated that magnetite can be recovered in the dry beneficiation of coal when the surface moistures of both the coal and magnetite are controlled. Use of a high-frequency screen can improve recoveries only for conditions where the surface moisture of the coal is high.

Acknowledgements:

I would like to give thanks to God, the Almighty, for giving me the strength and abilities throughout the duration of the project.

My sincere gratitude goes to Prof Natasia Naudé for her guidance, valuable advice, expertise, and support throughout the research project and the writing of the thesis, and for not letting me give up.

My sincere gratitude and appreciation goes to the Coaltech Research Association for their financial assistance and valuable feedback and support. A special thank you to the Department of Materials Science and Metallurgical Engineering for their technical support and use of equipment.

I acknowledge with gratitude the support of Tronox Limited for the provision of high-titanium magnetite samples and Martin & Robson for the provision of the magnetite sample.

I would like to extend my truthful thankfulness and appreciation to my parents (Pieter and Judy Pieterse), my sister and brother-in-law (Andriette and Jan Nel) for their financial and emotional support.

My gratitude goes to friends for their constant support and encouragement.

A special thank you for the English editing of this thesis that was carried out by Dr. K. C. Sole of Sole Consulting.

Lastly, I would like to give express thanks to all the people that have added valuable advice and knowledge to this study: without your contributions this project would not have been a success.

Plagiarism declaration

| | |
|----------------|--|
| Full names | Jumandie Pieterse |
| Student number | 10372742 |
| Topic of work | Recovery of magnetite from coal by dry beneficiation |

Declaration

1. I understand what plagiarism is and am aware of the University's policy in this regard.
2. I declare that this thesis is my own original work. Where other people's work has been used (either from a printed source, internet or any other source), this has been properly acknowledged and referenced in accordance with the requirements as stated in the University's plagiarism prevention policy.
3. I have not used another student's past written work to hand in as my own.
4. I have not allowed, and will not allow, anyone to copy my work with the intention of passing it off as his or her own work.

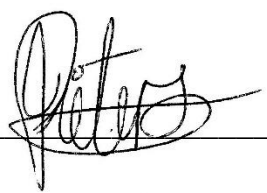
Signature 

Table of Contents

| | |
|--|----|
| 1. Introduction | 1 |
| 1.1. Background | 1 |
| 1.2. Problem statement | 3 |
| 1.3. Objectives..... | 3 |
| 1.4. Hypothesis..... | 4 |
| 1.5. Thesis organisation..... | 4 |
| 2. Literature Review | 5 |
| 2.1. Introduction | 5 |
| 2.2. Coal in South Africa..... | 5 |
| 2.2.1. A history of coal in South Africa..... | 5 |
| 2.2.2. A history of coal mining in South Africa..... | 7 |
| 2.2.3. Greenside and New Denmark Collieries..... | 9 |
| 2.3. Methods of coal beneficiation | 11 |
| 2.4. Dry beneficiation of coal..... | 15 |
| 2.4.1. Fluidization gas separation | 15 |
| 2.4.2. X-ray transmission | 17 |
| 2.4.3. Air jigs | 18 |
| 2.5. Air dense medium fluidized bed | 19 |
| 2.6. Magnetite in South Africa..... | 24 |
| 2.6.1. A history of magnetite in South Africa..... | 24 |
| 2.6.2. A history of the recovery of magnetite in South Africa..... | 27 |
| 2.6.3. Surface properties of magnetite | 28 |
| 2.7. High-titanium magnetite in South Africa..... | 30 |
| 2.8. Magnetic separation | 31 |
| 2.8.1. A history of magnetic separation | 31 |
| 2.8.2. Magnetic properties of materials | 34 |
| 2.8.3. The physics of magnetic separation..... | 36 |
| 2.8.4. Magnetic separators | 37 |
| 2.8.5. Dry magnetic separation | 39 |
| 2.9. Conclusion..... | 42 |
| 3. Methodology..... | 43 |



| | | |
|----------|---|----|
| 3.1. | Introduction | 43 |
| 3.2. | Sampling and characterisation of coal | 44 |
| 3.2.1. | Air drying..... | 44 |
| 3.2.2. | Screening..... | 44 |
| 3.2.3. | Splitting of AFE and ROM coal samples | 44 |
| 3.2.4. | Splitting of NDC coal sample | 46 |
| 3.2.5. | Coal classification..... | 47 |
| 3.2.5.1. | Particle size distribution | 47 |
| 3.2.5.2. | Proximate analysis..... | 48 |
| 3.2.5.3. | Calorific value | 48 |
| 3.2.5.4. | X-ray diffraction analysis..... | 49 |
| 3.3. | Sampling and characterization of magnetite and high-titanium magnetite..... | 49 |
| 3.3.1. | Drying | 49 |
| 3.3.2. | Splitting..... | 50 |
| 3.3.3. | Classification..... | 51 |
| 3.3.3.1. | Particle size distribution | 51 |
| 3.3.3.2. | X-ray diffraction analysis..... | 51 |
| 3.3.3.3. | X-ray fluorescence analysis | 51 |
| 3.3.3.4. | Scanning electron microscopy (Phase 1) | 52 |
| 3.3.3.5. | Quantitative evaluation of minerals by scanning electron microscopy..... | 52 |
| 3.3.3.6. | Hydrophobicity test..... | 53 |
| 3.4. | Sample preparation..... | 53 |
| 3.4.1. | Summary of experimental procedure..... | 54 |
| 3.4.2. | Preparation of wet and dry samples | 56 |
| 3.4.3. | Screening..... | 58 |
| 3.4.4. | Magnetic separation | 59 |
| 4. | Results | 61 |
| 4.1. | Mineralogical characteristics of coal samples..... | 61 |
| 4.1.1. | Particle size distribution..... | 61 |
| 4.1.2. | Proximate analysis | 61 |
| 4.1.3. | Calorific value..... | 62 |
| 4.1.4. | X-ray diffraction | 62 |
| 4.2. | Mineralogical characterization of magnetite and high-titanium magnetite | 63 |



| | | |
|----------|--|-----|
| 4.2.1. | Particle size distribution..... | 63 |
| 4.2.2. | X-ray diffraction | 64 |
| 4.2.3. | X-ray fluorescence | 65 |
| 4.2.4. | Scanning electron microscopy | 65 |
| 4.2.5. | Quantitative evaluation of minerals by scanning electron microscopy | 67 |
| 4.2.6. | Hydrophobicity | 68 |
| 4.3. | Phase 1: Losses of magnetite on coarse surfaces | 70 |
| 4.3.1. | Recovery of magnetite | 70 |
| 4.3.2. | Effect of sample mass on magnetite recovery | 72 |
| 4.3.3. | Magnetite losses per tonne..... | 74 |
| 4.3.4. | Nodule formation in magnetite | 75 |
| 4.4. | Phase 2: Effects of different screens on recovery of magnetite and high-titanium magnetite from the medium | 76 |
| 4.4.1. | Recovery of magnetite and high-titanium magnetite in the magnetic fraction.. | 76 |
| 4.4.1.1. | 3 mm screen..... | 76 |
| 4.4.1.2. | 13.2 mm screen..... | 77 |
| 4.4.1.3. | 3 mm high-frequency screen | 78 |
| 4.4.1.4. | Influence of moisture content on magnetic recovery in the magnetic fraction | 79 |
| 4.4.2. | Recovery of magnetite in the magnetic, middling, and non-magnetic fractions | 82 |
| 4.4.3. | Magnetite losses per tonne..... | 87 |
| 4.4.4. | Effect of moisture on media loss | 93 |
| 5. | Conclusions | 96 |
| 6. | Recommendations | 98 |
| | Bibliography | 99 |
| | Appendix 1..... | 106 |
| | Appendix 2..... | 107 |
| | Appendix 3..... | 107 |
| | Appendix 4..... | 109 |
| | Appendix 5..... | 110 |

List of Figures

| | |
|---|----|
| Figure 1: Bohou air dense medium fluidized bed system (Kalenda, North, & Naude, 2019)... | 3 |
| Figure 2: The Karoo Basin stratigraphy (Götz, Ruckwied, & Wheeler, 2018) | 6 |
| Figure 3: Map showing the extent of the Molteno coal field in the Eastern Cape Province (Pinheiro, Pretorius, Boshoff, & Barker, 1999) | 7 |
| Figure 4: Coal fields of South Africa (Pinetown, Ward, & Van der Westhuizen, 2007) | 9 |
| Figure 5: Locations of Greenside and New Denmark collieries (Mogodi, 2012) | 10 |
| Figure 6: Processing cycle for cleaning coal (Kumar & Kumar, 2018) | 11 |
| Figure 7: Generic preparation plant flowsheet according to subsystem and coal size (Kumar & Kumar, 2018)..... | 13 |
| Figure 8: Flotation cell (Kramer, Gaulocher, Martins, & Leal Filho, 2012) | 14 |
| Figure 9: Schematic diagram of FGX dry separator showing the different products (Zhang et al., 2011) | 16 |
| Figure 10: A belt sorter using X-ray transmission technology (Robben et al., 2014) | 18 |
| Figure 11: Expansion and contraction of a bed of particles due to jiggling action (Gupta & Yan, 2016)..... | 19 |
| Figure 12: Schematic air dense medium fluidized bed (CSIR, Pretoria)..... | 20 |
| Figure 13: Schematic diagram of a dry separator with air dense medium fluidized beds (Zhenfu & Qingru, 2001)..... | 21 |
| Figure 14: Schematic diagram illustrating the performance indicators and variables that affect ADMFB performance (Mohanta et al., 2013) | 22 |
| Figure 15: The Palabora Complex in South Africa (Groves & Vielreicher, 2001) | 25 |
| Figure 16: Geology of the Palabora Igneous Complex (Vielreicher, Groves, & Vielreicher, 2000) | 26 |
| Figure 17: South Africa's iron deposits (Utembe, Faustman, Matatiele, & Gulumian, 2015) | 27 |
| Figure 18: Rotation symmetries and equilateral crystal faces of an octahedral crystal (Ootaki & Wolken, 1973) | 29 |
| Figure 19: Development of permanent magnet materials (Svoboda, 2004) | 32 |
| Figure 20: Schematic representation of a magnetic separator (Svoboda, 2004)..... | 33 |
| Figure 21: Graphical illustration of ferromagnetic, ferrimagnetic, paramagnetic, and diamagnetic materials (Sinatra, 2010) | 34 |
| Figure 22: Magnetic susceptibility of common rock types (Clark & Emerson, 1991)..... | 36 |
| Figure 23: Different types of wet low-intensity drum magnetic separators (Svoboda, 2004)..... | 38 |
| Figure 24: Pattern of the magnetic field around a magnetic drum (Svoboda, 2004)..... | 40 |
| Figure 25: Dry drum magnetic separator with top feed (Svoboda, 2004) | 41 |

| | |
|---|----|
| Figure 26: Arrangement of magnetic poles in a drum magnetic separator (Svoboda, 2004) .. | 41 |
| Figure 27: Splitting of AFE and ROM coal samples with a rotary splitter | 45 |
| Figure 28: Splitting of NDC coal sample with rotary and riffle splitter..... | 46 |
| Figure 29: Laboratory sieve shaker..... | 48 |
| Figure 30: Splitting of magnetite for the AFE and ROM coal tests using a rotary splitter | 50 |
| Figure 31: Splitting of magnetite and high-titanium magnetite for use with the NDC coal using a rotary splitter. | 51 |
| Figure 32: Hydrophobicity measurement | 53 |
| Figure 33: Experimental procedure | 55 |
| Figure 34: Mixing of NDC coal and magnetite samples | 57 |
| Figure 35: Further splitting of magnetite samples | 58 |
| Figure 36: Magna chute | 60 |
| Figure 37: Particle size distributions of coal samples..... | 61 |
| Figure 38: X-ray diffraction analysis of ROM and AFE samples | 63 |
| Figure 39: Particle size distribution of magnetite samples | 64 |
| Figure 40: Secondary-electron image of magnetite | 66 |
| Figure 41: Secondary-electron image of magnetite with clay. | 66 |
| Figure 42: Secondary-electron image of magnetite with a size fraction of +1700 μm | 67 |
| Figure 43: QEMSCAN analysis showing agglomerations in the magnetite sample | 68 |
| Figure 44: QEMSCAN of high-titanium magnetite..... | 68 |
| Figure 45: Contact angle of hydrophobicity test..... | 69 |
| Figure 46: Force diagram of Young's equation and associated contact angle measurement.(Simpson, Hunter, & Aytug, 2015) | 69 |
| Figure 47: Recovery versus loss of magnetite | 71 |
| Figure 48: Magnetite sticking to wet coal..... | 72 |
| Figure 49: Magnetite recovered from the different magnetic fraction from the LIMS | 73 |
| Figure 50: Loss of magnetite per tonne of coal | 75 |
| Figure 51: Nodules formed during screening of the wet coal samples..... | 75 |
| Figure 52: Recovery of magnetite and high-titanium magnetite using 3 mm screen | 77 |
| Figure 53: Recovery of magnetite and high-titanium magnetite using 13.2 mm screen | 78 |
| Figure 54: Recovery of magnetite and high-titanium magnetite using 3 mm high-frequency screen | 79 |
| Figure 55: Magnetite recovery as a function of surface moisture of the magnetite | 80 |
| Figure 56: Magnetite recovery as a function of surface moisture of the coal..... | 80 |

| | |
|---|-----|
| Figure 57: High-titanium magnetite recovery as a function of surface moisture of the high-titanium magnetite | 81 |
| Figure 58: High-titanium magnetite recovery as a function of the surface moisture of the coal | 82 |
| Figure 59: Percentages of magnetite and high-titanium magnetite deporting to the magnetic fraction (3 mm screen) | 83 |
| Figure 60: Percentage of magnetite and high-titanium magnetite deporting to the magnetic fraction (13.2 mm screen) | 84 |
| Figure 61: Percentage of magnetite and high-titanium magnetite deporting to the magnetic fraction (3 mm high-frequency screen)..... | 84 |
| Figure 62: Effect of magnetite surface moisture on recovery of magnetite in the magnetic fraction | 85 |
| Figure 63: Coal surface moisture in comparison to recovery of magnetite in the magnetic fraction | 85 |
| Figure 64: High-titanium magnetite surface moisture in comparison to recovery of high-titanium magnetite in the magnetic fraction | 86 |
| Figure 65: Coal surface moisture in comparison to recovery of high-titanium magnetite in the magnetic fraction | 87 |
| Figure 66: Loss of magnetite samples per tonne of coal for -13.2 mm screen | 88 |
| Figure 67: Loss of magnetite per tonne of coal for -3 mm screen | 88 |
| Figure 68: Loss of magnetite per tonne of coal for -3 mm high-frequency screen..... | 89 |
| Figure 69: Loss of magnetite in wet coal samples | 90 |
| Figure 70: Loss of magnetite per tonne of coal as a function of moisture of the magnetite.... | 91 |
| Figure 71: Loss of magnetite per tonne of coal as a function of moisture of the coal..... | 91 |
| Figure 72: Loss of high-titanium magnetite per tonne as a function of surface moisture of the high-titanium magnetite | 92 |
| Figure 73: Loss of high-titanium magnetite per tonne as a function of surface moisture of the coal | 92 |
| Figure 74: Loss of magnetite as a function of surface moisture of magnetite | 93 |
| Figure 75: Loss of magnetite as a function of surface moisture of coal | 94 |
| Figure 76: QEMSCAN image of magnetite..... | 107 |
| Figure 77: Microscope image of magnetite sticking to the surface moisture of coal | 109 |
| Figure 78: Clumps of magnetite and fine wet coal magnified at 1.25x..... | 109 |

List of Tables

| | |
|---|-----|
| Table 1: Hydrophobicity of materials (Drzymala, 2007)..... | 29 |
| Table 2: AFE and ROM sample labels | 45 |
| Table 3: Sample preparation methods for magnetite and high-titanium magnetite samples ... | 47 |
| Table 4: Proximate analyses of coal samples | 62 |
| Table 5: Calorific values of coal samples | 62 |
| Table 6: X-ray diffraction results for magnetite and high-titanium magnetite | 64 |
| Table 7: X-ray fluorescence analysis of magnetite (%)..... | 65 |
| Table 8: Magnetite losses..... | 74 |
| Table 9: Total recovery of magnetite during initial test work. | 108 |
| Table 10: Recovery of magnetite in different fractions | 108 |
| Table 11: Magnetite recovery with 3 mm screen..... | 110 |
| Table 12: High-titanium magnetite recovery with 3 mm screen | 111 |
| Table 13: Magnetite recovery with 13.2 mm screen..... | 112 |
| Table 14: Recovery of high-titanium magnetite with 13.2 mm screen..... | 113 |
| Table 15: Magnetite recovery with 3 mm high-frequency screen | 114 |
| Table 16: High-titanium magnetite recovery with 3 mm high-frequency screen | 115 |
| Table 17: Recovery of magnetite in different fractions | 116 |
| Table 18: Recovery of high-titanium magnetite in different fractions | 117 |
| Table 19: Magnetite and high-titanium magnetite losses per ton | 118 |
| Table 20: Comparison of moisture content and loss of magnetite..... | 119 |

1. Introduction

1.1. Background

Beneficiation is the separation of gangue material from a desired mineral to create a concentrated product (Whitten, 1972). Coal is beneficiated to produce a workable product for either thermal or metallurgical coal (Noble & Luttrell, 2015). Thermal coal is used in power plants to generate electricity, while metallurgical coal, also known as coking coal, is used as feedstock in the production of steel and various other ferrous metals. Beneficiation includes the breaking down of coal into specific particle sizes, removal of impurities, selective removal of harmful air pollutants, and lowering the moisture and ash contents. The degree of beneficiation is determined by the intended use of the coal.

Wet beneficiation of coal has been most commonly used globally for processing (Dwari & Rao, 2007). Extra steps in wet beneficiation include dewatering and waste disposal, which can lead to environmental problems (Noble & Luttrell, 2015). Owing to recent economic struggles and water shortages, other methods, such as dry beneficiation, are being investigated (Chen & Wei, 2003). Dry beneficiation appears to be an acceptable alternative due to the lower capital cost of waterless processing. Dry beneficiation processes include the use of air-fluidized beds, magnetic separation, jigs, and X-ray fluorescence (XRF) sorters, to name a few.

The focus of this study is the use of dry magnetic separation for the recovery of magnetite from the medium used in dry fluidized-bed separation of coal.

Coaltech Research Association (Coaltech), a collaborative research organisation funded by the South African coal industry, is investigating the use of a new dry dense medium separation (DMS) process (fluidized bed), developed in China, as an alternative to the current wet DMS processing. Magnetite is widely used as the medium in wet DMS beneficiation. This study evaluated the recovery and re-usability of magnetite as a medium in dry DMS. The recovery of the medium (magnetite) is critical to ensure acceptable medium consumption levels because this has an influence on the economic viability of the process.

Magnetic separation started in 1792 with the patenting of the recovery of magnetite by magnetic separation by W. Fullarton (Svoboda, 2004). Magnetite occurs in a naturally magnetic state: it is a ferromagnetic mineral that is strongly attracted to a magnetic field with a magnetic susceptibility of 625×10^{-6} – $1156 \times 10^{-6} \text{ m}^3/\text{kg}$ (Howie, Zussman, & Deer, 1992). Owing to its ferromagnetic nature, a low-intensity magnetic separator (LIMS) can be used to recover magnetite.

Coal is classified as a weakly diamagnetic material (Dwari & Rao, 2007). The difference in magnetic susceptibility between coal and magnetite is used to recover the magnetite medium in wet DMS processes in the coal industry. During dry DMS, the magnetite medium can also be recovered by use of a dry magnetic separator.

During the dry magnetic recovery of magnetite, it is important to ensure that there is no contamination of the magnetite by fine coal and clay material. The most significant current concern regarding the proposed dry DMS unit is recovery of the medium (magnetite).

China has a large coal industry that struggles with water shortages (Chen & Yang, 2003). Owing to the lack of usable water, research in clean coal technology (CCT) has become popular. One of the methods to achieve CCT is use of an air dense medium fluidized bed (ADMFB), as shown in Figure 1. An ADMFB uses gas to create DMS of particles (Luo, Zhu, Fan, Zhao, & Tao, 2007). The aim of this project was to study the recovery of the magnetite used as medium in this application.

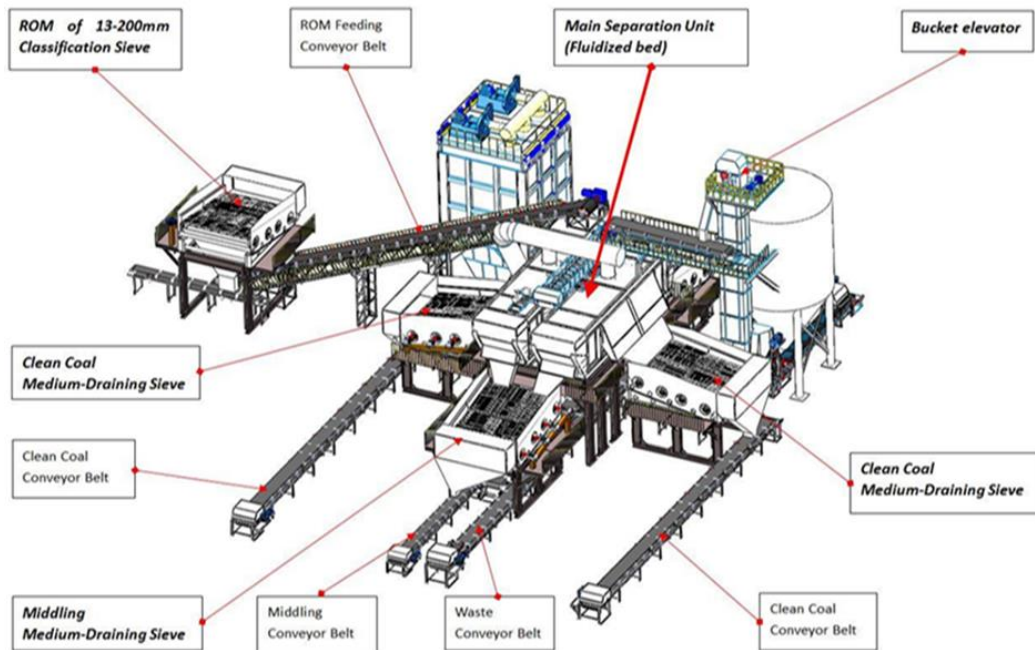


Figure 1: Bohou air dense medium fluidized bed system (Kalenda, North, & Naude, 2019)

1.2. Problem statement

Owing to the importance and scarcity of water, different methods of coal beneficiation are being studied. Dry beneficiation of coal is promising because it uses little to no water. The Bohou process, implemented in China, shows promise in this field. Although magnetite is commonly used as a medium in the dry DMS process, the loss of magnetite should be studied, because this has a significant influence on the process economics and feasibility. Re-use of magnetite in the system plays a vital role in reducing the overall process cost of dry DMS.

1.3. Objectives

The study aimed to evaluate the use and recovery of magnetite in the dry beneficiation of coal. In summary, the objectives of this study were to:

- Conduct a comprehensive study into previous work done on the use of magnetite in coal beneficiation;
- Identify sources of magnetite in South Africa;
- Determine the recovery and loss of magnetite to the oversize (Phase 1);

- Determine the recovery of magnetite from the medium (Phase 2);
- Compare the use of magnetite with that of high-titanium magnetite.

1.4. Hypothesis

Magnetite can effectively be recovered during the dry beneficiation of coal compared to that of the wet beneficiation process.

1.5. Thesis organisation

The body of this thesis is organised into three parts that give information on the study, excluding the introduction, conclusion, and recommendations.

Chapter 2 focuses on the literature study. This includes the background of both coal and magnetite, the historical use of magnetite, and the future use for magnetite in the field of beneficiation.

Chapter 3 discusses the methodology of the study. The chapter includes descriptions of the steps used in sampling, and the mixing and separation of the samples.

Chapter 4 discusses the results obtained from the study, as well as an analysis of the losses.

Chapter 5 is based on the conclusions drawn from the results.

Chapter 6 contains a summary of future work and recommendations that can assist with better understanding of the study.

2. Literature Review

2.1. Introduction

Coal is an important commodity in South Africa, with a rich history in the development of the country. From the discovery of coal to the processing by coal mines today, new techniques have been discovered for the beneficiation of coal. Coal is found in the north-eastern region of South Africa (Coulter, 1957).

The use of magnetite in the processing of coal has been used since the early days of DMS methods in coal production. With an ample supply of magnetite available, new methods are being investigated for the use of this commodity. Owing to the strong magnetic properties and high density of magnetite, it is easy to recover during the processing of coal, making it an ideal medium to use during beneficiation. Magnetite is found in the Palabora Igneous Complex (PIC) as a by-product of the carbonatite-hosted copper deposit, as well as in Namakwa in the Northern Cape (Lurie, 1977).

Environmental constraints are forcing countries to look into new, more economically friendly methods of coal preparation. Thus, there is a need for the study of dry DMS beneficiation of coal using magnetite.

2.2. Coal in South Africa

2.2.1. A history of coal in South Africa

The coal seams in South Africa formed about 200 million years ago (Hand, 2002). The highest concentration of coal is found in the Ecca group of the Karoo Basin (Cadle, Cairncross, Christie, & Roberts, 1993), shown in Figure 2. The Ecca group contains three sub groups: the Pietermaritzburg Formation, the Volksrust Formation, and the Vryheid Formation. The coal seams formed when the Vryheid Formation was deposited (Wilson & Anhaeusser, 1998a). South Africa contains 70% of the coal found in Africa (Snyman & Botha, 1993).

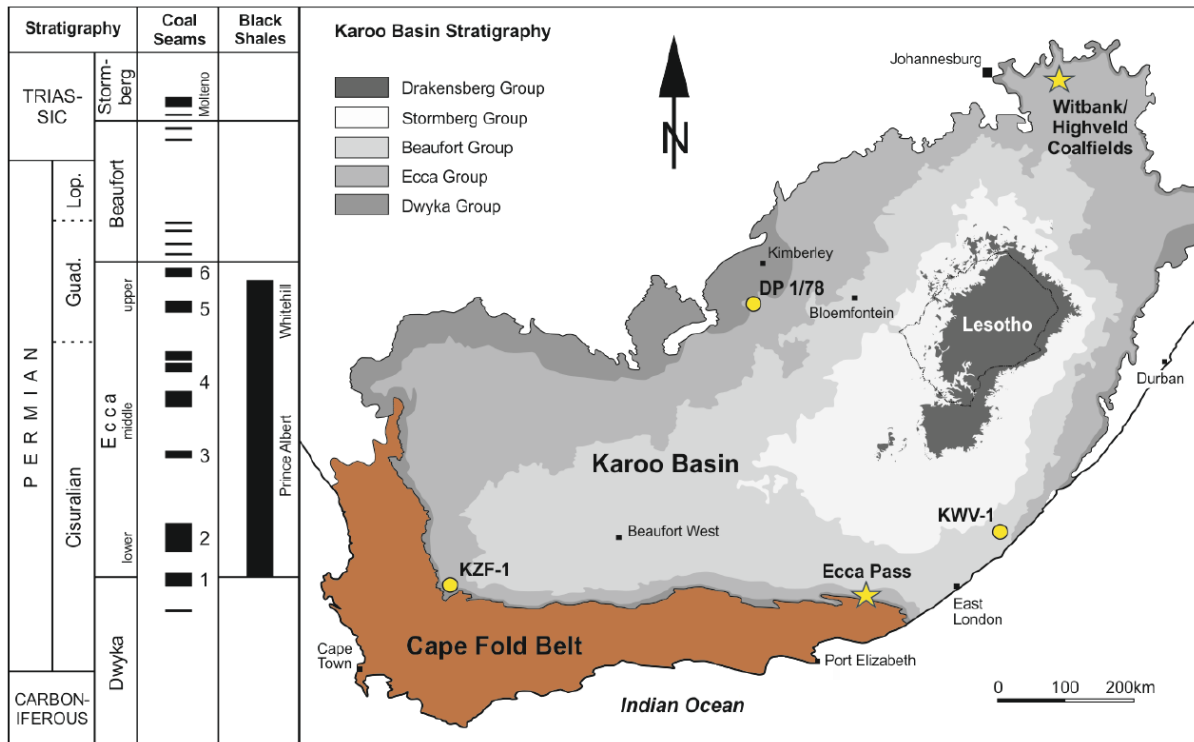


Figure 2: The Karoo Basin stratigraphy (Götz, Ruckwied, & Wheeler, 2018)

The Vryheid Formation is classified as a delta-plain environment (Wilson & Anhaeusser, 1998a). During the formation, the area was categorized by widespread peat-forming periods (Catuneanu et al., 2005). The peat swamps of the Vryheid Formation caused the coal seams to occur in fluvial succession (Johnson, Anhaeusser, & Thomas, 2006). The coal was formed when the peat was covered by sediments (McCarthy, 2013). The peat consisted mostly of carbon, hydrogen, and water. As the peat was covered by sediments and water, the oxygen in the peat was replaced with water. The peat was converted to coal due to the high pressure and temperature that occurred. At a low temperature and pressure, peat is converted to lignite; at higher temperature and pressure, the peat is converted to bituminous coal; at extreme temperature and pressure, the coal is converted to anthracite (McCarthy, 2013).

The higher the temperature and pressure, the higher is the carbon content (McCarthy, 2013). Lignite contains roughly 70% carbon, bituminous coal contains roughly 85%, and anthracite contains roughly 83% carbon.

Mud is usually buried with the peat during sedimentation (McCarthy, 2013). The mud forms bands in the peat. Mud is incombustible, so it forms the residue or ash of the coal.

2.2.2. A history of coal mining in South Africa

The first coal mine in South Africa opened in 1864 in the town of Molteno in the Eastern Cape (Peatfield, 2003), shown in Figure 3. The development of coal mines increased with the discovery of the Kimberly diamond fields and the Witwatersrand gold fields. With the rise of mining in South Africa, new coal mines opened near Vereeniging and in (then) Natal.

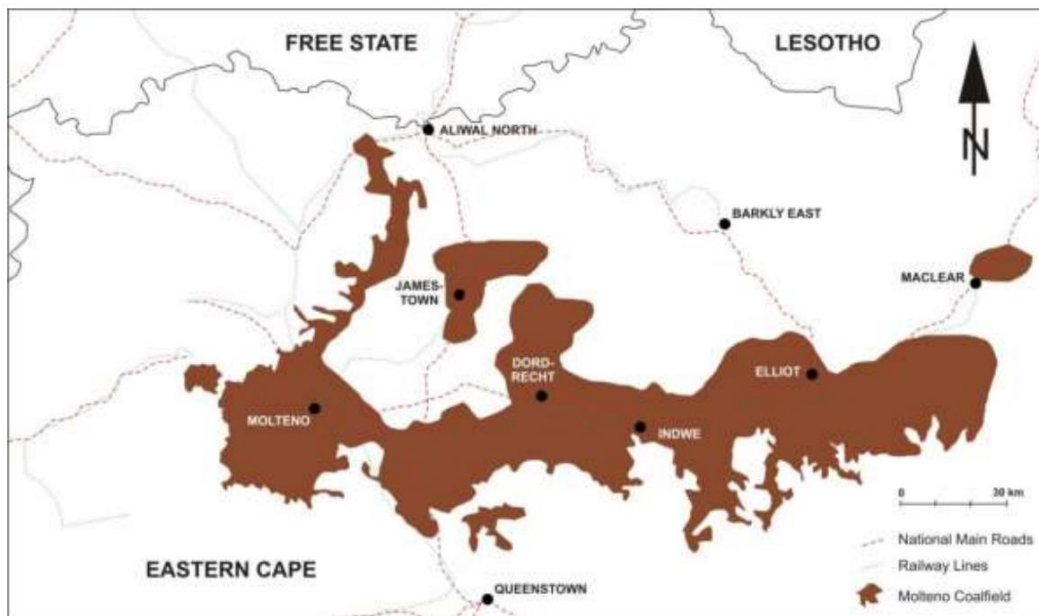


Figure 3: Map showing the extent of the Molteno coal field in the Eastern Cape Province
(Pinheiro, Pretorius, Boshoff, & Barker, 1999)

Molteno became a major supplier of coal for the Kimberly diamond fields (Knowles, 1936). In 1882, the mine produced 6000 tonnes of coal; this grew to 70 000 tonnes by 1897. Owing to the expansion of railroads to the (then) Natal and Transvaal coal fields, the mine closed in 1920.

After the discovery of gold on the Witwatersrand, coal was discovered in Boksburg (1887) and in Witbank in 1890 (Peatfield, 2003). Witbank became an important supplier of coal for the country's mines, industries, and railways. Owing to the growth

in the gold industry and other mining activity, the need for more coal grew, resulting in further development of the coal fields (Eberhard, 2011).

The Natal coal fields were situated close to the sea, making it ideal for export (Alexander, 2007), whereas Transvaal provided coal for the gold mining industry. The railways in South Africa were an important catalyst for the development of the coal industry. South Africa produced 10.3 million tonnes of coal in 1919, with 64.5% produced in the Transvaal and 27.3% produced in Natal (Alexander, 2007). It was estimated that South Africa produced 24.9 million tonnes of coal in 1944, with 70.6% produced in the Transvaal (Alexander, 2007).

In the early days, when coal was needed for the gold and diamond mines, coarse coal was screened by hand. Coal smaller than 6 mm was called 'duff' (de Korte, 2015). The duff, which mostly consisted of run-of-mine (Sachkov, Nefedov, Orlov, Medvedev, & Sachkova) coal, was usually discarded, while the coarse coal was supplied to the end-users. Mine owners realised that, to be more sustainable, they would have to mine the whole seam. Owing to the low quality of the coal, a new way to upgrade the coal needed to be created. The earliest method was by hand picking (Coulter, 1957).

It was important to find better ways to upgrade the coal. A coal preparation plant was constructed in 1909 in Witbank (Coulter, 1957). A jig plant was constructed in the coal preparation plant. Numerous new coal processing plants were then constructed in Witbank and Natal. Owing to the need for better coal, it became crucial to install jigs at a number of coal mines (de Korte, 2015).

DMS using magnetite became popular in the 1950s (de Korte, 2015). Jigs were gradually replaced due to the better performance of the DMS.

The first oil made from coal was produced in Sasolburg, South Africa, in 1955 (Peatfield, 2003). The oil crisis that occurred in 1973 and the low-ash contract that was signed between the Transvaal Coal Owners Association and the Japan Steel Mills caused an export boom in the 1970s (de Korte, 2015).

Events in the 1970s caused major changes in the South African coal processing industry (de Korte, 2015). The Richards Bay Coal Terminal (RBCT) was built as an export port for coal, along with a railway that connected Witbank and Richards Bay.

The need for coking coal for the Iron and Steel Corporation (Iscor) led to further development of the coal fields in the Natal region (Hand, 2002). The largest beneficiation plant was commissioned in 1980 at Grootegeluk (Peatfield, 2003). The plant was designed to supply 2 million t/a of coking coal for Iscor and 4 million t/a of steam coal to the Matimba Power Station.

The growth in the coal industry led to 104 operating coal mines by 1987 (Peatfield, 2003), with most coal produced in Mpumalanga. The Witbank, Highveld, and Eastern Transvaal coal fields contribute roughly 80% of the coal production in South Africa (Peatfield, 2003). A map of South Africa’s coal fields is shown in Figure 4.

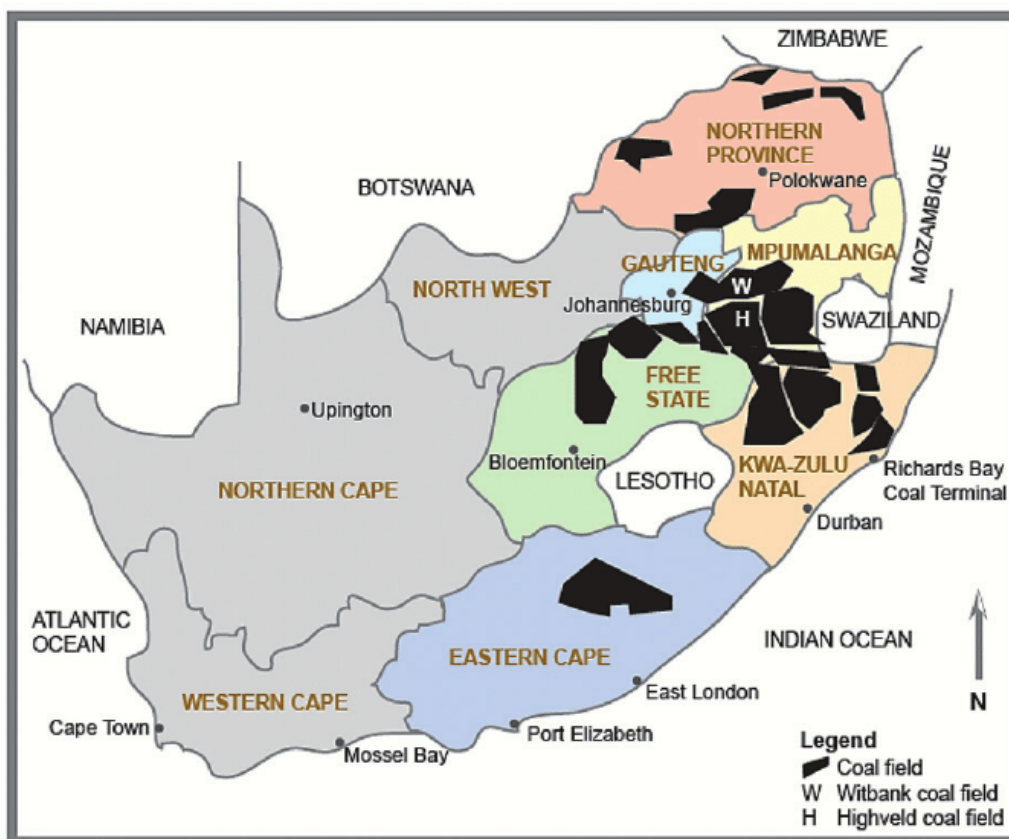


Figure 4: Coal fields of South Africa (Pinetown, Ward, & Van der Westhuizen, 2007)

2.2.3. Greenside and New Denmark Collieries

Both Greenside Colliery and New Denmark Colliery are located on the Vryheid Formation of the Ecca Group (Hancox & Götz, 2014). Greenside Colliery is an Anglo American-owned coal mine situated 15 km from Emalahleni (van Vollenhoven, 2017).

No. 4 seam coal is currently being extracted for export and local use. Greenside Colliery has a life of mine expectancy until the year 2031. The mine is estimated to have 201 million tonnes of coal in-situ and 124 million tonnes of coal in ROM reserves (Nefedov, Orlov, Medvedev, Sachkova, & Sachkov, 2018). The mine produces 3.6 million tonnes of ROM coal per annum.

New Denmark Colliery (NDC) is also an Anglo American-owned coal mine, situated close to Standerton. NDC is the deepest coal mine in South Africa, reaching down to roughly 200 m below the surface (Hancox & Götz, 2014). The mine was opened in 1982 and production started in 1984 (Mogodi, 2012). The mine has a life expectancy until 2039, with a resource base of 147 million tonnes. Annual coal production is 5.4 million tonnes. The locations of both mines are shown in Figure 5.

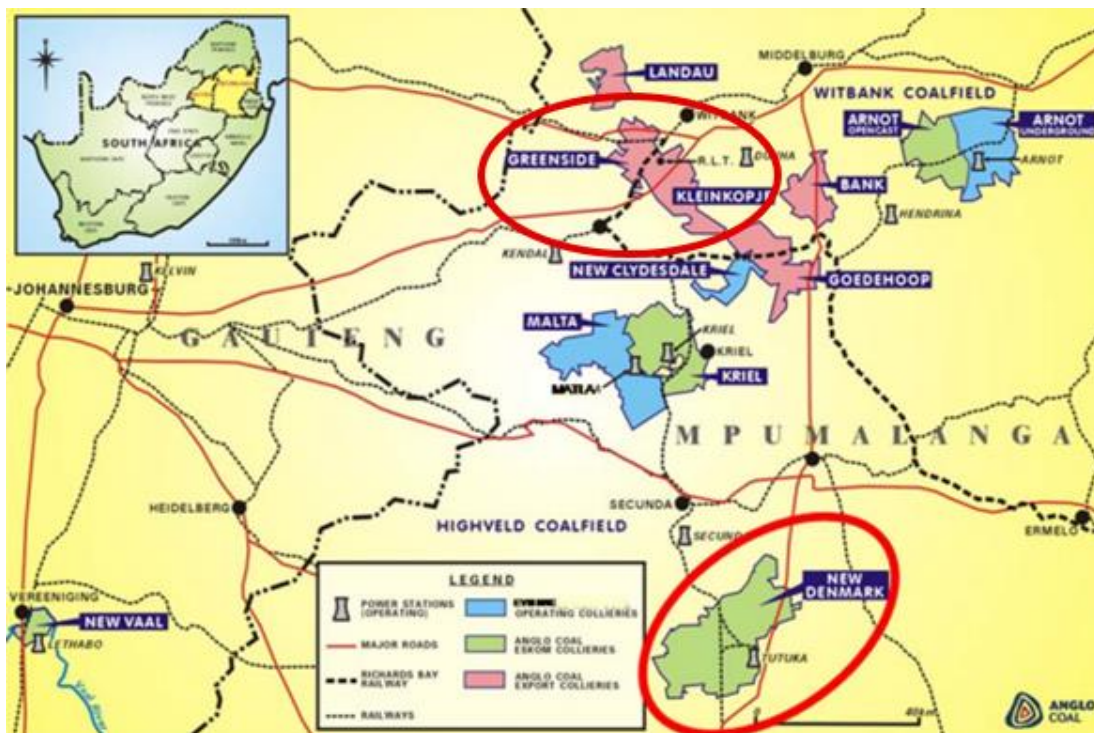


Figure 5: Locations of Greenside and New Denmark collieries (Mogodi, 2012)

2.3. Methods of coal beneficiation

The beneficiation of coal refers to its upgrading to a cleaner and graded product (Hand, 2002). Coal is upgraded to improve the grade by regulating its size and by reducing the mineral matter content. The coal goes through classification and crushing, cleaning and washing, and dewatering, as shown in Figure 6.

ROM coal is the coal that is directly delivered to the coal processing plant (CPP) from the mine (Sanders, 2007). The coal is sent to the processing plant or to a stockpile to be worked later. The stockpile is created to allow for a constant feed to the wash plant. The coal passes through a crusher to reduce the top size. Crushing may include two stages, depending on the top size that is desired and the liberation characteristics (Kumar & Kumar, 2018). The ROM material is crushed to three different fractions, comprising coarse (> 50 mm), small (0.5 to 50 mm), and fines (< 0.5 mm). Each size fraction is treated separately. Screening is most commonly used to size the coarser particles of coal, whereas fine coal is sized using fine coal sieves or classifying cyclones.

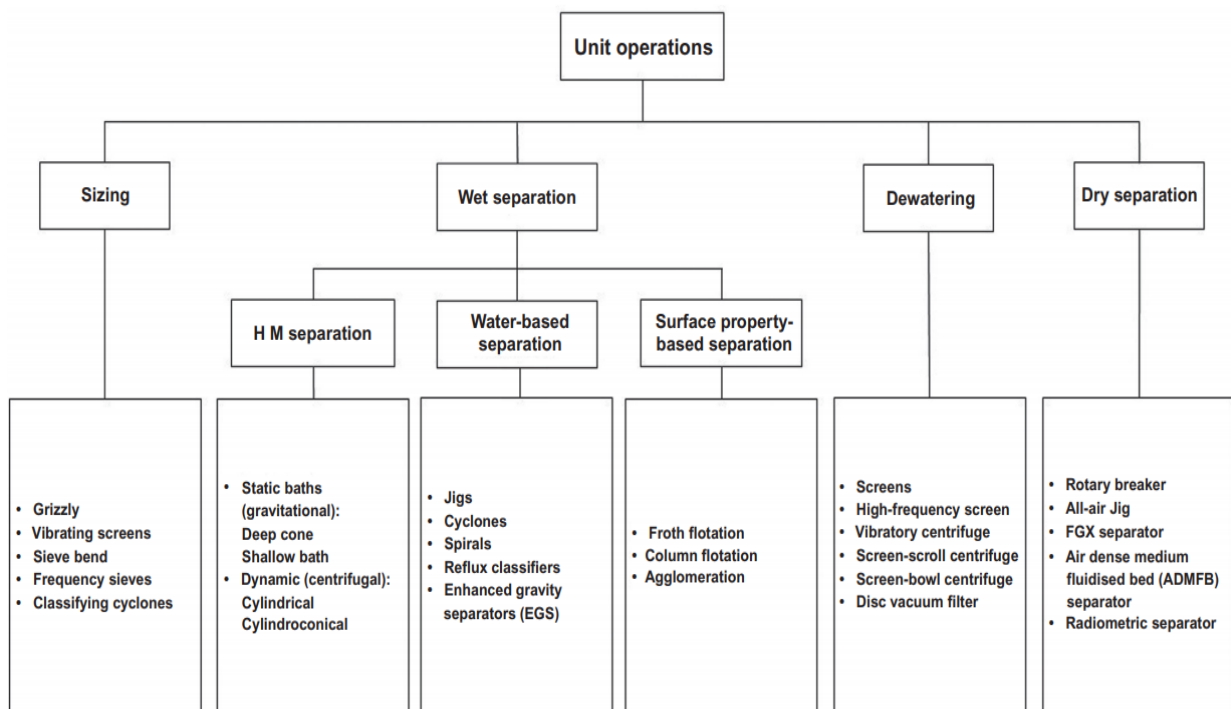


Figure 6: Processing cycle for cleaning coal (Kumar & Kumar, 2018)

After crushing, the coal is washed. Washing can be done with jigs, heavy-medium systems, cyclones, or by flotation (Kumar & Kumar, 2018). Prewashing is carried out to remove an adequate amount of non-combustible material. The removal of additional material is undertaken to relieve the downstream circuit of preventable overloading. Prewashing also minimises the creation of fines: fine coal can be expensive and difficult to treat.

The coal is further screened to separate it according to coarse and fine size fractions. The coal is separated to obtain different final products. Coarse- and intermediate-sized coals are cleaned by gravity separation, while fine coal is cleaned using flotation (Hand, 2002). The coal is beneficiated to remove impurities and sulfur, and reduce the ash content (Sanders, 2007). Through the removal of unwanted material, the coal is upgraded to a better quality.

The type of washing depends on the size, density, and surface wettability of the coal. The jigs, heavy-medium systems, cyclones, or flotation equipment used for separating the coal during washing within a somewhat narrow size range of particles perform well because of their characteristic processing effectiveness and geometry (Kumar & Kumar, 2018). Owing to the large range of particle sizes found in ROM coal, a variety of types of cleaning processes are used in a plant (Figure 7). Jigs, heavy-medium baths, and heavy-medium cyclones are used to treat both coarse- and intermediate-sized particles.

Of the coal preparation methods used in South Africa, 85% is processed by dense medium separation (DMS) (Robl, Oberlink, & Jones, 2017). DMS is preferred because of the very high levels of near-gravity material that is found in South African coal. Near-gravity material is material that has a density of within a range of 0.1 of the relative density of the coal. Finely ground magnetite is typically employed in the density separation. The magnetite ($-45\ \mu\text{m}$) is dispersed in water. The desired density is achieved by adding magnetite to the suspension. During DMS, particles with a lower density will float to the top of the medium, while those with a higher density will sink to the bottom. The particles are separately removed from the top and bottom. The magnetite used during DMS is recovered from the wash water by magnetic separation and then recycled back into the dense medium circuit.

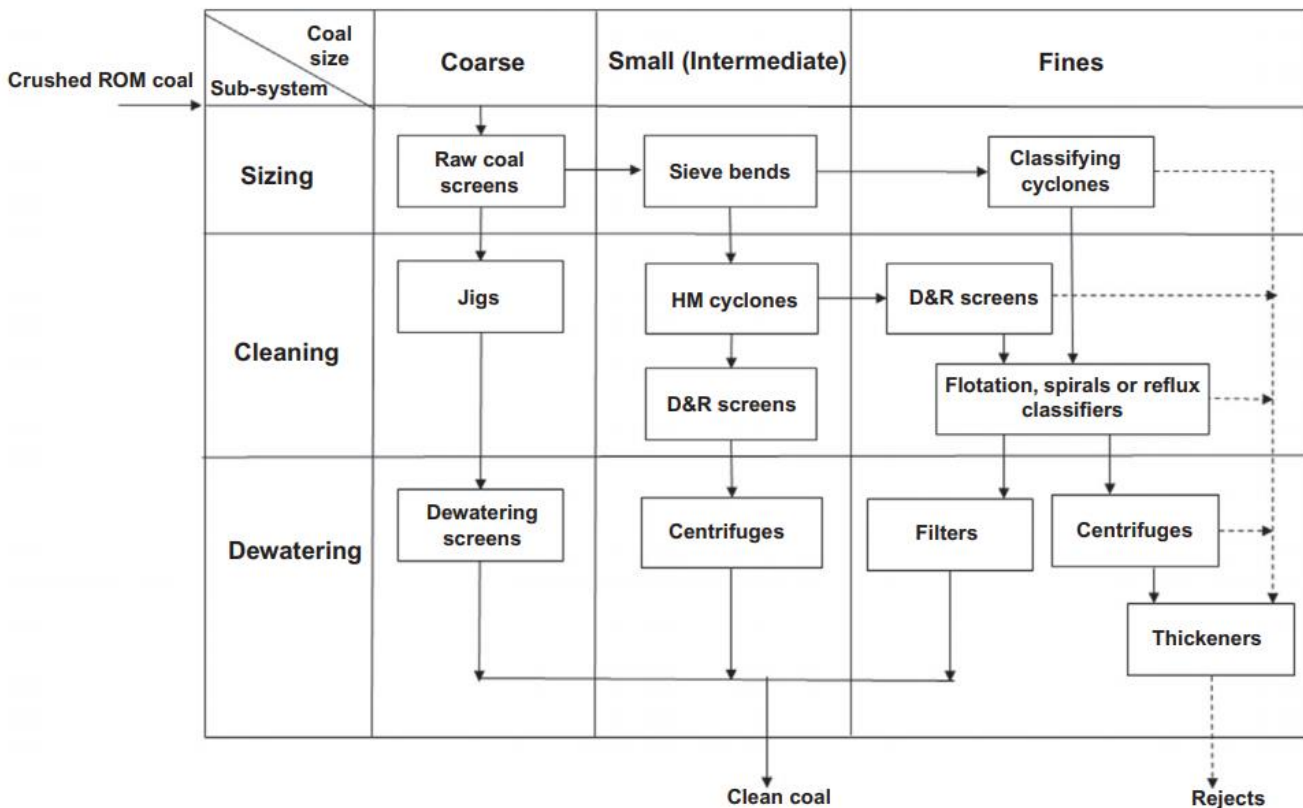


Figure 7: Generic preparation plant flowsheet according to subsystem and coal size (Kumar & Kumar, 2018)

Intermediate coal particles (1–50 mm) are treated using cyclones, whereas coarse particles (> 50 mm) are usually separated in dense medium drums (Robl et al., 2017). Dense medium cyclones (DMC) work on the same principle as conventional cyclones. In a DMC, the fluid density can be increased to achieve the desired separation density by the addition of magnetite.

Another form of gravity separation is jig washing. Jig washing is also based on the principles of DMS (Robl et al., 2017), but the particles are separated using water as the medium. The water is pneumatically or hydraulically pulsated through the coal particles. The pulsation of the water stratifies the particles based on their density. The result is that lighter particles accumulate at the top of the particle bed and heavier particles at the bottom.

The amount of near-gravity material in the coal is the leading factor determining whether a jig or DMS is employed (Robl et al., 2017). With a percentage of the feed of between 1% and 7% near gravity, almost any separation process will work effectively,

but jigs are usually used for these conditions (Wills & Finch, 2015). When the near-gravity material is greater than 10%, a DMS process is used, although the process needs to be closely controlled. With a near-gravity material content above 25%, the dense medium process is difficult, although it can be used in limited situations.

The simplest method of separating coarse from fine coal is size separation (Robl et al., 2017). The approach is simple and used wherever possible. The size separation is dependent on the size difference between the coal particles. When screening is not efficient in separating the coal, a classifying cyclone is used.

Fine particles (less than 150 μm) are separated using flotation (Robl et al., 2017; Wills & Finch, 2015). Flotation uses the difference in particle hydrophobicity to separate the particles. The particles are agitated in a flotation cell while air bubbles from the bottom of the cell move through the particles (Figure 8). The coal, which is hydrophobic, adsorbs onto the air bubbles and rises to the top where the particles form a stable froth layer. The froth layer is then collected to remove the fine coal.

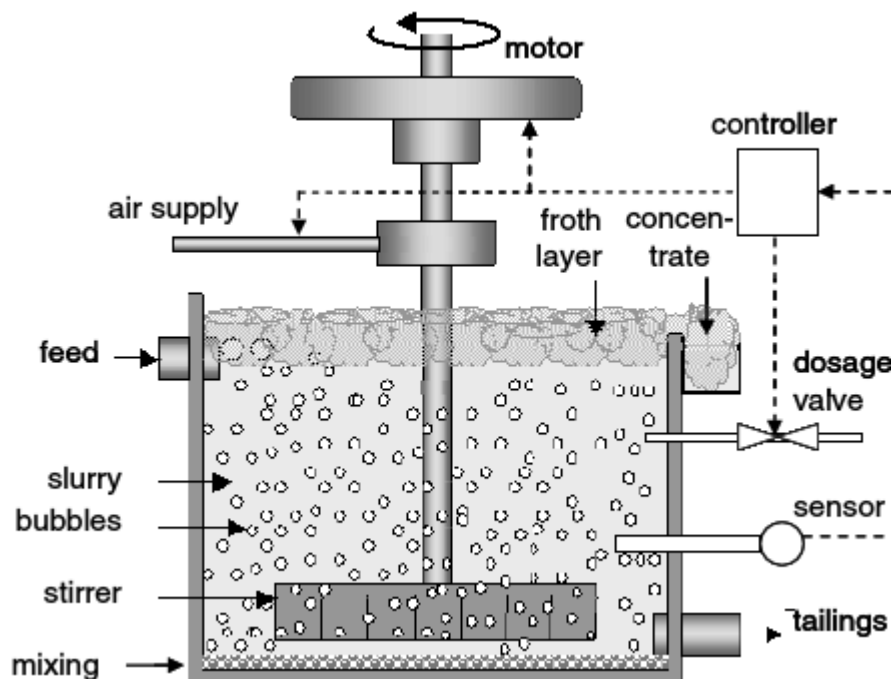


Figure 8: Flotation cell (Kramer, Gaulocher, Martins, & Leal Filho, 2012)

2.4. Dry beneficiation of coal

South Africa's coal processing industry has become efficient in processing raw coals and producing a high quality product (de Korte, 2015). The Witbank area has as many as 60 coal processing plants currently operating, with many producing export thermal coal.

Most plants use a two-stage process to clean the coal (de Korte, 2015). The first stage is the processing of the raw coal to produce the export coal. The second stage is processing the discarded coal to produce thermal coal for Eskom. It is common to use dense medium drums or cyclones to process the coarse coal and a spiral is used for the finer coals. The above processes use vast amounts of water to process the coal.

Owing to concerns about water quality and water wastage, alternative methods of processing coal need to be found. Water used during processing may become acidic due to the presence of pyrite (Tiwary, 2001). The effect of acidic water can be severe if it comes in contact with the surrounding water reserves. Pyrite can degrade water by lowering its pH, making it unsuitable for use by the local communities.

South Africa is a country that is prone to droughts (Baudoin, Vogel, Nortje, & Naik, 2017). Recent droughts have had a major impact on water availability for the country. Droughts affect both communities and industry. A new way of dry processing thus needs to be used to prevent unnecessary loss of water.

Dry beneficiation of coal does not require any water to be added. Two methods of dry beneficiation are currently used in South Africa; namely, fluidization gas separation (FGX) and X-ray transmission (XRT) sorting (De Korte, 2013). Dry separation of coal is less effective than that of wet sorting (De Korte, 2013).

2.4.1. Fluidization gas separation

FGX is an air-table dry separator, as shown in Figure 9. The FGX dry separator uses a modified air-table mechanism to clean coal (Akbari, Zhang, Sayeh, Mohanty, & Rahimi, 2012). The table consists of a perforated separating deck that is fluidised by three air chambers underneath the table (Zhang, Akbari, Yang, Mohanty, & Hirschi, 2011). The table includes a vibrating mechanism and a hanging support mechanism.

The deck is suspended at an angle, is lined with riffles on the surface, and can be moved in a longitudinal or lateral direction (Akbari et al., 2012). The particles on the table are separated by density, with the air flowing upwards causing fluidization and gravity weighing down the solid particles. The output consists of three streams: the clean coal, middlings, and refuse.

The combination of vibration and air bubbles results in a pseudo-fluid-like medium that separates the particles based on their specific densities (Z. Luo et al., 2008). The flow pattern inside an FGX table is similar to a helix or spiral (Zhang et al., 2011) as the material moves along the bed. The particles experience a stratifying force while on the separating deck: they are pushed up due to the fluidizing force created by the air, or downward by the pulling force due to gravity.

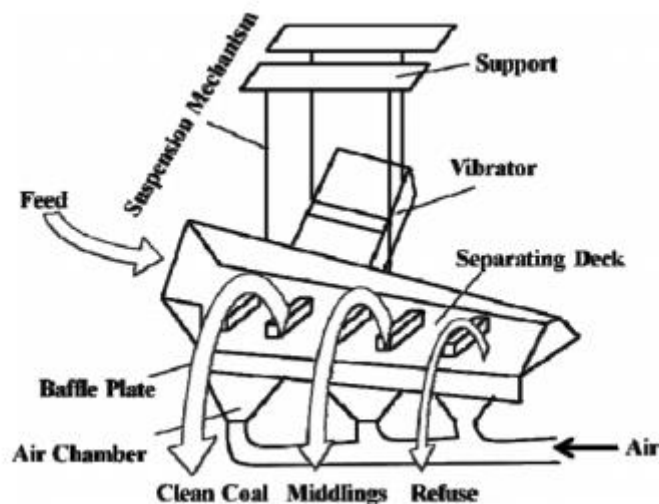


Figure 9: Schematic diagram of FGX dry separator showing the different products (Zhang et al., 2011)

The vibrating fluidized bed was created to separate dry fine coal particles from gangue material with the use of gas moving through the bed (Z. Luo et al., 2008). The fluidized gas bed is suited for coarse coal (6 to 50 mm). Coal particles smaller than 6 mm are not efficiently beneficiated with an FGX bed separator.

Different parameters affect the efficiency of the FGX dry separator. The first parameter is the feeder frequency and the deck vibration frequency (measured in hertz, Hz) (Akbari et al., 2012). The position of the clean coal splitter is important to separate the clean coal from the middlings, as well as the position of the refuse stream splitter. A

clean coal air flow valve can be adjusted to control the fluidization air flow rate. The angles of both the longitudinal and lateral decks can be adjusted as needed for the feed material.

2.4.2. X-ray transmission

XRT is a method of separation that is based on the surface characteristics and physical size of particles (Von Ketelhodt & Bergmann, 2010). Separation is achieved by applying an electrical X-ray source to the sorter feed material. The feed moves past the scanner while X-rays penetrate the material. The scans are then converted into digital image data. The data are used to evaluate the shape, size, texture, and inclusions in the material (Von Ketelhodt & Bergmann, 2010). The data are used to determine if each particle meets a predefined criteria (Robben, De Korte, Wotruba, & Robben, 2014). Based on the criteria, an array of high-speed air valves ejects the selected particles from the feed (Figure 10). Depending on the type of feed, either the discard or product is ejected. If there is more discard in the feed, it would be more economical to eject the product; if there is more product in the feed, it will be more economic to eject the discard. Using the appropriate method can reduce operating costs by reducing compressed air consumption.

The top and bottom sizes of the material need to be small enough to ensure that the air blasts can effectively separate the material (Robben et al., 2014). The feed must also have a clear minimum undersize in order to be operationally stable. Typical sizes of the material can be grouped as 20–30 mm, 30–60 mm, and 60–100 mm.

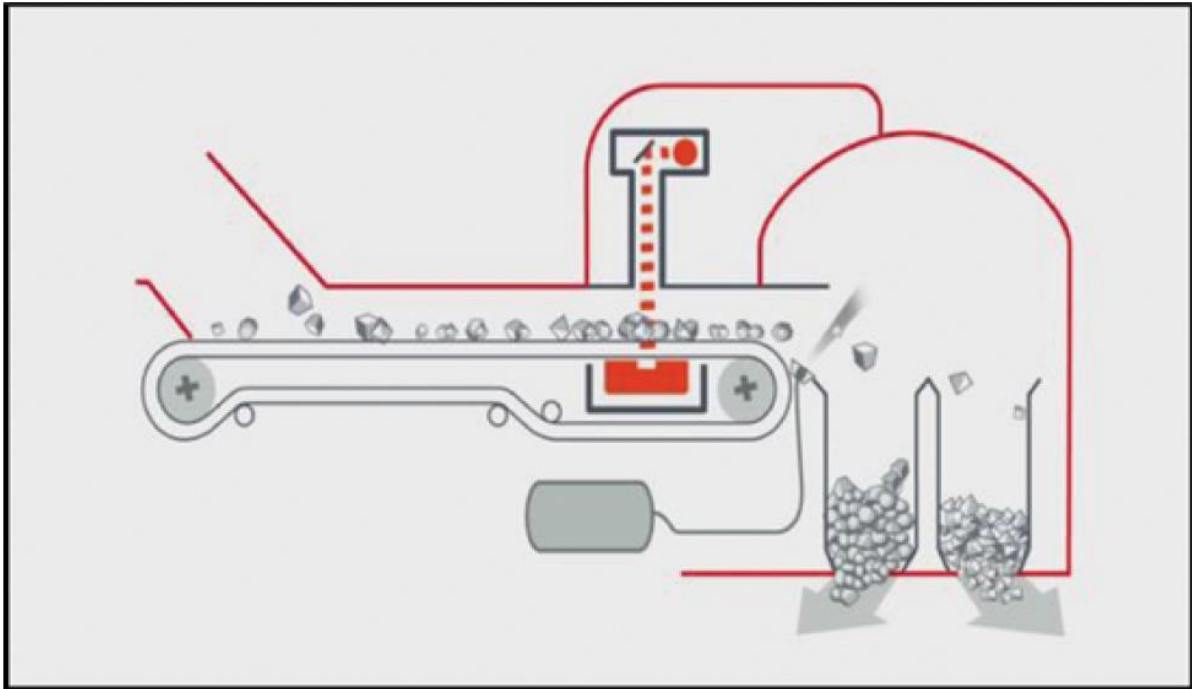


Figure 10: A belt sorter using X-ray transmission technology (Robben et al., 2014)

2.4.3. Air jigs

Similar to the methods described above, air jigs are based on separating material using an air flow. Air jigs were the historically preferred method of dry separation (Weinstein & Snoby, 2007). With significant improvement in modern-day air jigs, this technology is no longer limited to the recovery of coal, but can also be used in the separation of waste material (Ambrós, Cazacliu, & Sampaio, 2016). Unfortunately, the separation efficiency of the air jig is lower than that of water jigs, but it is more economic and environmentally friendly (Ambrós, Sampaio, Cazacliu, Miltzarek, & Miranda, 2017).

Stratification in a jig takes place due to repeated pulses (of air or water) moving through the particles (Figure 11). Once the pulsating action ends, the particles settle under the force of gravity (Gupta & Yan, 2016). The bed expands as the air or water moves through the particles and the bed contracts when the air or water stops. With the pulsating motion, heavier particles deport to the bottom and lighter particles settle on top. The pulsating action is repeated until the stratification is complete. It can take up to 300 cycles per minute of pulsation to achieve stratification.

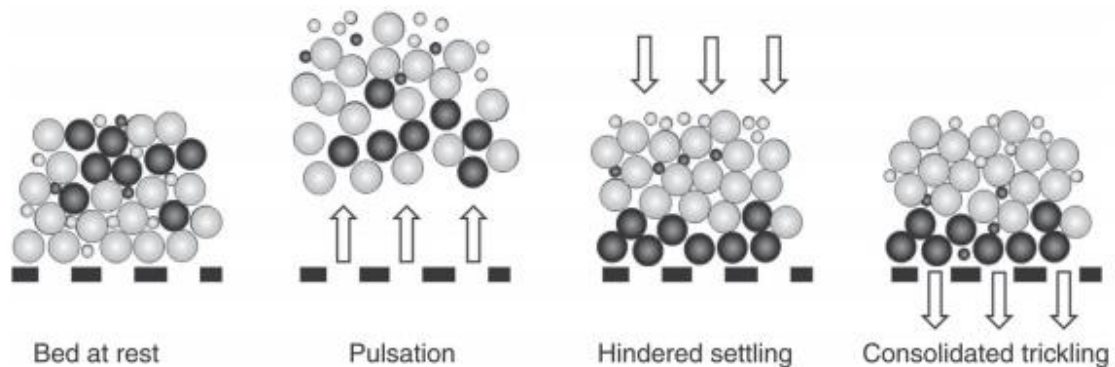


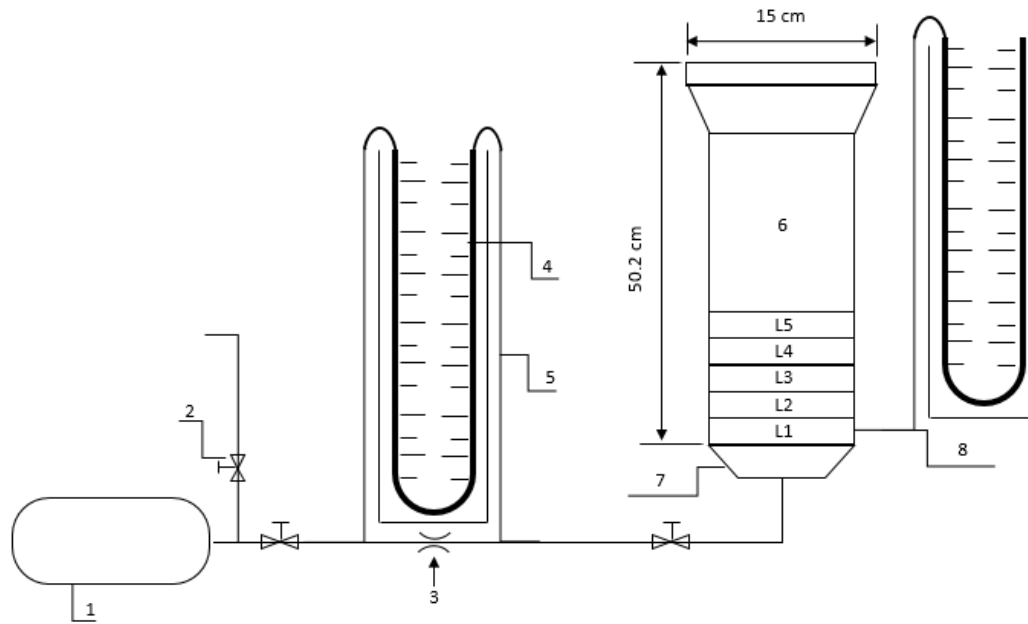
Figure 11: Expansion and contraction of a bed of particles due to jiggling action (Gupta & Yan, 2016)

In this test work, the FGS, XRT, and air jigs were not used: the test work was based on the Bohou method that employs an air dense medium fluidized bed (ADMFB). Although all three methods show promise for the dry beneficiation of coal, each with unique characteristics, the ADMFB was used to better understand the Bohou process.

2.5. Air dense medium fluidized bed

Clean Coal Technology (CCT) was developed to address environmental issues regarding coal and its processing (Robl et al., 2017). CCTs focus on reducing sulfur production that causes acid rain and the reduction of nitrogen oxide gases.

Fluidized-bed combustion (FBC) technology was created to reduce and control the emissions of nitrogen and sulfur (Kim, Amouzegar, & Ao, 2015). Gas is passed through a bed of particles, causing motion: the resulting phenomenon is called fluidization (Peng, Moghtaderi, & Doroodchi, 2017). The resulting fluid-like medium has many properties and characteristics of a normal fluid, including the ability to free-flow under gravity (Figure 12).



1. Compressed air; 2. Air bleed valve; 3. Orifice; 4. U-type manometer; 5. Pipe connector; 6. Perspex fluidised bed; 7. Distributor; 8. Bed pressure drop

Figure 12: Schematic air dense medium fluidized bed (CSIR, Pretoria)

The particles act as a fluid as the gas passes through them, with the fluid flow depending on the particle size and rate of the gas flow (Peng et al., 2017). When the gas flow is slow, it simply moves through the gaps in the particles. As the gas flow is increased, larger particles start to rearrange themselves to accommodate the flow. As the gas flow increases further, the particles are thrown into a state of turbulent motion as the gas moves through, causing density separation. When upper part of the bed is tipped, the upper surface remains relatively horizontal and the bed can be assumed to be a heterogeneous mixture of the fluid and solids (Mohanta, Rao, Daram, Chakraborty, & Meikap, 2013).

The fluidized bed uses gravity to separate the coal from the ash and other unwanted minerals (Robl et al., 2017). Thus, an object with a lower density than the bed will float to the top of the bed and an object with a higher density will sink to the bottom of the bed (Peng et al., 2017). Owing to the flexibility of changing the bed density, objects with different densities compared with that of the bed can be made to sink or float. The contact of the coal particles with the fluidization medium is significantly greater when compared with that of other packed beds (Peng et al., 2017).

The ADMFB is an alternative approach to the dry beneficiation of coal (Mohanta et al., 2013), as shown in Figure 13. The configuration of the fluidized bed, the feed characteristics, and the operating conditions play a significant part in the effectiveness of the ADMFB. The first ADMFB was described in 1926 by T. Fraser and H.F. Yancey (Fraser & Yancey, 1925). It used river sand as the fluidizing medium to separate the coal. A feed size of the coal of -50 mm to +10 mm was proposed and the bulk density of the fluidizing medium was 1.45 g/cm³ (Mohanta et al., 2013). However, the first ADMFB was not tested on a pilot or commercial scale.

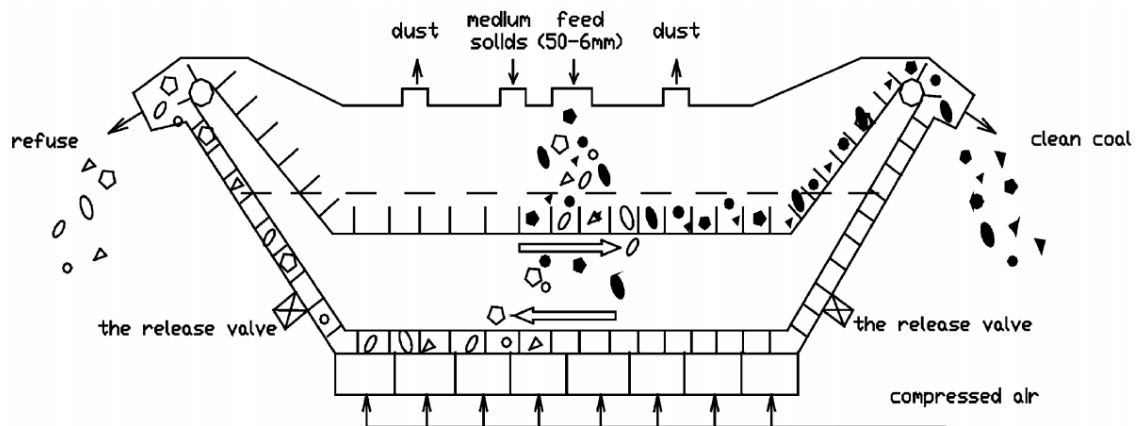


Figure 13: Schematic diagram of a dry separator with air dense medium fluidized beds (Zhenfu & Qingru, 2001)

Experiments carried out using the fluidized bed in the 1970s to test continuous flow conditions used different ratios of a mixture of magnetite and sand particles for the medium (Lohn, 1971). Additional test work was done by H.N. Asthana and S. Sarkar in 1969 and A.W. Deurbrouck in 1979 (Asthana & Sarkar, 1969; Weintraub, Deurbrouck, & Thomas, 1979). These authors suggested that the density of the medium should be formed using magnetite with a range of 1.7 to 2.2 g/cm³ and sand with a range of 1.2 to 1.4 g/cm³. A mixture of both sand and magnetite could be used to make up the densities for the intermediate ranges.

Additional work done by E. Douglas in 1966 combined the effect of fluidization with the effects of the vibrating table (Douglas & Walsh, 1966). The resulting bed contained an inclined vibrating channel with a porous base that was filled with dry sand. The improved bed was found to effectively treat a feed size between 0.7 mm and 75 mm with adjustment of the operating techniques (Mohanta et al., 2013). Figure 14 indicates

the variables that can affect ADMFB performance. Three important factors need to be considered: namely, the feed characteristics, the bed stability, and the operating conditions.

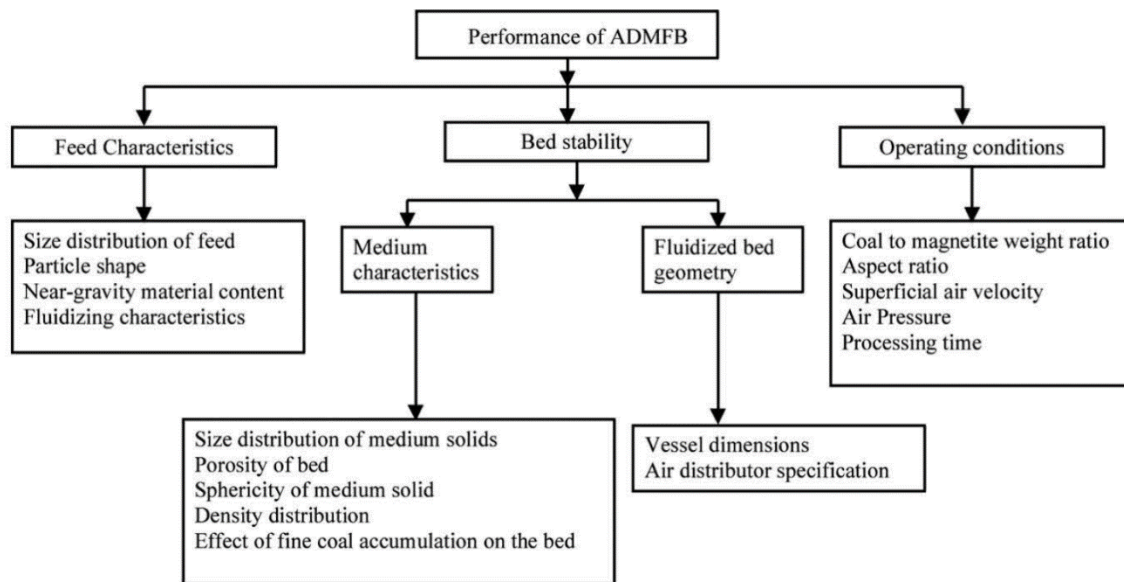


Figure 14: Schematic diagram illustrating the performance indicators and variables that affect ADMFB performance (Mohanta et al., 2013)

Work on dry beneficiation technologies started in 1967 in China (Chen & Yang, 2003). A pneumatic separator was originally designed, but was later discontinued due to low beneficiation efficiency and dust pollution. The Mineral Processing Research Centre at the China University of Mining and Technology (CUMT) started with dry coal beneficiation technology and the ADMFB research in 1984. The first ADMFB used an air–solid suspension as a medium. An improved ADMFB that was used in coal beneficiation was developed by CUMT in 2003 (Chen & Yang, 2003). A working plant has been operating at the Qitaihe Coal Company since 1994. The plant has dimensions of 5000 mm × 2000 mm × 350 mm, a capacity of 50 t/h, and a beneficiation size of 6 mm to 50 mm of coal. The fluidizing medium is composed of 0.15 mm to 3 mm magnetite (Mohanta et al., 2013). Additional improvements have been made to accommodate coal larger than 50 mm by using a deeper fluidized bed (Chen & Yang, 2003).

Continual work has been done on the ADMFB to improve the beneficiation process. The fluidizing quality of the medium solids was improved during beneficiation of fine coal by applying a vibration energy to the ADMFB. A magnetically stabilized fluidized bed was developed for fine coal (1 mm to 6 mm) (Fan, Chen, Zhao, & Luo, 2001). Further work by L. Wei allowed for a dual-density bed that produced three different product densities (Wei, Chen, & Zhao, 2003).

Additional work on the ADMFB has been carried out by the University of Pretoria, North-West University, and the University of the Witwatersrand. The University of Pretoria evaluated the use of ilmenite as a possible medium in an ADMFB (Kalenda, 2017). This was found to be a viable medium for use as an alternative to magnetite in the extraction of coal.

Evaluation of alternative solid media for coal beneficiation using an ADMFB was carried out at the University of the Witwatersrand (Chagwedera, Bada, & Falcon, 2018). The study used magnetite, pyrrhotite, silica sand, granulated blast furnace slag, and coal discards. The study found that pyrrhotite was the best replacement for magnetite, with the ideal replacement being a mixture of 40% pyrrhotite and 60% magnetite.

Work at North-West University on destoning of fine coal in a fluidized bed looked at the possibility of using an ADMFB for particles that are less than 2 mm (Le Roux, Campbell, & Langner, 2016). The study evaluated the bed with and without additional vibration, as well as using different media (magnetite, sand, and fine coal discards). It was found that the results were skewed due to particle size owing to particle-to-medium adhesion.

The dry beneficiation of duff coal was investigated using a dense medium fluidised bed (DMFB) to remove impurities from the duff coal (-5.6 mm to +0.5 mm) using magnetite, sand, and fine discard coal as media (Langner, 2016) (North-West University). Although magnetite did segregate the coal particles, it did not improve the overall destoning of the bed. It proved difficult to remove the magnetite from the coal, whereas sand proved to have better separation efficiency.

A study of fluidized-bed dry dense medium coal beneficiation (North, Engelbrecht, Oboirien Bilainu, De la Rey, & Mashinini, 2017), University of Pretoria, investigated if separation of solid particles by density was possible with a fluidized bed and if the medium affected the observed split in the densities of the bed. The media used were magnetite, sand, and ilmenite. The study found that magnetite needed to be demagnetized in order to achieve fluidization. Further investigation into magnetite as a medium was recommended.

The use of magnetite as a medium for an ADMFB has been evaluated by numerous people and academic institutions. From the above-mentioned research, it is evident that magnetite has the possibility to be a viable medium for the ADMFB.

2.6. Magnetite in South Africa

2.6.1. A history of magnetite in South Africa

The Palabora Igneous Complex (PIC), shown in Figure 15, formed around 2 billion years ago (Lurie, 1977). The complex was formed when carbonate-rich magma intruded into the granitic country rock. The intrusion occurred in several stages, creating pipe-like structures that were concentrically arranged around the intrusions. The early intrusions mainly consisted of pyroxenite, syenite, and carbonatite. Later intrusions were rich in syenite. Copper mineralization occurred due to ascending fluids (Solovova, Ryabchikov, Kogarko, & Kononkova, 1998).

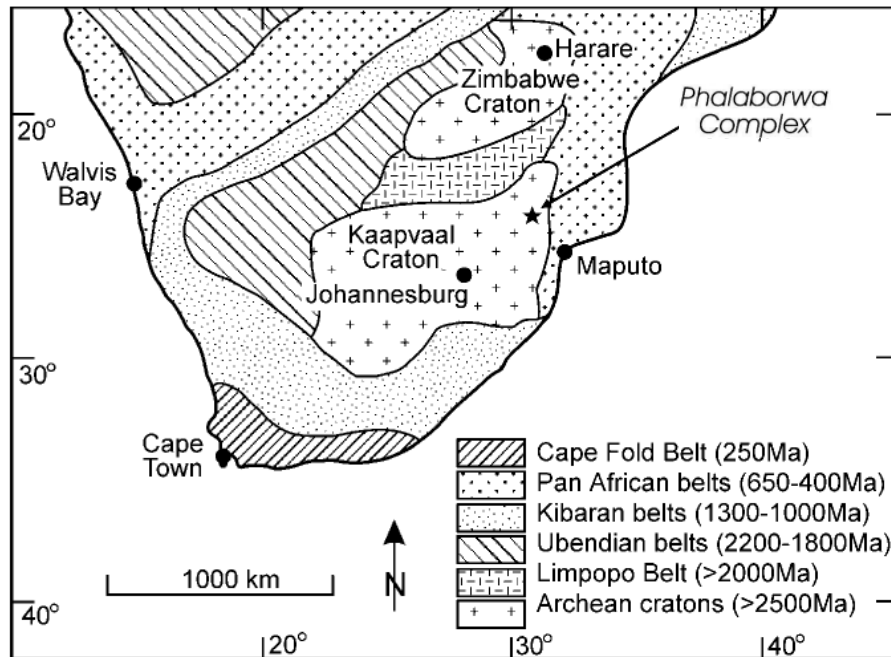


Figure 15: The Palabora Complex in South Africa (Groves & Vielreicher, 2001)

The PIC is unique because it is the only carbonatite-hosted copper deposit in the world that is economically viable (Wilson & Anhaeusser, 1998a). More than fifty different minerals have been found in the PIC (Wilson & Anhaeusser, 1998b). The inner part of the PIC contains foskorite and carbonatite, both of which contain magnetite (Southwood & Cairncross, 2017). The foskorite and carbonatite rocks host copper sulfides, which are mined at Phalaborwa, as well as apatite and magnetite (Figure 16). Foskorite contains roughly 30% magnetite by mass (Wilson & Anhaeusser, 1998b), but can vary up to a magnetite content of 50%. The carbonatites contain roughly 20% magnetite, but can reach up to 30% magnetite. The titania content of the magnetite can be as low as 1% in the carbonatite and as high as 8% in the foskorite.

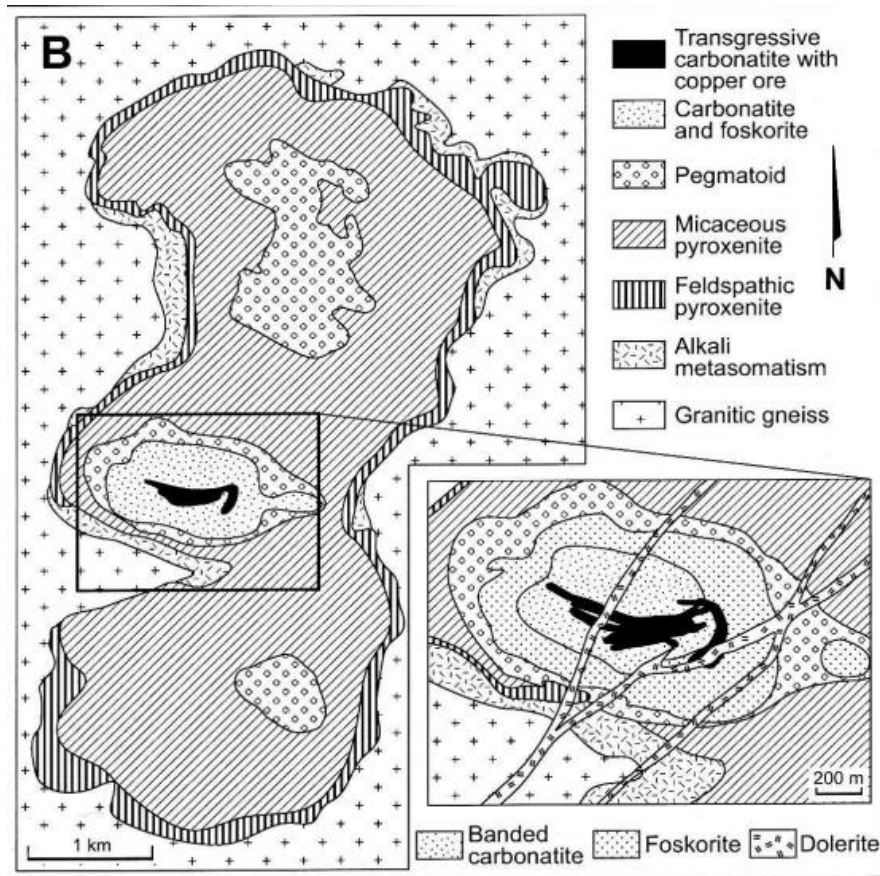


Figure 16: Geology of the Palabora Igneous Complex (Vielreicher, Groves, & Vielreicher, 2000)

Another magnetite deposit occurs at Vergenoeg, which is part of the Bushveld Complex (Borrok, Kelsner, Boer, & Essene, 1998). The intrusion (which cuts through the Rooiberg Group) comprises fluorite, apatite, ilmenite, and magnetite. The complex was formed due to felsic magma interacting with hydrothermal solutions. The bulk of the magnetite did not form in the early stages, but in later alterations while replacing fayalite. The highest concentration of magnetite is found in the upper part of the Vergenoeg deposit. Magnetite is commonly found with a hematite coating. Figure 17 displays the location of iron deposits found in South Africa.

Another source of magnetite is found in the Merensky Reef of the Bushveld Complex (Harney, Merkle, & Von Gruenewaldt, 1990). Magnetite is found in the Upper Zone of the Bushveld Complex (Johnson et al., 2006). The zone contains 24 magnetite layers, with the thickest being up to 6 m and the smallest being just a couple of millimetres thick. Magnetite makes up to 8% of the volume of the Upper Zone. Towards the top of

the Upper Zone, the magnetite changes into high-titanium magnetite, and further on into ilmenite.

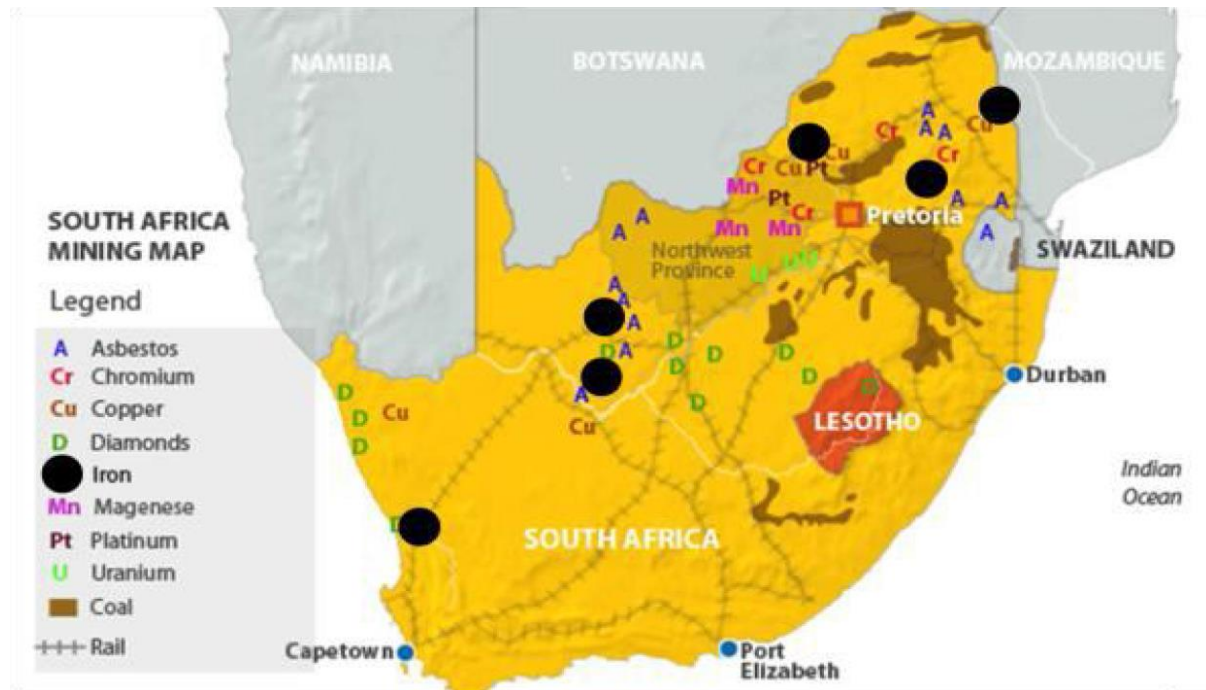


Figure 17: South Africa's iron deposits (Utembe, Faustman, Matatiele, & Gulumian, 2015)

2.6.2. A history of the recovery of magnetite in South Africa

Historical research indicates that metal mining in South Africa started as early as the ninth century (Van der Merwe & Scully, 1971). Archaeological evidence indicates that South Africa has a long history with iron ore. The site at Lolwe (Loolekop) in Phalaborwa contained mineshafts and galleries (Eriksson, 1989). It is estimated that roughly 10 000 tonnes of ore-containing rock was removed from Lolwe. The ore was mainly copper deposits consisting of malachite and azurite (Van der Merwe & Scully, 1971). Magnetite pebbles were found freely available on the surface level, with the pebbles small enough to be easily carried away. The original mining technique involved warming up the rocks with fire and then driving gad and chisels into the rock with hammer stones.

Modern-day mining started as early as the 1930s to remove apatite and vermiculite from the PIC (Southwood & Cairncross, 2017). Palabora Mining Company (PMC) started in 1956 to develop the area for the removal of low-grade copper from the surrounding carbonatite and foskorite rocks. The large-scale open-cast copper mine

started in 1965 (Basson et al., 2017). The open-cast mine was later followed by underground block carving in 2003. Block carving is widely used in underground mining by collapsing the ore into the empty cavities underneath. Palabora Copper produces medium- and coarse-grade magnetite.

The magnetite is crushed, milled, and put through a flotation process with the copper ore (Surmon, 2019). The magnetite is recovered from the copper flotation tailings by magnetic separation. The magnetite is prepared by de-sliming of the tailings from the copper flotation. The fine non-magnetic fraction is removed in a hydro-separator. The magnetite has an iron content of between 60% and 65%. The magnetite is then either re-ground to upgrade the magnetite to an iron content of 67% or pumped into storage dams.

The magnetite has been sold as fines to the coal washing industry. Magnetite is used as a heavy medium in coal washing due to its high specific gravity when compared with that of coal (Dey, Mishra, Dutta, & Tiwary, 1997), as well as its lower viscosity and abundance. It is predicted that as much as 197 Mt of magnetite has been removed from the open pit mine at Loolekop. It has been suggested that magnetite recovery will continue until 2040 (Surmon, 2019).

The mine was sold in 2013 to a consortium that comprised the Industrial Development Corporation of South Africa and China's Hebei Iron and Steel Group (Southwood & Cairncross, 2017). The sale led to the renaming of the mine as Palabora Copper (Pty.) Ltd.

2.6.3. Surface properties of magnetite

Magnetite is a black mineral that is commonly found in igneous rocks (Klein, Dutrow, Dana, & Klein, 2002). The crystal shape is most commonly octahedral, as shown in Figure 18, with sharp pointed edges.

Magnetite is a hydrophilic mineral (Tang et al., 2018). Hydrophobicity represents the ability of water molecules to penetrate the interior of a material (Drzymala, 1994). A solid material is hydrophobic when a water drop does not spread over the solid material, but remains a droplet. A contact angle can be measured from the water droplet to indicate the hydrophobicity. Table 1 (Drzymala, 2007) indicates the

hydrophobicity of different minerals. It can be seen that magnetite is hydrophilic with a contact angle of 0°.

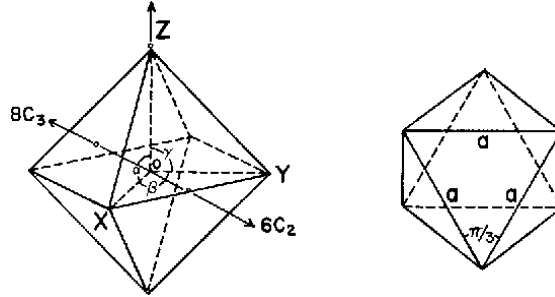


Figure 18: Rotation symmetries and equilateral crystal faces of an octahedral crystal (Ootaki & Wolken, 1973)

Table 1: Hydrophobicity of materials (Drzymala, 2007)

| Strongly hydrophobic* | | Hydrophobic | | Weakly Hydrophobic | | Hydrophilic** = 0 |
|---------------------------|------|-------------------------------|-----------|--------------------------|-------|--------------------------------|
| Material | | Material | | Material | | Material |
| 1 | 2 | 3 | 4 | 5 | 6 | 7 |
| Paraffin C_nH_{2n+2} | 90+ | Sulfides | 44–0 | Fluorite, CaF_2 | 10–13 | Gypsum $CaSO_4 \cdot 2H_2O$ |
| Teflon, C_2F_4 | 90+ | Silicon carbide SiC | 27.6 | Arsenic, As_2O_3 | 9.3 | Ferrosilicon |
| Sulfur, S | 63.2 | Coal | 26–0 | Perovskite, $CaTiO_3$ | 9 | Dolomite $CaMg(CO_3)_2$ |
| Mercury, Hg | 45.6 | Indium, In | 25 | Scheelite, $CaWO_4$ | 9 | Magnetite Fe_3O_4 |
| Ge | 39.7 | Jodargyrite, AgI | 23.5 | Diamond, C | 7.9 | Halite, NaCl |
| Si | 35.4 | Cassiterite, SnO_2 | 22– | Tin, Sn | 7.5 | Brown coal |
| Talc | 35.2 | Silver, Ag | 14 | Boric acid, H_3BO_3 | 6.4 | Kaolinite |
| | | Ilmenite, $FeTiO_3$ | 14 | Graphite, C | 6.2+ | Hematite, Fe_2O_3 |
| | | Molybdenite, MoS_2 | 5.9+ | PbJ_2 | 6 | Quartz, SiO_2 |
| | | | | Gold, Au | 5 | Calcite, $CaCO_3$ |
| | | | | Barite, $BaSO_4$ | 5 | Anhydrite, $CaSO_4$ |
| | | | | Corundum, Al_2O_3 | 4 | Bones |
| | | | | HgO | 3.3 | Tourmaline |
| | | | | HgJ_2 | 3 | Vegetables |
| | | | | Copper, Cu | 3 | Iron, Fe |
| | | | | | | Amber |
| | | | | | | Ice, D_2O |

* Flotometric method can measure contact angles in degree smaller than 90°.

** Other hydrophilic materials: chromite, malachite, smithsonite, azurite, rutile, zircon, mica.

2.7. High-titanium magnetite in South Africa

High-titanium magnetite is found in the Upper Zone of the Bushveld Complex (Klemm, Snethlage, Dehm, Henckel, & Schmidt-Thome, 1982) in massive layers. The magnetite found in the Upper Zone is enriched in Ti, Mg, Al, and Si (Klemm, Henckel, Dehm, & Von Gruenewaldt, 1985). The high-titanium layers are found between cumulus-magnetite and olivine gabbro layers. The high-titanium layers are of economic importance due to the contained tin, vanadium, and iron (Sachkov et al., 2018). As high as 2.3% V_2O_5 can be found in the high-titanium magnetite layers, whereas the main magnetite layer only contains about 1.6% V_2O_5 . Additional high-titanium magnetite is found in the Vergenoeg deposit of the Bushveld Complex (Borrok et al., 1998). The pipe-shaped complex cuts through the Rooiberg rhyolites. High-titanium magnetite is found with ilmenite and magnetite in the deposit.

Mining for copper in the PIC results in the mining of by-product high-titanium magnetite (Vielreicher et al., 2000), which occurs in the main mass of foskorite in the complex. The high-titanium magnetite found in the PIC is of lower quality than that found in the Bushveld Complex, and is stockpiled for when it can be used. It is estimated that roughly 26 400 Mt of high-titanium magnetite exists in the Bushveld Complex (Ratshomo, 2014).

High-titanium magnetite is sold as iron ore to be used predominantly in production of steel, vanadium salt, and as a raw material for cast iron (Sachkov et al., 2018).

Another source of high-titanium magnetite is found along the west coast of South Africa (Carelse, 2012). Namakwa Sands is operational in Brand-se-Baai (north of Cape Town). The heavy mineral sands of the area have been of interest since the 1930s when Haughton studied the placer deposits that were found along the west coast of South Africa. The first comprehensive study of the distribution and mineralogy of the heavy mineral deposits was done by Toerien and Groeneveld in 1957 (Coetzee, Toerien, & Groeneveld, 1957). Owing to the discovery of a 35 m-thick heavy-mineral-bearing sand deposit in 1987, the Namakwa Sands Ltd heavy mineral mine was established in 2002. The mine produces mainly ilmenite, zircon, and rutile (Philander & Rozendaal, 2015).

The heavy mineral sand is part of a siliciclastic arenaceous deposit (Philander & Rozendaal, 2015). The siliciclastic deposit is largely made up of quartz and other silicate minerals that have been deposited by streams or other mechanical processes. An arenaceous deposit refers to the particles resembling or being made up of sand. The dunes are classified into east and west areas. The east area is mostly made up of unrelated dune deposits, whereas the west area comprises transitional shallow marine-aeolian environments. The result is a difference in bulk chemistry and mineralogy, and a better heavy-mineral grade and high percentages of the gangue minerals, such as garnets and pyroxenes (Philander & Rozendaal, 2015).

2.8. Magnetic separation

2.8.1. A history of magnetic separation

Magnetite is the most magnetic naturally occurring material found on earth. William Fullarton procured the patent for the separation of iron ore using magnetic attraction in 1792; since then, the field of magnetic separation has grown rapidly (Dean & Davis, 1941). Commercialized magnetic separation became popular in the 1860s for removing iron from brass (Elvers & Ullmann, 1990). In 1895, the Wetherill's magnetic separator was invented. The separator could separate two components that were considered to be non-magnetic. Until then, only coarse and moderately strong magnetic materials could be separated.

A steady improvement in equipment and the range of ores that could be treated began in the early nineteenth century (Svoboda, 2004). High-intensity magnetic separation was inaugurated, which allowed the separation of paramagnetic materials (Elvers & Ullmann, 1990). Further growth came with the development of permanent magnetic materials and the enhancement in their properties. Three main innovations took place to improve the future of magnetism: the first was the use of feeble steel-based magnets; the second improvement came in the 1940s when permanent magnets appeared on the market and were able to compete with the electromagnets already on the market; the third occurred in the 1970s when rare-earth magnets became available. Figure 19 indicates the development of permanent magnetic materials over

time. As materials improved, so did the strength of the magnets.

Another contributing achievement was the introduction of ferromagnetic bodies to the magnetic separator. An important contribution was made by Frantz (1937): a magnetic separator was developed that consisted of an iron-bound solenoid packed with ferromagnetic steel ribbons (Fraas, 1973). The magnetic separator provided the basis for the present-day high-intensity magnetic separators (HIMS). The magnetic separator made it possible to extract weakly magnetic and diamagnetic materials down to microns in size.

Recent research has focussed on eddy-current separators, magnetic fluids, and magnetic carriers (Svoboda, 2004). Renewed research into magnetic separation is due to numerous economic, environmental, and social challenges. The main aims are the recycling of metals from industrial waste and the removal of biological objects in the bio-scientific field.

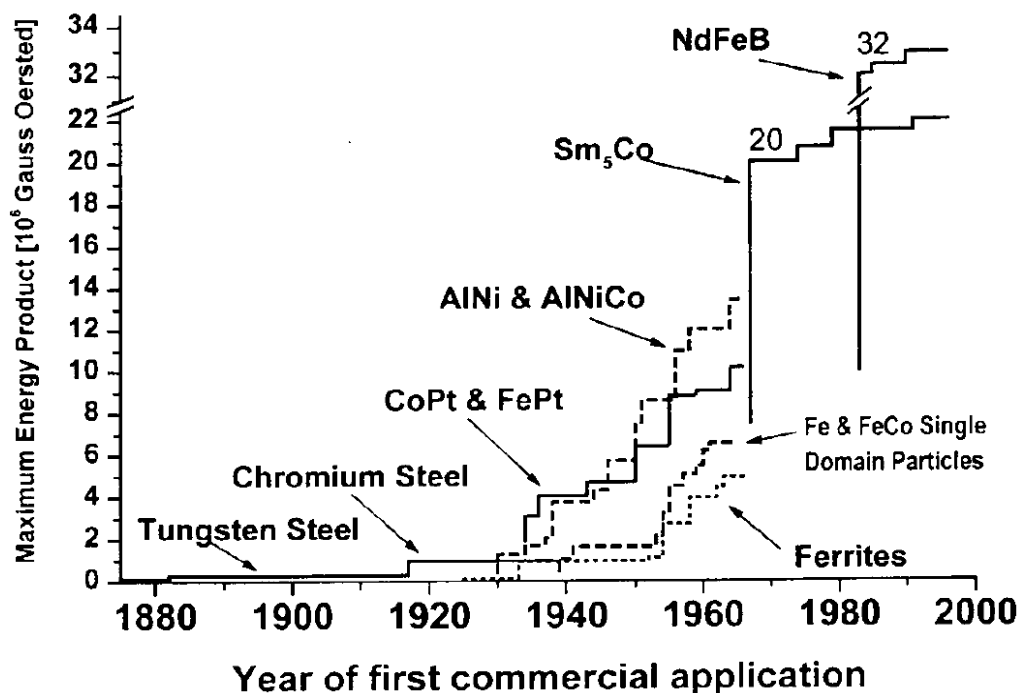


Figure 19: Development of permanent magnet materials (Svoboda, 2004)

Magnetic separation is based on the separation of materials using an external magnetic force (Svoboda, 2004). To remove the material, the magnetic forces need to overcome other competing forces acting on the material. These may include

gravitational, inertial, hydrodynamic, and centrifugal forces. The theory of separation is shown in Figure 20. The feed enters the magnetic separator and is split into two or more compounds. Once the competing forces are overcome, the magnetic material will move with the magnetic forces towards the side and the non-magnetic material will stay on the non-magnetic side. The product that passes through the magnetic field is known as the tails; the product that remains is the magnetic concentrate known as the mags (Parker, 1977). Materials that are in the middlings will be a mixture of the magnetic and non-magnetic materials. Owing to inter-particle forces, such as electromagnetic and electrostatic forces, non-magnetic material is pulled towards the magnetic fraction (Oberteuffer, 1974).

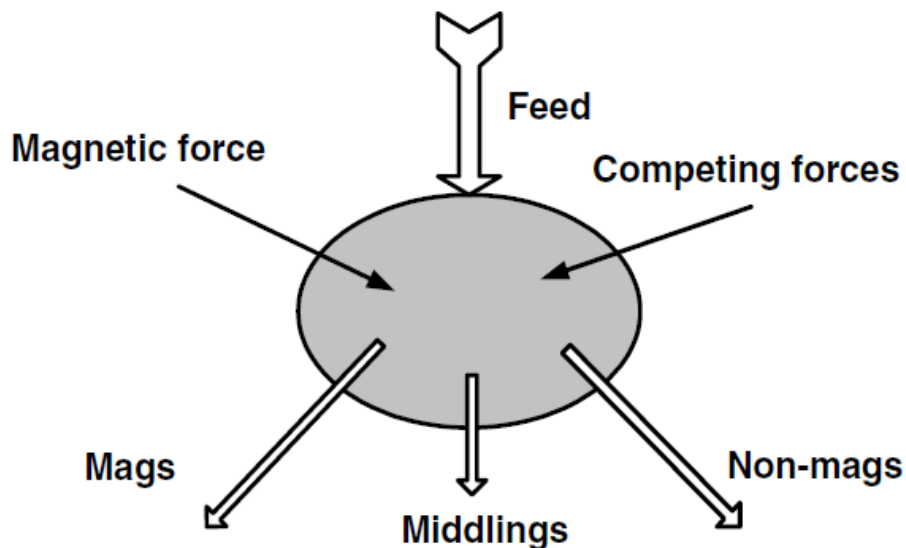


Figure 20: Schematic representation of a magnetic separator (Svoboda, 2004)

The efficiency of a magnetic separator is expressed by the recovery or grade of the magnetic fraction (Oberteuffer, 1974). Recovery is the ratio of magnetic material found in the magnetic fraction compared with that in the original feed; grade refers to the fraction of the magnetic material in the magnetic fraction. Both recovery and grade are used as measurements of the effectiveness of the separation of a magnetic separator.

Magnetic separation can be classified into two general groupings (Oberteuffer, 1974): the first is purification of a feed that contains magnetic components and produces a non-magnetic product; the second is the concentration of the magnetic material to produce a magnetic product.

2.8.2. Magnetic properties of materials

All materials have certain magnetic properties (Svoboda, 2004). Materials can be divided into five categories based on their magnetic properties. These groups are diamagnetic, paramagnetic, ferromagnetic, antiferromagnetic, and ferromagnetic. The last three groups have a higher magnetic susceptibility than those materials in the diamagnetic and paramagnetic groups.

Ferromagnetism is the strongest type of magnetic force (Parker, 1977): the interaction between neighbouring atoms is so strong that the magnetic moments of all the particles align parallel with each other (Figure 21). Ferromagnetic material is used to make permanent magnets that are used in everyday life.

Paramagnetic materials comprise material that is weakly attracted by an externally applied magnetic field, causing internally induced magnetic fields that align with an external magnetic field (Parker, 1977). The effect of a magnetic field on a paramagnetic material is shown in Figure 21.

Diamagnetic materials are repelled by a magnetic field (Parker, 1977). An applied magnetic field creates an induced magnetic field in the opposite direction in a diamagnetic material. The magnetic alignment is thus in the opposite direction to the applied magnetic field, creating a repulsive force, as shown in Figure 21.

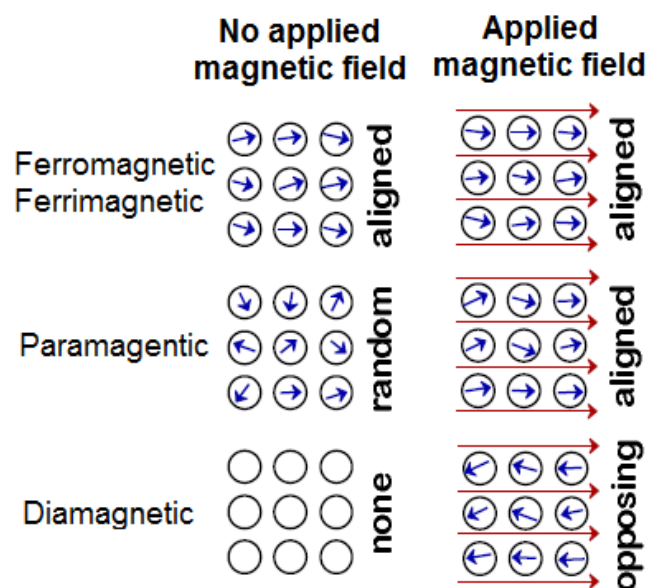


Figure 21: Graphical illustration of ferromagnetic, ferrimagnetic, paramagnetic, and diamagnetic materials (Sinatra, 2010)

Another classification method is to separate materials into three groups: namely, strongly magnetic, weakly magnetic, and non-magnetic materials (Svoboda, 2004). Strongly magnetic material only needs a weak magnetic field to be recovered (Svoboda, 2004). Strongly magnetic materials need a weak field of roughly 0.15 T, with a field gradient of 0.5 T/m. Strongly magnetic materials include iron, magnetite, maghemite, and pyrrhotite.

Weakly magnetic materials need a stronger magnetic field created by magnetic induction to recover the material (Svoboda, 2004). The magnetic induction can be up to 1 T, with a field gradient ranging from 50 to 500 T/m. This group comprises mainly iron and manganese oxides, ilmenite, and wolframite.

Non-magnetic materials cannot be easily recovered using magnetic separation (Svoboda, 2004). This group includes diamagnetic materials, as well as aluminium, rutile, pyrite, and garnets. Owing to developments in magnetic separation, the range of materials that can be treated by magnetic separation is increasing.

Magnetite is a strongly magnetic material with the formula Fe_3O_4 (Svoboda, 2004). It is a ferrimagnetic mineral with two distinct lattices, each magnetized in an opposite direction. The two cations (Fe^{2+} and Fe^{3+}) form distinct layers in the crystal lattice. Magnetite has a density of 5 200 kg/m^3 . It is commonly used in the processing of coal due to its density and easy recovery using magnetic separation. Figure 22 summarises the magnetic susceptibility of different minerals. Magnetite has the highest magnetic susceptibility of the listed minerals due to its highly ferromagnetic properties. Figure 22 also illustrates that materials with a higher percentage of magnetite are more magnetically susceptible.

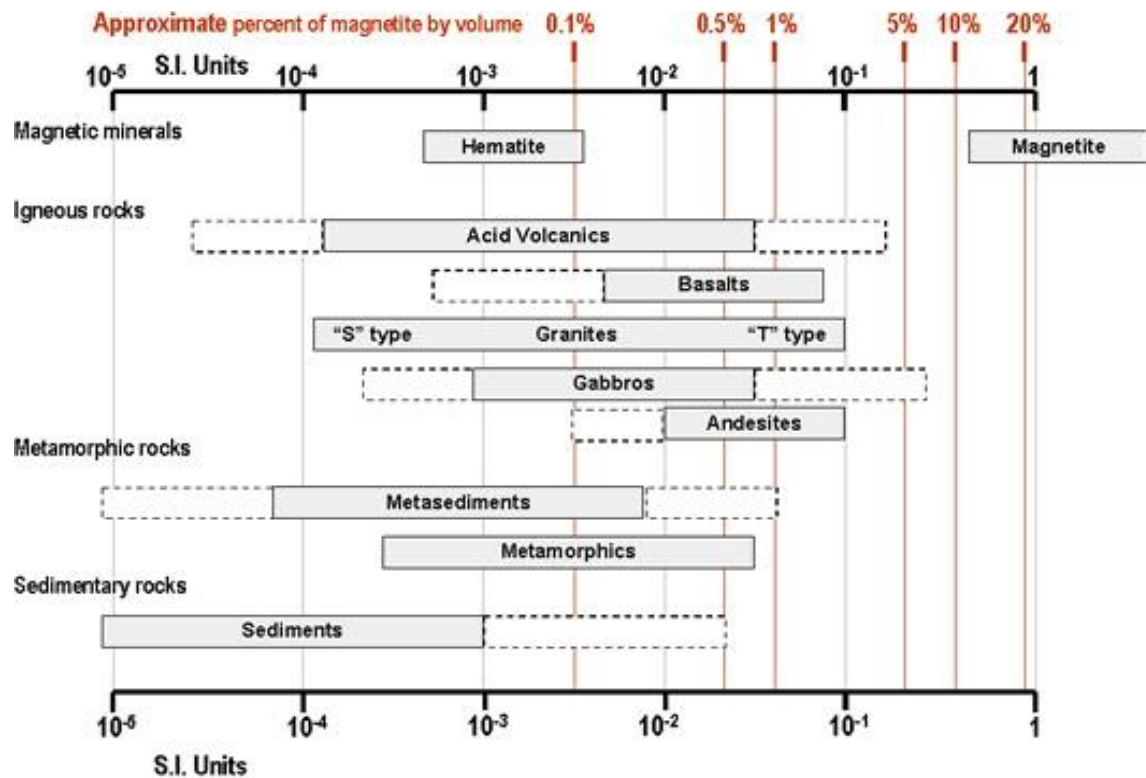


Figure 22: Magnetic susceptibility of common rock types (Clark & Emerson, 1991)

2.8.3. The physics of magnetic separation

An enormous range of devices is used for magnetic separation, with a vast range of applications. Magnetic separation is used in chemical engineering, food and drink manufacturing, the tobacco industry, manufacturing, and in the metal industry (Parker, 1977). A classification system was introduced in 1960 by Devaney. The classification is divided into four groups: low-intensity dry magnetic separation, low-intensity wet magnetic separation, high-intensity dry magnetic separation, and high-intensity wet magnetic separation. The importance of each force is a function of the type of the separator and of the mode in which it operates (Svoboda, 2004).

It is important to remember that the competing forces acting on a particle need to be overcome during magnetic separation (Parker, 1977). As previously mentioned, these include gravitational, inertial, hydrodynamic, and centrifugal forces. The magnetic force, F_m , can be expressed by Equation 1:

$$F_m = \frac{1}{2} \mu_0 (\kappa - \kappa_m) \vartheta \nabla (H^2) \quad (1)$$

where ϑ is the particle volume, κ is the particle susceptibility per unit of volume, κ_m is the susceptibility of the particle-bearing medium. The magnetic field strength, H , is expressible as Equation 2:

$$H = -\nabla V \quad (2)$$

where V is magnetic potential. The success of the separation depends on the relative strengths of the combination of competing forces acting on the particles (Parker, 1977). Further limitations are set by the size of the particles that need to be separated.

2.8.4. Magnetic separators

Magnetic separation can be classified according to a wide range of categories. The categories can be based on the medium that carries the feed (wet or dry), the requirements of the system, how the magnetic field is generated, or the magnitude of the magnetic field and the magnetic gradient (Svoboda, 2004). The two categories that are of importance to this project are the medium and the magnitude of the magnetic field and magnetic gradient. The medium can be either wet or dry, in combination with a low- or high-intensity magnetic field and gradient. The classification is thus split into four groups; namely, wet low-intensity magnetic separation, wet high-intensity magnetic separation, dry low-intensity magnetic separation, and dry high intensity magnetic separation.

The most common wet LIMS is the drum separator (Svoboda, 2004). It is generally used to recover ferromagnetic solids from a slurry feed. The magnetic drum separator is most commonly used for the recovery of the media in DMS plants and in the beneficiation of magnetite ores.

The drum is constructed in such a way that it is partially submerged in water (Svoboda, 2004). The material is carried through the magnetic system while the magnetic material is removed from the tank. The feed ranges in size between 20 μm and 6 mm. The construction of the drum is determined by the objective of the separation process.

The three most common designs are concurrent (A), counter-rotation (B), and counter current (C), as shown in Figure 23.

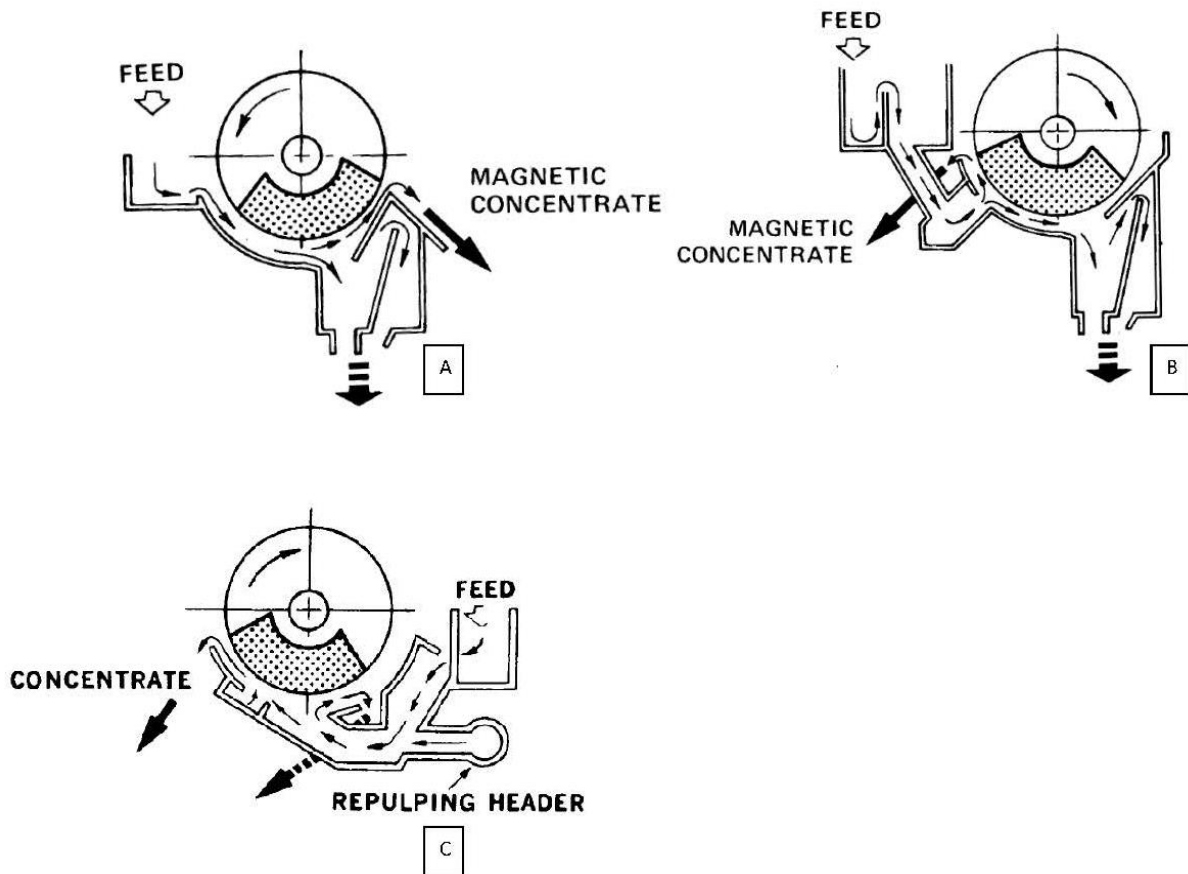


Figure 23: Different types of wet low-intensity drum magnetic separators (Svoboda, 2004)

A concurrent tank is shown in Figure 23A. The feed is introduced through a feed box (Svoboda, 2004). The flow direction is the same as that of the drum rotation. The tailings are discharged through an opening at the bottom, while the mags are picked up by the magnet in the drum and pass through an opening between the drum shell and the tank wall.

In the counter-rotation tank (Figure 23B), the feed is introduced through a special feed box on the side of the tank (Svoboda, 2004). The feed is introduced in the opposite direction to the drum rotation. Owing to the difference in direction, the magnetic material is removed almost immediately, whereas the tailings are free to flow along the base of the drum and through the opening at the bottom.

In the counter-current tank, shown in Figure 23C, the tailings flow counter to the rotation of the drum when leaving the tank (Svoboda, 2004). The feed enters through the bottom of the tank and is pushed up using wash water jets. The tailings are removed at the opposite side of the tank when the slurry overflows.

Further work was done to create HIMS for weakly magnetic material (Norrgran & Orlich, 1988). HIMS were produced to work with a wet or a dry medium. The dry separators have a magnetized rotor where the magnetic force opposes the gravitational and centrifugal forces inside the separator, whereas the wet high-intensity magnetic separator (WHIMS) uses a matrix that is magnetized by an externally produced magnetic field.

Owing to the approximate gauss range of magnetite (1000 Gs) and its strong magnetic attraction, low-intensity magnetic separation is needed for the removal of magnetite (Norrgran & Orlich, 1988). Dry low-intensity magnetic separation is most commonly used for the removal of tramp iron, improving the concentration of strongly magnetic iron minerals, and the recovery of iron from blast furnaces and steel mill slags (Svoboda, 2004).

2.8.5. Dry magnetic separation

Different types of dry low-intensity separators exist; namely, magnetic pulleys, plate magnets, grate magnets, suspended magnets, and drum magnetic separators (Svoboda, 2004). The drum magnetic separator is most widely used of the dry magnetic separators. It uses a permanent ferrite magnetic roller and can treat particle sizes from a few centimetres to several microns. The general design for all drum magnetic separators is the same, with the magnet being stationary within a rotating belt.

On larger drum magnetic separators, the magnets are arranged in three to nine magnetic blocks (Svoboda, 2004). The magnets are arranged so that the blocks are of alternating polarity, covering an angle between 90° and 120°, as shown in Figure 24. The alternating polarity of the magnets is suitable for the removal of tramp iron and the concentration of coarse particles.

There is a variety in diameter and width in the production of drum magnetic separators (Svoboda, 2004). Ferrite drum diameters are usually bigger (ranging from 600 mm to 1500 mm) than those of rare-earth drums (380 to 1000 mm).

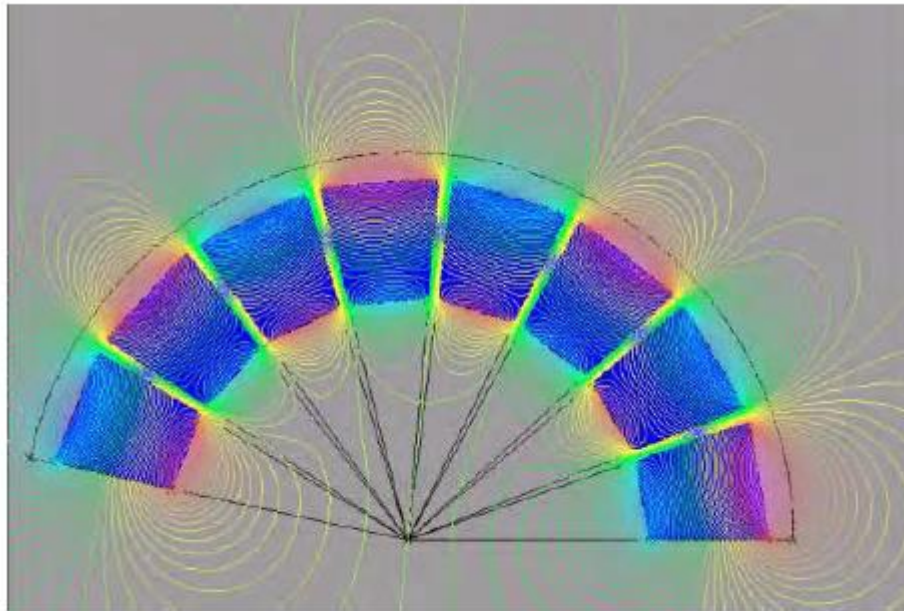


Figure 24: Pattern of the magnetic field around a magnetic drum (Svoboda, 2004)

The most common type of drum magnetic separator is fed from the top, as shown in Figure 25, but a drum magnetic separator can also be fed from the bottom (Svoboda, 2004). As the feed falls onto the drum, the nonmagnetic material leaves the drum at the bottom, while the magnetic material stays attached to the drum and is carried by the magnetic field until it leaves the drum. It has been stated that a drum magnetic separator with a top feed will produce the highest magnetic removal, as well as removal of materials with small amounts of magnetic material (Svoboda, 2004).

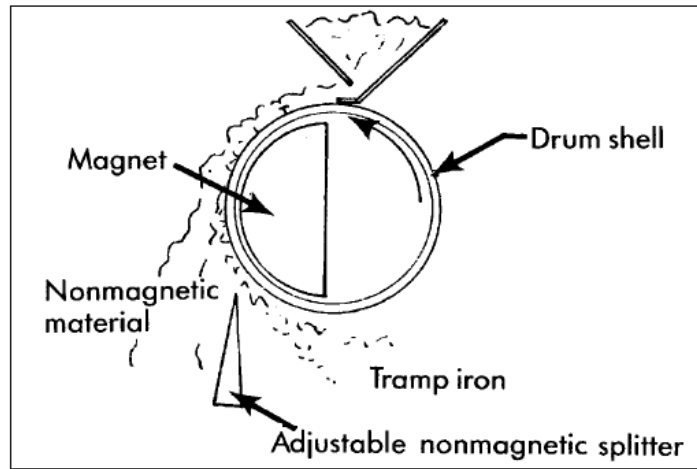


Figure 25: Dry drum magnetic separator with top feed (Svoboda, 2004)

D. M. Hopstock (1975) derived the equation shown in Equation 3 (Svoboda, 2004) for the radial and azimuthal magnetic forces in a drum separator:

$$B_r = B_0 \cos\left(\pi \frac{\theta}{\theta_0}\right) \exp\left(\frac{-\pi(r - R)}{\theta_0 R}\right) \quad (3)$$

where B_r is the remnant magnetic induction, B_0 is the magnetic induction on the surface of the drum, θ is the azimuthal component of the magnetic induction, r is the radius vector, and R is the radius (Figure 26). This equation was found to be a good fit to experimental data from a number of different magnetic configurations (Svoboda, 2004).

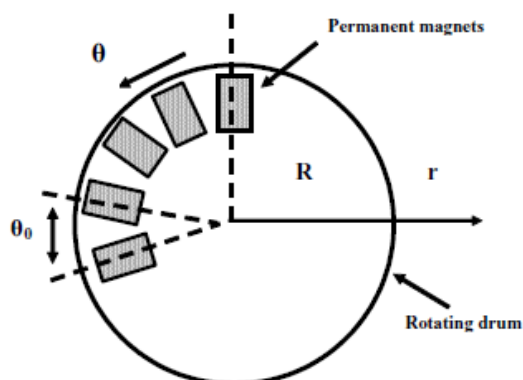


Figure 26: Arrangement of magnetic poles in a drum magnetic separator (Svoboda, 2004)

2.9. Conclusion

At the end of this chapter, there should be a clear understanding of the properties of magnetite and the properties of magnetic separation. This chapter includes a thorough investigation into coal and magnetite in South Africa. Emphasis was placed on the production and reserves of coal and magnetite deposits found in South Africa.

South Africa has a long history with coal. The first coal mine opened in 1864 in Molteno in the Eastern Cape. Shortly thereafter, coal was discovered in Mpumalanga, Natal, and parts of Gauteng. The development of the national rail system led to an increase of coal production in South Africa and new methods of coal production.

Coal is upgraded by regulating its size and by reducing the mineral matter content. The coal goes through classification and crushing, cleaning and washing, and dewatering to be upgraded. The most common ways to clean coal use forms of gravity separation, such as jigs, cyclones, and spirals.

China has created a new method of dry beneficiation that uses an ADMFB, in which coal is passed through an air dense fluidized bed that uses magnetite as the density medium. As the coal passes through the bed, gangue material is removed and discarded while clean coal is recovered.

Magnetite has been used in South Africa as early as the ninth century. The Palabora Igneous Complex at Lolwe (Phalaborwa) and the Vergenoeg Formation and Merensky Reef, which are part of the Bushveld Complex, contain magnetite that is a by-product of current mining activities.

Owing to the abundance of magnetite in South Africa and the need for clean coal technologies, it is logical to look at magnetite as a viable medium in the dry beneficiation of coal. The high magnetic properties of magnetite can prove to be an advantage in the recovery of the medium for further use during the cleaning of coal.

3. Methodology

3.1. Introduction

The experiments were designed to evaluate the recovery of magnetite from the finer fractions (-3.2 mm) and losses to the oversize fraction from the dry beneficiation of coal. The Bohou process served as a guide for the design of the methodology and experiments. Parameters were set up, including the control of moisture and the mixing ratios of the samples.

Two coal samples were obtained from Greenside Colliery in Witbank. The coal consisted of No. 1, 4, and 5 seam coals and was labelled as ROM (run of mine) or AFE (feed to plant). Both coal samples were wet when collected. The third sample was collected from New Denmark Colliery (NDC) in Secunda. The coal was mined from the No. 4 seam. The sample received was dry. Coal from Greenside Colliery was used in Phase 1 of the test work, while the two samples from NDC were used in Phase 2 of the test work.

The magnetite sample was provided by Martin & Robson and collected from Broodsnyers Farm, Mpumalanga. Magnetite was initially used for the experiments, but a high-titanium magnetite was identified as a possible alternative and was also included in the test work. The sample was semi-wet. The high-titanium magnetite sample was supplied from Namakwa Sands through Tronox. The sample was dry.

All samples were air dried to ensure that there was no surface moisture. American Society for Testing and Materials (ASTM) standards were used to ensure that the correct methods and sampling handling were followed. If no standard was available, the methods were discussed and approved by the supervisor.

The test work was divided into two phases. During Phase 1, the loss of magnetite to the oversize was investigated. This phase used the ROM and AFE coals from Greenside Colliery and a magnetite sample.

Phase 2 investigated the recovery of magnetite and high-titanium magnetite from the coal medium. The NDC coal was used for this phase. The second phase also included

the use of normal and high-frequency screens to investigate other possibilities to improve recovery.

3.2. Sampling and characterisation of coal

3.2.1. Air drying

The most significant concern for the test work was to have a controlled moisture content. The coal samples needed to be air dried for the coal to be in equilibrium with the atmosphere at ambient temperature. In accordance with ASTM D3302/D3302M-17, the coal was laid out in a layer that did not surpass the thickness of twice the nominal top size of the coal (Zhu, 2014). This was achieved by spreading the coal in thin layers on a plastic-covered floor. The room was closed off to avoid dust and excess air flow.

The coal was left to dry overnight. The coal samples were weighed at one-hour intervals until the mass loss was less than 0.1% per hour. Drying of the coal removed the surface moisture, but did not remove residual internal moisture. The air-drying process also ensured that mass of the sample would be stable during the testing (Speight, 2015).

3.2.2. Screening

After air-drying, the samples were screened using a vibrating horizontal screen. The screen size was selected to be 13.2 mm, in accordance with that used by the Bohou process. The oversize (50 mm to 13.2 mm) was collected to determine the magnetite losses to the oversize.

3.2.3. Splitting of AFE and ROM coal samples

Two coal samples were received from Witbank, labelled AFE and ROM. The samples were split according to D2234/D2234M-16 (2016) and ASTM D3302/D3302M-17 (2017). Precautions were taken to ensure that there were minimal losses due to dust and particle degradation. The standard was used to ensure that the samples would be as representative as possible in terms of mass and composition.

The bulk samples of both AFE and ROM were just over 40 kg. Both samples were manually mixed before being split with a mechanical splitter using a ten-way Dickie Stockler rotary splitter. The sample was passed through the rotary splitter three times with mixing in between, according to ASTM D2234/D2234M-16, to ensure sufficient mixing. The samples were split into two batches weighing ± 20 kg each using the rotary splitter. The samples were then passed through the rotary splitter again to obtain 20 samples of ± 2 kg each, as shown in Figure 27. The final AFE samples had an average mass of 2043.2 g with a maximum deviation of 2.1% or 41.1 g. The final ROM samples had an average mass of 2026.1 g and a maximum deviation of 2.3% or 47.5 g.



Figure 27: Splitting of AFE and ROM coal samples with a rotary splitter

The samples were named as indicated in Table 2, where the sample label indicates the method of testing; for example, A13 was an air-dried sample (both coal and magnetite were dry), A14 was a sample where the coal had surface moisture, but the magnetite was air dried; A15 comprised air-dried coal and magnetite containing surface moisture. The methods of preparation are discussed in Section 3.2.1.

Table 2: AFE and ROM sample labels

| Sample ID | Method |
|-----------|---------------|
| A13 | Dry |
| A14 | Wet coal |
| A15 | Wet magnetite |
| R13 | Dry |
| R14 | Wet coal |
| R15 | Wet magnetite |

3.2.4. Splitting of NDC coal sample

The bulk sample (roughly 60 kg) of the NDC coal was separated into 54 samples using manual and mechanical splitting. The sample was hand mixed before being passed through a ten-way Dickie Stockler rotary splitter to homogenize the sample, in a similar manner to that of the AFE and ROM samples. The bulk sample was then split into ten portions. These portions were added together and passed through the rotary splitter again. The process was repeated three times to ensure that the samples were mixed (ASTM D2234/D2234M-16). The sample was split into three samples of 20 kg each. The 20-kg samples were passed through the rotary splitter to give ten samples of 2 kg. Finally, the 2-kg samples were passed through a riffle splitter. The final samples weighed 1035 g on average, with a deviation of 4% or 41.4 g (Figure 28).

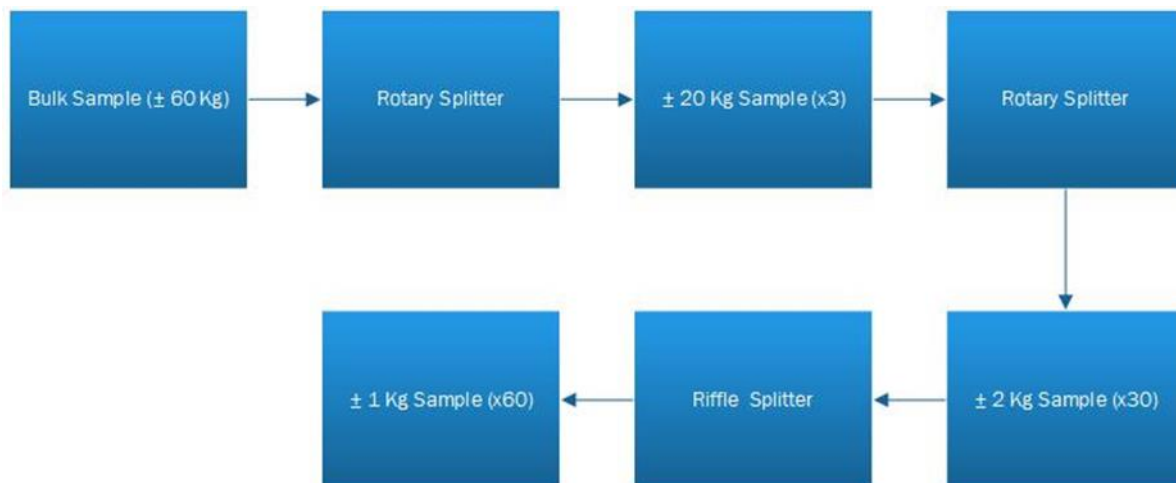


Figure 28: Splitting of NDC coal sample with rotary and riffle splitter.

The names of the split samples are indicated in Table 3. The same method was used for both the magnetite and high-titanium magnetite. Table 3 indicates which samples contained the dry coal and magnetite, the wet magnetite, and the wet coal. The dry, wet magnetite, and wet coal labels are the same as in Table 2, but labels were also created for a 13.2 mm normal screen, a 3 mm normal screen, and a 3 mm high-frequency screen.

Table 3: Sample preparation methods for magnetite and high-titanium magnetite samples

| Screen | Repetitions | Method | Screen | Repetitions | Method | Screen | Repetitions | Method |
|----------------|-------------|----------|-------------|-------------|----------|---------------------|-------------|----------|
| 13.2 mm normal | ×1 | Dry | 3 mm normal | ×1 | Dry | 3 mm high-frequency | ×1 | Dry |
| | ×1 | Wet mag | | ×1 | Wet mag | | ×1 | Wet mag |
| | ×1 | Wet coal | | ×1 | Wet coal | | ×1 | Wet coal |
| | ×5 | Dry | | ×5 | Dry | | ×5 | Dry |
| | ×5 | Wet mag | | ×5 | Wet mag | | ×5 | Wet mag |
| | ×5 | Wet coal | | ×5 | Wet coal | | ×5 | Wet coal |
| | ×10 | Dry | | ×10 | Dry | | ×10 | Dry |
| | ×10 | Wet mag | | ×10 | Wet mag | | ×10 | Wet mag |
| | ×10 | Wet coal | | ×10 | Wet coal | | ×10 | Wet coal |

3.2.5. Coal classification

It is vital to determine the chemical composition and physical properties of the coal sample to have a clear understanding of its properties. One of each of the representative samples was used for a particle size distribution (PSD) test, calorific value analysis, proximate analysis, and X-ray diffraction (XRD) analysis.

The samples for the proximate, calorific, and XRD analyses were pulverised to the specifications of the tests. The PSD was carried out according to the ASTM D4749-87 (2012) standard.

3.2.5.1. Particle size distribution

A PSD of the coal sample was determined. The test was performed using a laboratory sieve shaker (Figure 29) with a sample of 1031.1 g of coal. The sieve series included 26 500 µm, 19 000 µm, 13 200 µm, 8000 µm, 5600 µm, 4000 µm, 2800 µm, 2000 µm, 1400 µm, and 1000 µm sizes. The sample was sieved for 10 min at a frequency of 40 Hz according to ASTM D4749-87 (2012) to ensure representative results. The sample on each sieve was weighed and recorded. The final mass was added to check for sample losses.



Figure 29: Laboratory sieve shaker

3.2.5.2. Proximate analysis

Proximate analysis determines the rank of the coal (Mayoral, Izquierdo, Andrés, & Rubio, 2001). The rank is determined by the ash, moisture, volatile matter, and fixed carbon contents. The coal is heated in a furnace according to ASTM D5142 (2009).

The ash content is mostly composed of sulfates and oxides. The ash content is determined by burning the coal sample to remove the organic matter (Speight, 2015). The moisture content of the coal sample was calculated from the mass loss as the coal sample was heated and the water evaporated. The volatile matter was calculated from the percentage of volatile products that were released when the coal sample was heated. The fixed carbon was calculated from the mass remaining after the ash, moisture, and volatiles have been removed (Speight, 2015).

The proximate analysis was performed by Mintek, Randburg.

3.2.5.3. Calorific value

The calorific value is an energy value directly linked to the heat content of coal (Speight, 2015). It is indicative of the combined heats of combustion of the organic matter (sulfur, hydrogen, nitrogen, and carbon) and the sulfur found in pyrite. The

calorific value was determined by combusting a 1.00 g of each coal sample in a bomb calorimeter in the presence of oxygen (ASTM D3286, 1996). The analysis was carried out by Mintek, Randburg.

3.2.5.4. X-ray diffraction analysis

XRD is a popular and powerful method used for the identification of elements and minerals (Zhu, 2014). It is of importance to know the chemical composition of a material because this will determine its chemical and physical properties. X-ray diffraction occurs when X-rays are scattered by the electrons of the atoms when a beam passes through a material without any change to the wavelength of the X-ray (Klug & Alexander, 1974). The diffraction that occurs creates a pattern that is used to identify the unit cell of the mineral, as well as the atoms within the unit cell.

The sample was pulverised to a fine powder and inserted into a mount to form a pressed pellet. The mount was then inserted into the XRD instrument, where an X-ray beam is directed at the sample at specific angles. The X-rays were diffracted and analysed to produce the identification of the minerals present in the pellet.

The XRD analysis was performed at the Stoneman Mineralogical Laboratory at the University of Pretoria.

3.3. Sampling and characterization of magnetite and high-titanium magnetite

3.3.1. Drying

Currently, there is no standard for drying of magnetite, so the same standard was used as for drying of the coal samples. The magnetite and high-titanium magnetite were dried using the same standard (ASTM D2234/D2234M-16) as for the coal samples, as described in Section 3.2.1.

3.3.2. Splitting

Phase 1 test work for the magnetite was carried out using the AFE and ROM coal samples. The samples were split using a ten-way Dickie Stockler rotary splitter. The samples were split according to ASTM D2234/D2234M-16. The samples were mixed three times before being split into the final samples.

The initial magnetite sample was roughly 10 kg. The sample was split into two samples of roughly 5 kg each. These samples were passed through the rotary splitter to obtain final samples with a mass of about 500 g each, as shown in Figure 30. The final samples had an average mass of 510.8 g, with a maximum deviation of 1.6% or 8.0 g.



Figure 30: Splitting of magnetite for the AFE and ROM coal tests using a rotary splitter

Both the magnetite and high-titanium magnetite samples were split using a small ten-way Dickie Stockler rotary splitter (magnetite was used in both Phases 1 and 2; high-titanium magnetite was only used in Phase 2). Both samples were split according to ASTM D2234/D2234M-16, as used in the coal sample preparation. The samples were considered homogeneous after they had been through the rotary splitter three times, mixing between each split.

Both samples were prepared using 7.5 kg of magnetite and high-titanium magnetite. After the sample was mixed three times, it was split into three samples, each containing about 2.5 kg of material. The split samples were passed through the rotary splitter again to produce a total of 30 samples of both magnetite and high-titanium magnetite, each weighing approximately 0.25 kg. The process is shown in Figure 31. The magnetite samples had an average mass of 252.5 g, with a maximum deviation of 1.1% or 2.7 g; the high-titanium samples had an average mass of 253.3 g, with a maximum deviation of 1.5% or 3.7 g.



Figure 31: Splitting of magnetite and high-titanium magnetite for use with the NDC coal using a rotary splitter.

3.3.3. Classification

It was important to understand the both physical and chemical characteristics of the magnetite samples. Multiple analyses were done on both samples, including XRD, X-ray fluorescence (XRF), quantitative evaluation of minerals by scanning electron microscopy (QEMSCAN), PSD, and hydrophobicity tests. The samples were pulverised to adhere to the standard for XRD testing. The hydrophobicity test was performed on a large piece of magnetite crystal.

3.3.3.1. Particle size distribution

PSD tests were carried out on both the magnetite and high-titanium magnetite samples. The tests were performed by using a laboratory sieve shaker. The samples were sieved for 10 min at a frequency of 40 Hz according to ASTM D4749-87 (2012). The sample mass remaining on each sieve was weighed and recorded. A rather small sample was used in order to sieve the sample. The final mass was added to check for sample losses. The PSD data were compared with that of magnetite from Shenhua, China, that is used in the Bohou process.

3.3.3.2. X-ray diffraction analysis

Both the magnetite and high-titanium magnetite samples were pulverised to a fine powder and sent for XRD testing at the Stoneman Mineralogical Laboratories at the University of Pretoria. The conditions employed are given in Section 3.2.5.4.

3.3.3.3. X-ray fluorescence analysis

XRF is carried out by bombarding a material with gamma rays to produce secondary (fluorescent) X-rays (Zhu, 2014). XRF analysis is most commonly used for the identification of the elemental and chemical composition of a material.

The sample is dried and pulverised, and the powder compressed in a pellet. An X-ray beam is directed at the sample and the beam is absorbed to produce a secondary, or fluorescent, x-ray that is distinct to a specific element (Zhu, 2014). From the information acquired, a quantitative analysis is performed to identify the elemental and chemical composition of the sample.

The XRF analysis was performed at the Stoneman Mineralogical Laboratories at the University of Pretoria, using a Thermo Fisher ARL Perform'X instrument.

3.3.3.4. Scanning electron microscopy (Phase 1)

The scanning electron microscope (SEM) is used to obtain a low-magnification (less than 1000 \times) image of an object (Goldstein et al., 2017). The image is obtained by directing an electron beam down an evacuated vacuum tube. The beam passes through a lens at the bottom and interacts with the sample. As the beam interacts with the sample, it moves along a grid, gathering point data. The image is formed by integration of the point data.

SEM analysis was undertaken at the University of Pretoria. The analysis was done on the top and bottom size fractions of the magnetite sample to observe surface characteristics of the magnetite. The top size fraction was +1100 μm and the bottom size fraction was -53 μm .

3.3.3.5. Quantitative evaluation of minerals by scanning electron microscopy

QEMSCAN is similar to SEM analysis. The QEMSCAN provides a size-by-size and particle-by-particle mineralogical analysis of a material sample (Butcher et al., 2000). The sample is prepared by creating a polished section. The sample is scanned with an electron beam and the intensity of the resulting energy-dispersive X-ray spectrum is measured. An image is created of the individual particles in the sample. Chemical analysis can be determined using the energy-dispersive X-ray spectrum. The image shows the size, shape, and chemical makeup of the particle.

QEMSCAN analyses of magnetite and high-titanium magnetite were carried out at LightDeepEarth laboratories in Pretoria. The QEMSCAN measurements were taken at

5 μm intervals and 1000 counts per second (cps) at each point with a Zeiss EVO50 instrument, with a spot size of 5 nA, 25 kV.

3.3.3.6. Hydrophobicity test

Hydrophobicity is the ability of water molecules to penetrate the interior of a material (Drzymala, 1994). A solid material is hydrophobic when a water drop does not spread over the solid material, but remains a droplet. A contact angle can be measured from the water droplet to indicate the hydrophobicity.

A water-drop test was performed on a magnetite crystal to obtain the contact angle. The test was done by setting the magnetite crystal on a flat surface with a syringe filled with water above it. The sample was placed in front of a magnifying camera with a light attached, as shown in Figure 32. A droplet of water was dropped on the magnetite crystal and the contact angle measured.

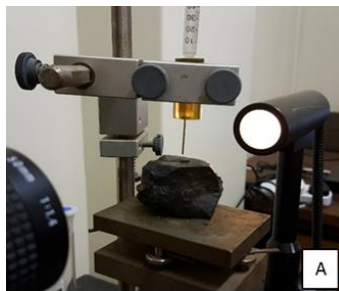


Figure 32: Hydrophobicity measurement

3.4. Sample preparation

During the sample preparation, the coal and magnetite samples were mixed. The AFE and ROM samples were mixed with magnetite for Phase 1. The NDC samples were mixed with both magnetite and high-titanium magnetite, and the tests were repeated in Phase 2.

The AFE and ROM samples were used to determine different options for the test work. The samples were tested in Phase 1 to determine the most appropriate method for the project. Based on the outcome of the AFE and ROM sample test work in Phase 1, the NDC samples were used in Phase 2 to test the recovery of the medium.

3.4.1. Summary of experimental procedure

Figure 33 indicates the experimental procedures followed during the test work, starting from screening of the samples to recovery of the magnetite samples.

The feed sample was dry screened with a 13.2 mm screen, and the oversize and undersize were collected. The undersize was weighed to account for the mass balance. The oversize was mixed with the magnetite and moisture was added, as described in Section 3.4.2. Initial test work was undertaken to determine how to add moisture to the coal and magnetite samples, as discussed in Section 3.4.2. The two methods were compared to determine which would be better suited to the project. The selected method was used in both Phases 1 and 2.

The prepared samples were dry screened with a 13.2 mm screen and the undersize and oversize fractions were collected. The oversize fraction was weighed for the mass balance and the undersize sample was used for further screening, as discussed in Section 3.4.3. The undersize samples were screened using a 3 mm laboratory screen in Phase 1; in Phase 2, three different screens (the 3 mm laboratory screen, a 13.2 mm laboratory screen, and a 3 mm high-frequency screen) were used (Section 3.4.3).

The samples were passed through a LIMS to separate the magnetic and non-magnetic particles (Section 3.4.4). Both the magnetic and non-magnetic fractions were washed on a magnetic chute to remove the non-magnetic material that could not be removed with the magnetic separator. Both fractions were weighed to calculate the amount of magnetite and the total magnetite that was recovered.

Detailed descriptions of each step are discussed in the following sections.

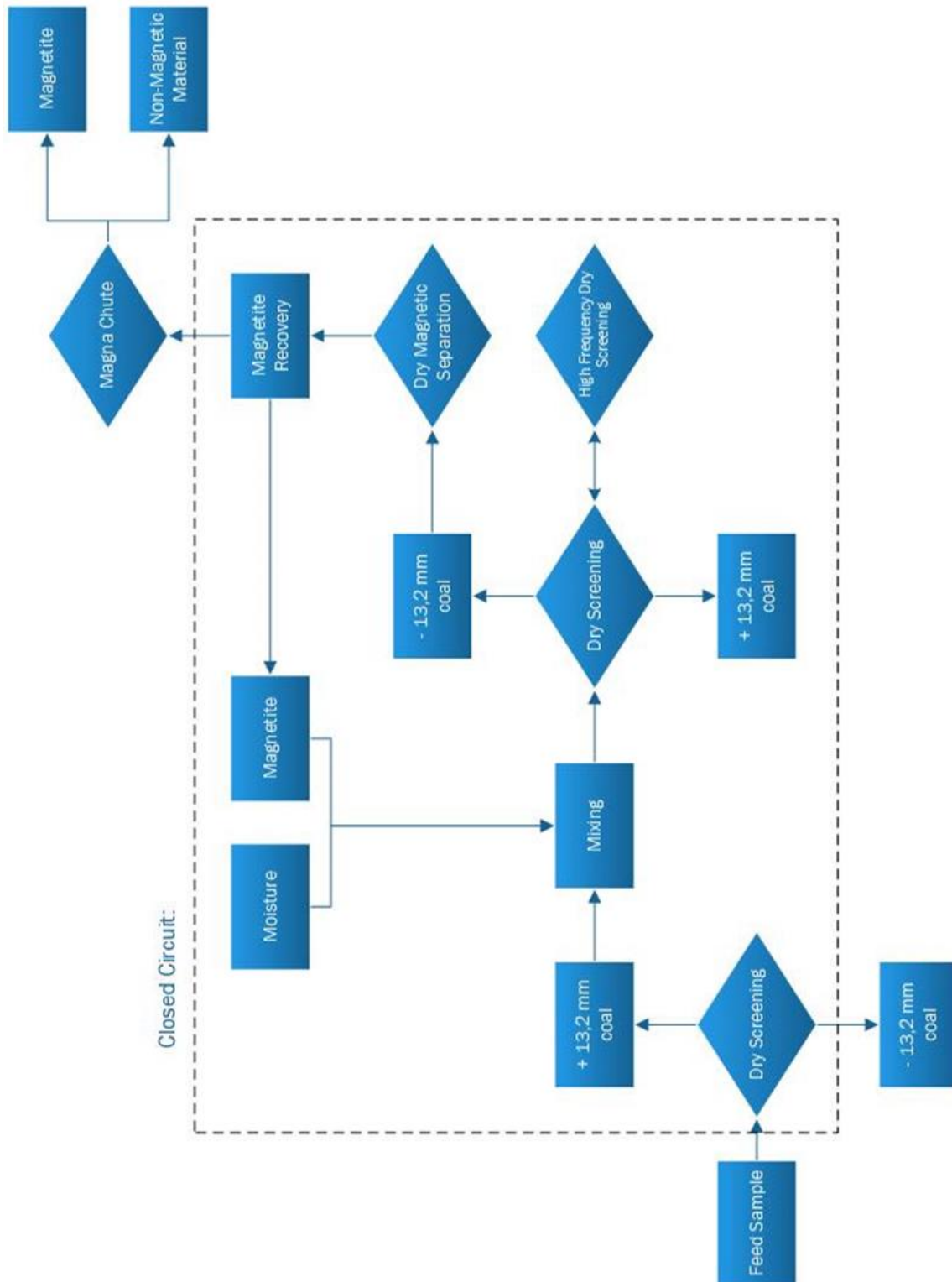


Figure 33: Experimental procedure

3.4.2. Preparation of wet and dry samples

Wet samples of the coal and magnetite samples with controlled moisture contents needed to be prepared before the samples could be mixed. Two different methods were used during the initial test work to prepare wet AFE and ROM coal samples. Initial test work was performed on the AFE and ROM samples to determine the method of adding moisture. Once the method was determined, the samples were mixed and the final test work was done. Final test work was using the AFE, ROM, and NDC samples.

The first group of samples was prepared by adding 5% water (calculated using the coal sample mass) to the coal sample and then draining the excess water. The second group of samples was prepared by leaving the coal sample overnight in water and draining the excess water the next day (AFE, ROM, and NDC). The wet samples were weighed to calculate the moisture content.

The different magnetite samples (magnetite and high-titanium magnetite) were prepared by adding 4% water (calculated from the magnetite sample mass) to the dry samples. Excess water was drained and the samples weighed to determine the moisture content.

Three samples each of the AFE and ROM coals were mixed with the different magnetite samples. The masses of the coal and magnetite samples were recorded for mass balance calculations.

The resulting samples were a dry coal and dry magnetite sample, a dry coal and wet magnetite sample, and a wet coal and dry magnetite sample. The same procedure was used to prepare the NDC coal samples. This resulted in nine dry samples, nine wet magnetite samples, and nine wet coal samples for both magnetite and high-titanium magnetite, as shown in Figure 34.

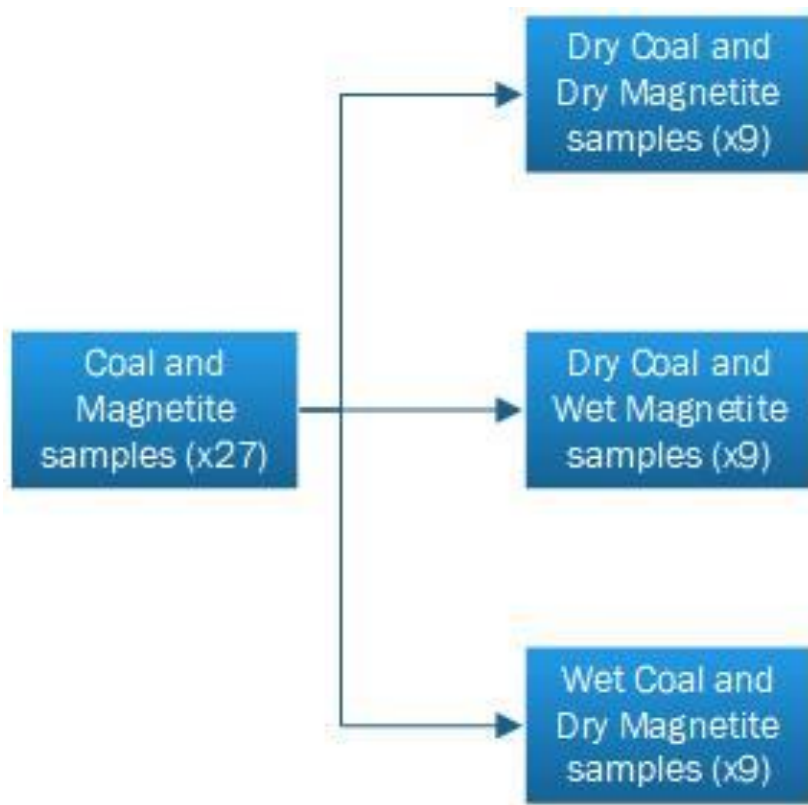


Figure 34: Mixing of NDC coal and magnetite samples

To test different sieve sizes and screen frequencies, the nine samples were further split into three categories based on the screen that was used; namely, 13.2 mm, 3 mm, and a 3 mm high-frequency screen, as shown in Figure 35. A further division was made to test the re-usability of the magnetite according to the number of screen repetitions; namely, one (x1), five (x5), and ten (x10) repeats. The different magnetite samples were used once, five, or ten times to determine the relative losses. After each use, the magnetite was re-mixed with the coal sample and screened again. The mass of magnetite recovered was recorded to calculate the overall losses, as discussed in Chapter 4.

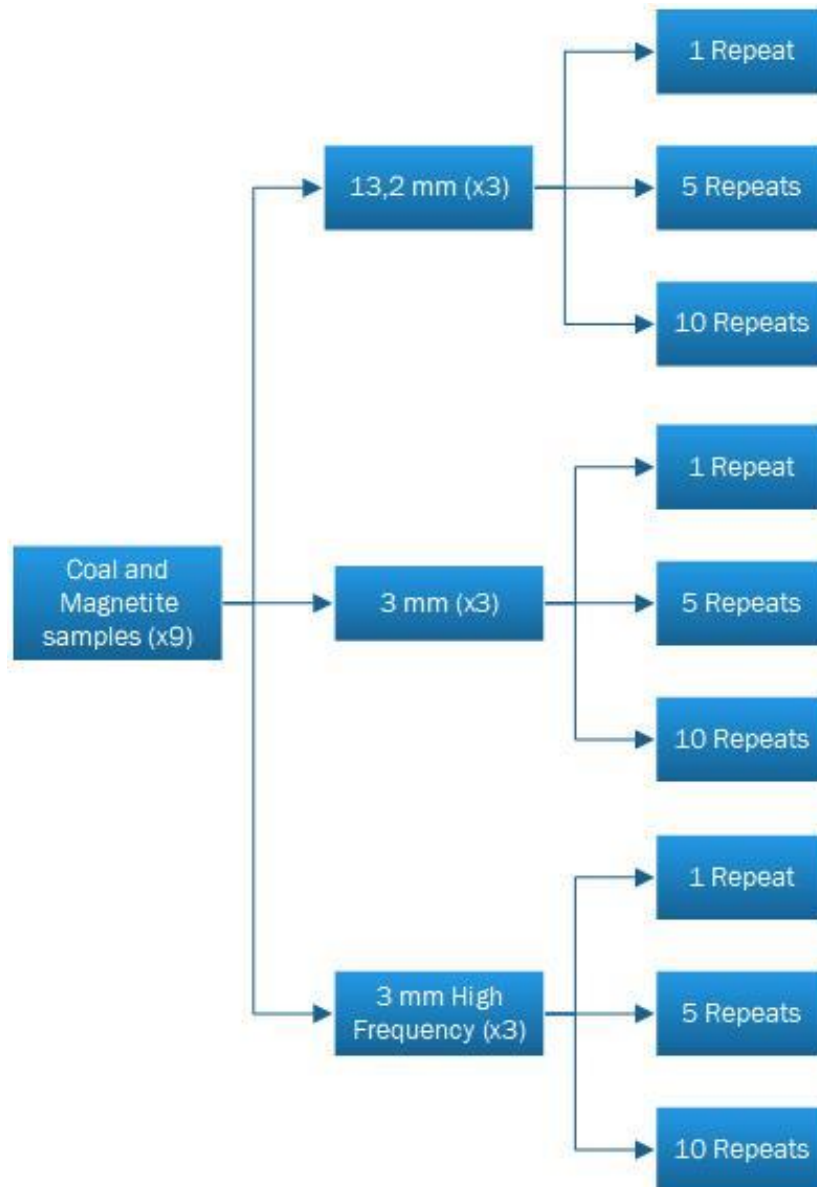


Figure 35: Further splitting of magnetite samples

3.4.3. Screening

The first batch of samples was screened using a 13.2 mm screen in a laboratory sieve shaker. The samples were screened for 10 min at 40 Hz. The undersize was collected and sent for magnetic separation. This test was repeated five and ten times to account for the disintegration of the magnetite and its effect on recovery.

The second batch of samples was screened using a 3 mm screen in a laboratory sieve shaker. The samples were screened for 10 min at 40 Hz, and repeated five and ten times. The undersize was collected and sent for magnetic separation.

The third batch of samples was processed using a high-frequency screen with a screen size of 3 mm. The samples were screened for 10 min at 47 Hz and up to 100 Gs. The experiment was repeated five times. The undersize was sent for magnetic separation.

3.4.4. Magnetic separation

Magnetite is highly magnetic and can be easily removed from the coal sample (Svoboda, 2004), thus a dry LIMS process was followed. This system is usually used for removing strongly magnetic material.

The undersize samples were passed through a permanent magnetic roll separator, with a magnetic induction between 710 and 1150 Gs. The roller separated the sample into magnetic and non-magnetic fractions. Both fractions were passed through a magnetic chute.

A magnetic (magna) chute consists of a metal plate placed on a magnet. A hopper is placed over the plate, through which the material is fed. The material moves over the plate: magnetic material will attach to the plate, while non-magnetic material will move over the plate. Once all the material has passed, the plate is lifted up and the magnetic material is released.

An Eriez Magna Chute BaFe was used to separate the finer fractions of magnetite and coal. This magna chute has an intensity of 1370 Gs. The magnetite was cleaned by pouring the sample with water over a flat tray that was in contact with a magnet. The sample was washed with water to remove the non-magnetic components. The tray was then raised above the magnet and the magnetic portion fell to the back to be collected. The magnetic sample was then dried and weighed. This method was used for measuring both the magnetite and high-titanium magnetite. The magna chute used is shown in Figure 36.



Figure 36: Magna chute

4. Results

4.1. Mineralogical characteristics of coal samples

4.1.1. Particle size distribution

The PSD results are shown in Figure 37. This indicates that the ROM sample was coarsest and the NDC sample finest. Only 31.34% of the NDC sample passed to the +13.2 mm size fraction, whereas 71.37% of the AFE and 81.37% of the ROM coal passed to the +13.2 mm size fraction. None of the coal samples were larger than 26.0 mm in size.

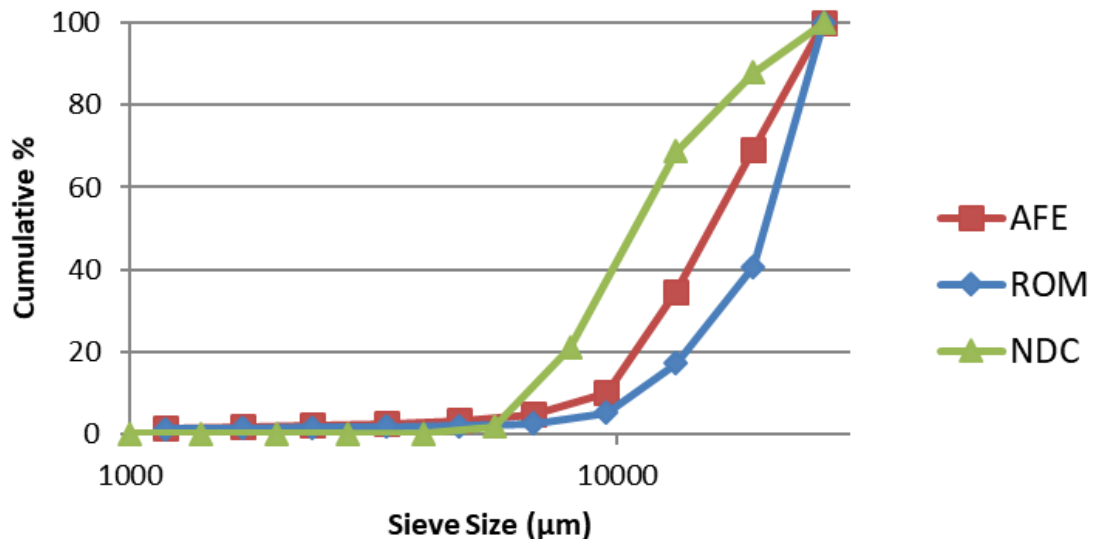


Figure 37: Particle size distributions of coal samples

4.1.2. Proximate analysis

Table 4 indicates the proximate analyses of the NDC, AFE, and ROM samples. The ROM sample had the highest inert moisture (2.39%) and volatile (22.82 %) contents. The AFE sample had the highest ash content (49.22%). The highest fixed carbon content (38.5%) was found in the NDC coal.

Table 4: Proximate analyses of coal samples

| Sample name | Initial mass (g) | Inert moisture (%) | Volatiles (%) | Ash (%) | Fixed carbon (%) |
|-------------|------------------|--------------------|---------------|---------|------------------|
| NDC | 1.0069 | 1.42 | 20.73 | 39.35 | 38.50 |
| AFE | 1.0022 | 1.61 | 20.14 | 49.22 | 29.03 |
| ROM | 1.0064 | 2.39 | 22.82 | 39.39 | 35.39 |

4.1.3. Calorific value

Table 5 indicates the calorific values (CV) of the coal samples. The NDC coal had the highest CV of 18.57 MJ/kg, followed closely by the ROM coal with a CV of 18.17 MJ/kg. The AFE coal had the lowest CV of 14.2982 MJ/kg.

Table 5: Calorific values of coal samples

| Sample name | Mass (g) | CV (MJ/kg) |
|-------------|----------|------------|
| NDC | 0.97 | 18.57 |
| AFE | 0.97 | 14.30 |
| ROM | 0.97 | 18.17 |

4.1.4. X-ray diffraction

Appendix 1 presents the results from XRD analysis of the ROM and AFE coal samples. The average values are given in Figure 38. The ROM sample contained calcite, dolomite, kaolinite, and quartz. The sample contained a high percentage of kaolinite (70.28%) and a low percentage of calcite (5.38%). The AFE sample contained calcite, dolomite, kaolinite, quartz, and some siderite. The sample had a high percentage of kaolinite (53.06%) and a low percentage of siderite (6.82%).

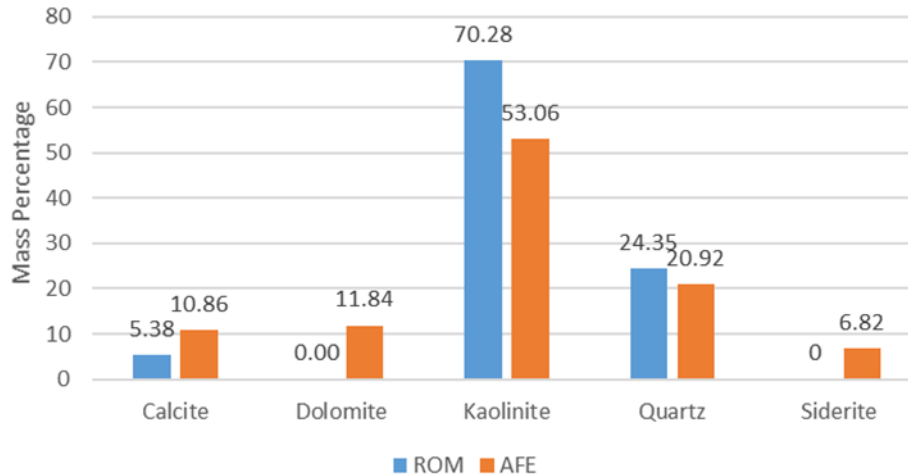


Figure 38: X-ray diffraction analysis of ROM and AFE samples

4.2. Mineralogical characterization of magnetite and high-titanium magnetite

4.2.1. Particle size distribution

The PSDs of the magnetite and high-titanium magnetite samples are compared with that of Shenhua magnetite obtained from the Bohou process, China, as shown in Figure 39. The high-titanium magnetite was the most coarse of the samples and the magnetite sample the finest. The 80% passing fraction occurred at 110 μm for the magnetite sample, 150 μm for the Shenhua magnetite, and 200 μm for the high-titanium magnetite sample. The high-titanium magnetite had a narrower size range than the magnetite sample.

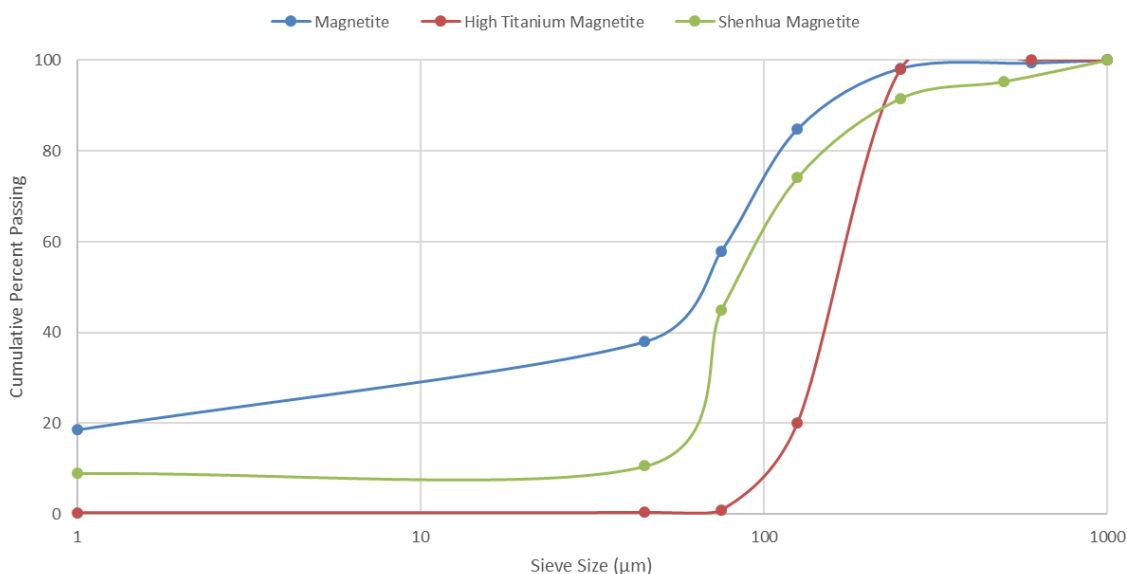


Figure 39: Particle size distribution of magnetite samples

4.2.2. X-ray diffraction

XRD results for the dried magnetite and high-titanium magnetite samples are shown in

Table 6. The magnetite sample consisted of 93.95% magnetite, with small amounts of calcite, dolomite, and ilmenite. The high-titanium magnetite had a lower percentage of magnetite (53.54%), higher concentrations of hematite (30.89%) and ilmenite (11.91%), and small amounts of rutile (3.16%) and quartz (0.5%). The sigma-three errors were very low on both samples, indicating a low variability of measurement errors.

Table 6: X-ray diffraction results for magnetite and high-titanium magnetite

| Magnetite | | | High Ti Magnetite | | |
|-----------|-------|------------------|-------------------|-------|------------------|
| | Mass% | 3 σ error | | Mass% | 3 σ error |
| Calcite | 2.48 | 0.66 | Hematite | 30.89 | 0.75 |
| Dolomite | 1.93 | 0.51 | Ilmenite | 11.91 | 0.78 |
| Ilmenite | 1.63 | 0.45 | Magnetite | 53.54 | 0.87 |
| Magnetite | 93.95 | 0.99 | Quartz | 0.5 | 0.3 |
| | | | Rutile | 3.16 | 0.42 |

4.2.3. X-ray fluorescence

Table 7 indicates the results obtained for XRF analysis of the dried magnetite sample. It comprised mainly iron (Fe) (67.09%), followed by silicon (Si) at 1.18%. Traces of other elements were also found within the magnetite. The “Bal” value refers to the balance material, this is the material that the instrument is unable to attribute to an element.

Table 7: X-ray fluorescence analysis of magnetite (%)

| | | | |
|--------------------------------|-------|----|-------|
| SiO ₂ | 2.52 | Fe | 67.09 |
| Cr ₂ O ₃ | 0.03 | Mn | 0.21 |
| Sn | 0.01 | Ti | 0.78 |
| Bal | 29.11 | Ca | 0.64 |
| Nb | 0.00 | Nd | 0.10 |
| Th | 0.00 | Pr | 0.05 |
| Zr | 0.01 | Ce | 0.03 |
| Sr | 0.01 | La | 0.02 |
| Rb | 0.00 | Ba | 0.01 |
| Pb | 0.03 | Cl | 0.29 |
| Zn | 0.02 | S | 0.19 |
| Cu | 0.06 | Si | 1.18 |
| Ni | 0.03 | | |

4.2.4. Scanning electron microscopy

Different size fractions of the magnetite sample were photographed using secondary-electron images, as shown in Figure 40. The magnetite is seen to have sharp edges and to be clean (without finer particles).

The magnetite sample was then mixed with clay and again viewed under the SEM (Figure 41). The objective was to determine if clay in coal could play a role in the recovery of magnetite from the dry beneficiation process. The samples were prepared by taking kaolinite clay and mixing it with magnetite at a 1:4 mass ratio. The objective was to see the interaction between the particles of the clay and the magnetite; specifically if the clay particles would attach to the magnetite particles. The magnetite

particles were rough and had sharp edges, whereas the clay particles were scattered around the magnetite particles. The clay particles were finer than the magnetite particles.

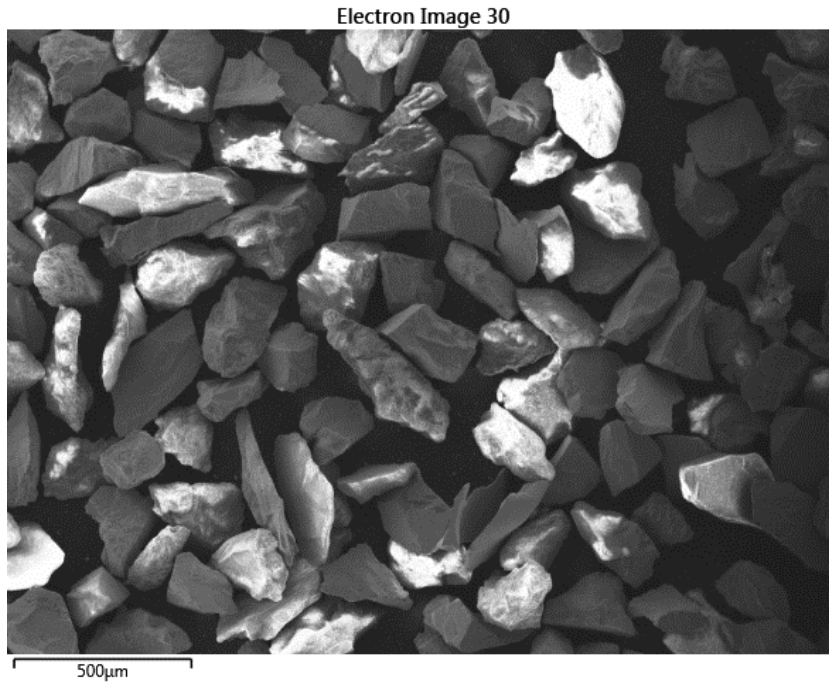


Figure 40: Secondary-electron image of magnetite

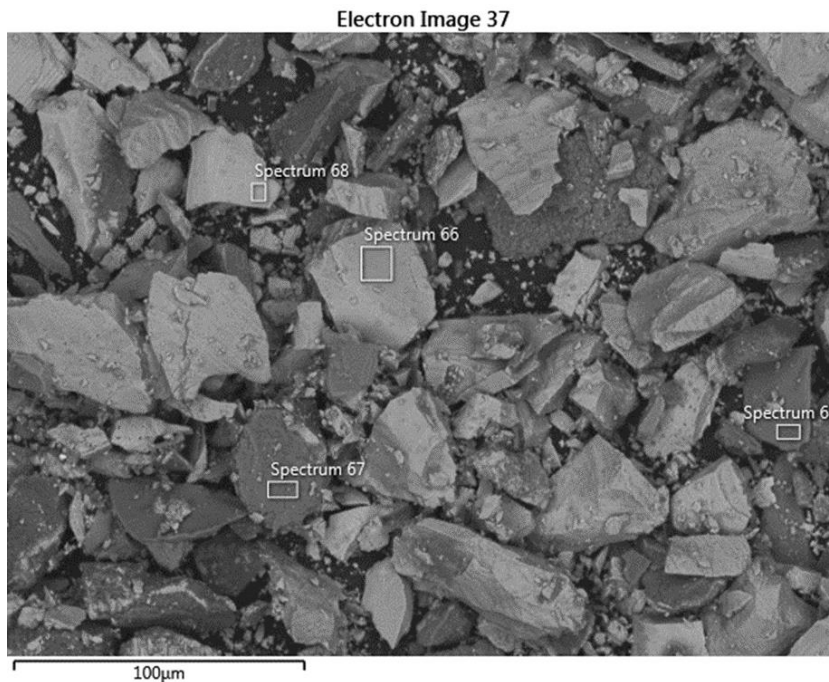


Figure 41: Secondary-electron image of magnetite with clay.

In the higher magnification image shown in Figure 42, clay was observed to adhere to the surface of a magnetite particle. The particles that stick to the magnetite are smaller than those of the magnetite. The kaolin particles appeared to coat the magnetite sample in a thin layer. Adhesion can be due to magnetic forces created by the magnetite (Gupta & Yan, 2016).

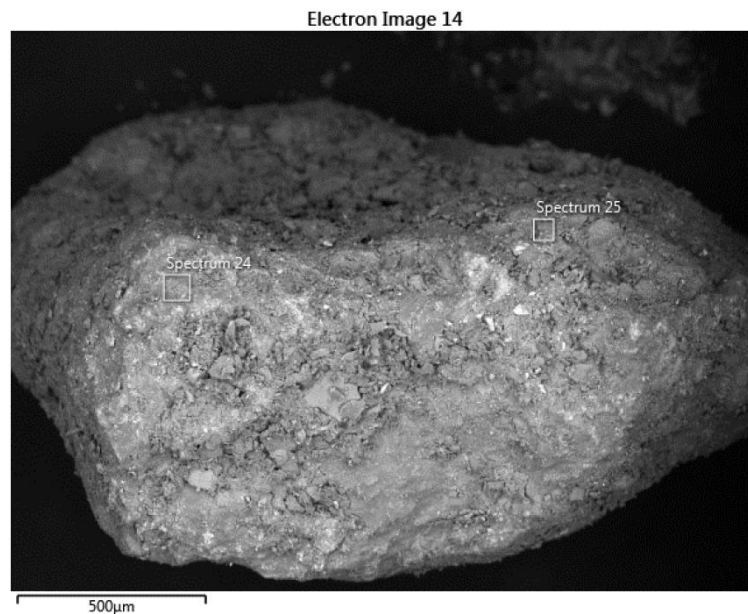


Figure 42: Secondary-electron image of magnetite with a size fraction of +1700 μm

4.2.5. Quantitative evaluation of minerals by scanning electron microscopy

Figure 43 shows a QEMSCAN analysis of the magnetite sample. The same rough and sharp edges that were seen in the SEM images are apparent. A large agglomeration can be seen in this and other images. Three different agglomerations are shown in Figure 76 in Appendix 2, with the legend indicating the minerals that are included. This agglomeration could be due to the magnetic forces of magnetite.

The high-titanium magnetite sample is shown in Figure 44. The sample surface was much smoother, and rounder when compared with the magnetite sample. The high-titanium magnetite did not show any of the agglomerations that were found in the magnetite sample. This is likely due to pure magnetite being ferromagnetic and high-titanium magnetite being less magnetic.

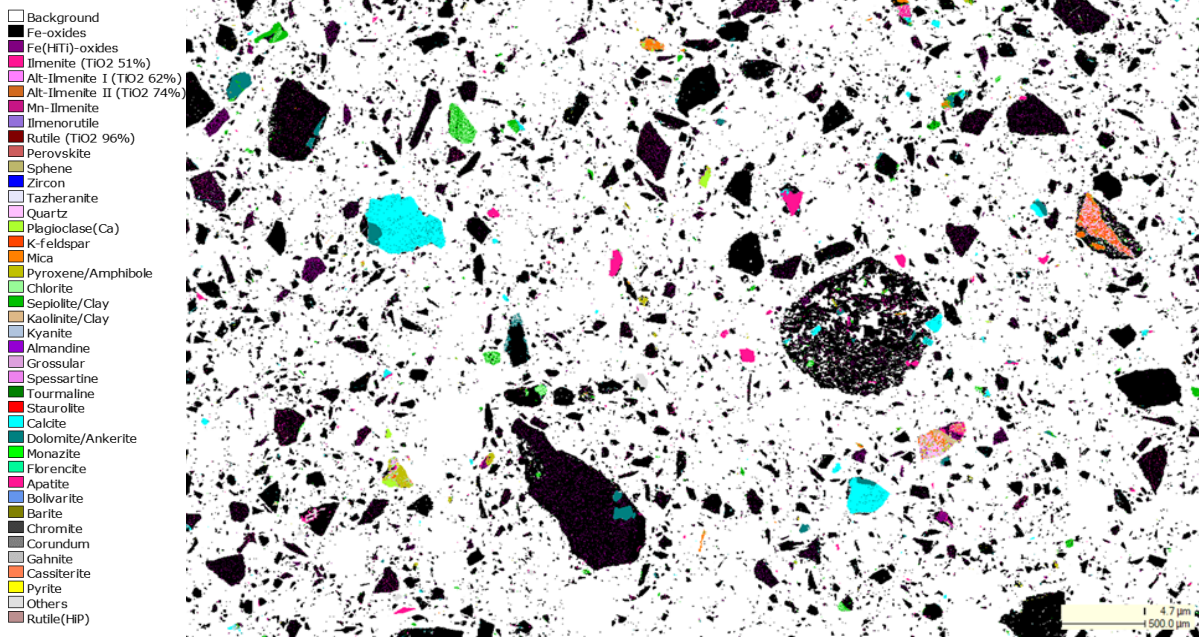


Figure 43: QEMSCAN analysis showing agglomerations in the magnetite sample

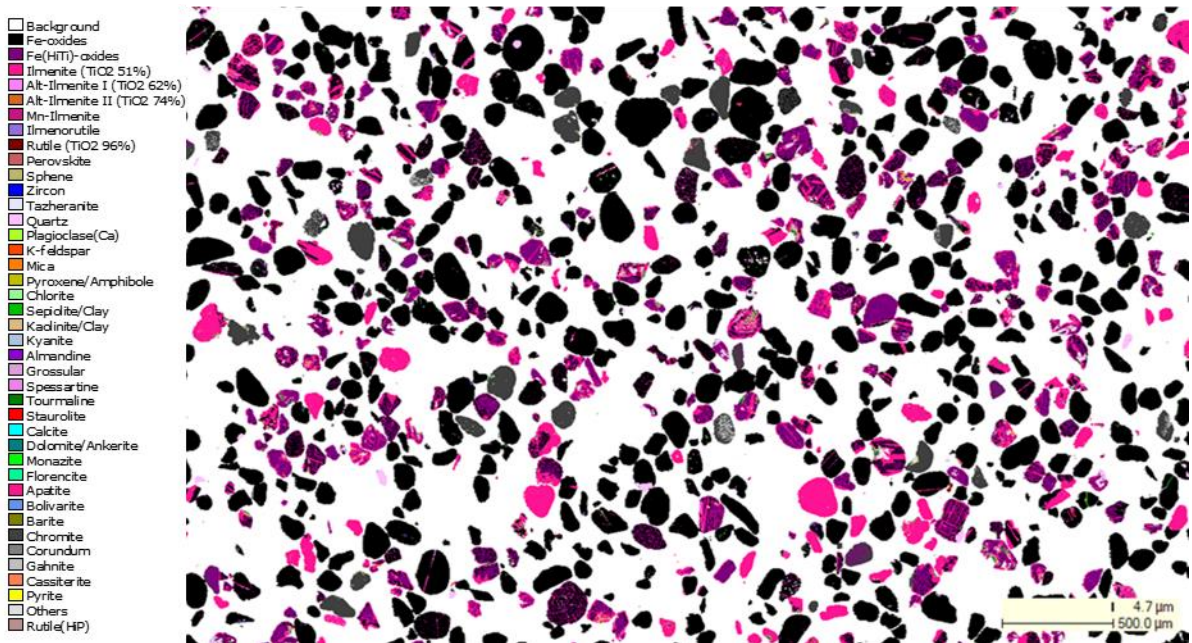


Figure 44: QEMSCAN of high-titanium magnetite

4.2.6. Hydrophobicity

When the water-droplet test was done on a magnetite crystal (Section 3.3.3.6), the contact angle could not be measured, which indicated a very hydrophilic surface (Figure 45). Figure 46 indicates the angles used to determine the hydrophobicity of a

sample. When compared with the data in Figure 45, it can be seen that the contact angle is above 90°. Table 1 indicates that the contact angle of a hydrophilic mineral is close to or at zero (Drzymala, 2007), which supports the claim that magnetite is hydrophilic.

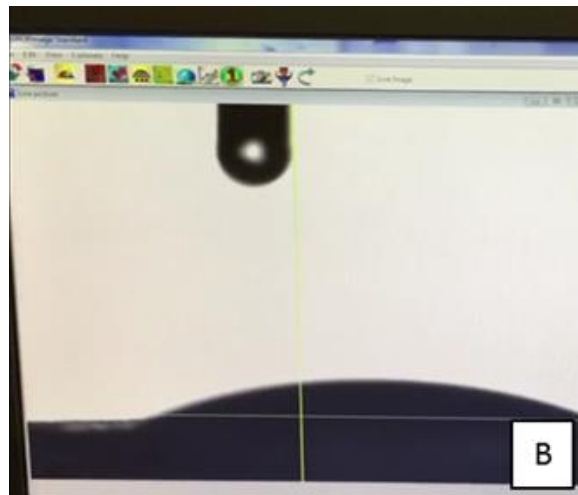


Figure 45: Contact angle of hydrophobicity test

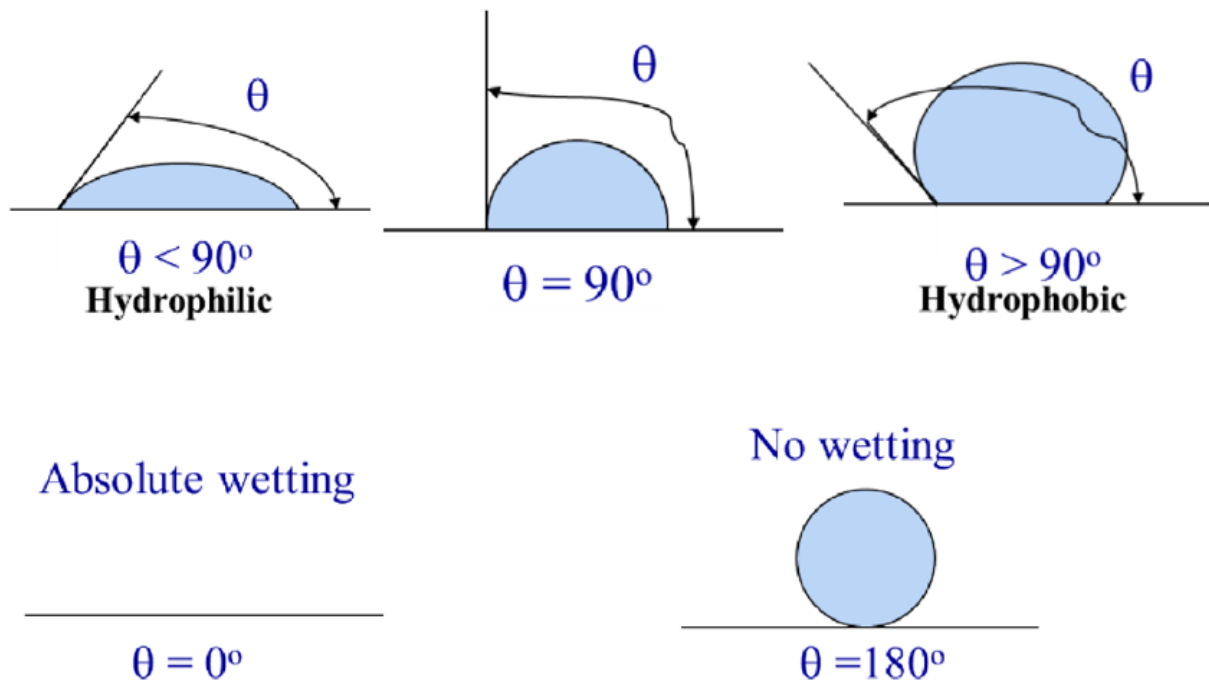


Figure 46: Force diagram of Young's equation and associated contact angle measurement. (Simpson, Hunter, & Aytug, 2015)

4.3. Phase 1: Losses of magnetite on coarse surfaces

Phase 1 work comprised studies using two coal samples (AFE and ROM) and the magnetite sample. The bulk samples were originally split into 20 subsamples of both AFE and ROM, as shown in Figure 34. Three samples each of AFE and ROM were prepared: sample 1 was dry coal and dry magnetite; sample 2 was wet coal and dry magnetite; sample 3 was dry coal and wet magnetite, as explained in Section 3.4.2. The samples were mixed and screened using a 13.2 mm sieve, as per Section 3.4.3. The samples were then passed through a dry LIMS, and the magnetic concentrate from the LIMS was passed through a magnetic chute to recover the magnetite (Section 3.4.4).

The wet coal samples were prepared by the two methods discussed in Section 3.4.2. The first method was to add 5% water and drain the excess. The sample was then weighed and the surface moisture calculated. The second method was to leave the coal samples in water overnight and drain the excess water the next day. The samples that were soaked in water overnight proved too wet to undertake the experiments: the samples that were submerged in 5% water yielded better results. Samples A14 and R14 had moisture contents of 2% and 1.4%, respectively; the samples that were left overnight had moisture contents of 4.8% (A14-2) and 2.8% (R14-2). The magnetite sample had an overall moisture of 1% when prepared in the same way.

4.3.1. Recovery of magnetite

The results are shown in Table 9 (Appendix 3) and comparison of the recovery and losses is shown in Figure 47. The highest recovery was found in the samples labelled as dry (>1% surface moisture). The dry AFE sample (A13) had a recovery of 93% and the dry ROM sample (R13) had a recovery of 92%. Thus, samples A13 and R13 showed the lowest losses of 7% and 8%, respectively.

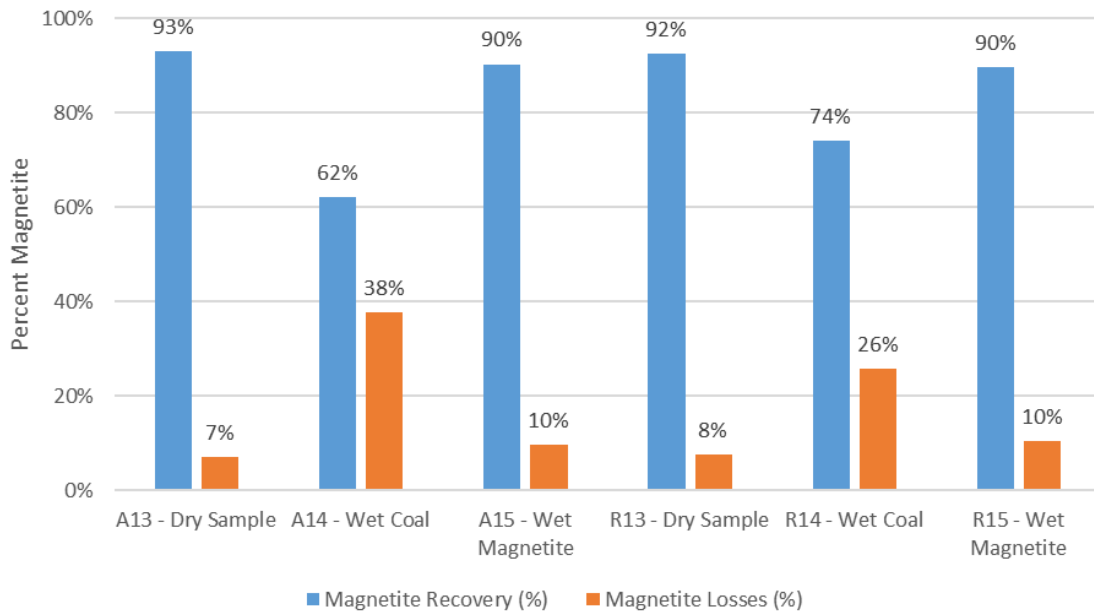


Figure 47: Recovery versus loss of magnetite

The wet coal (4.8% surface moisture for A14 and 2.8% surface moisture for R14) samples showed the highest losses of 38% and 26%, respectively, and lowest recoveries of 62% and 74%, respectively. The high losses were due to the magnetite sticking to the wet coal. The dry coal–wet magnetite system gave high recoveries, with 90% of the magnetite recovered from both the AFE (A15) and ROM (R15) samples. The results indicate that wet coal is a problem, as shown in Figure 48. The magnetite adhered to the surface moisture of the wet coal. Therefore, it is concluded that a feed coal containing a moisture content no higher than 1.4% limits the magnetite losses. The surface moisture of the coal plays a large role in the recovery of magnetite: unless the coal is completely dry, there will be a loss of magnetite.



Figure 48: Magnetite sticking to wet coal

4.3.2. Effect of sample mass on magnetite recovery

Table 10 (Appendix 3) indicates the mass of magnetite used in Phase 1 (discussed in Section 4.3.1) and the recovery of magnetite in each fraction. Figure 49 summarizes the recovery of magnetite from the different magnetic fractions taken from the LIMS; namely, the magnetic, middlings, and non-magnetic fractions.

Each fraction was passed through a magna chute to recover the magnetite. The percentage recoveries were calculated by comparing the recovered magnetite from the magna chute with the original mass of magnetite that was added to the sample.

This analysis showed that 93.0% of the A13 (>1% surface moisture) sample that was recovered by the LIMS was magnetite; the other 7% was non-magnetic material (Figure 49). Samples A14 and R14 (4.8% coal surface moisture for A14 and 2.8% coal surface moisture for R14) gave the lowest magnetic recoveries of 86.0% and 81.9%, respectively.

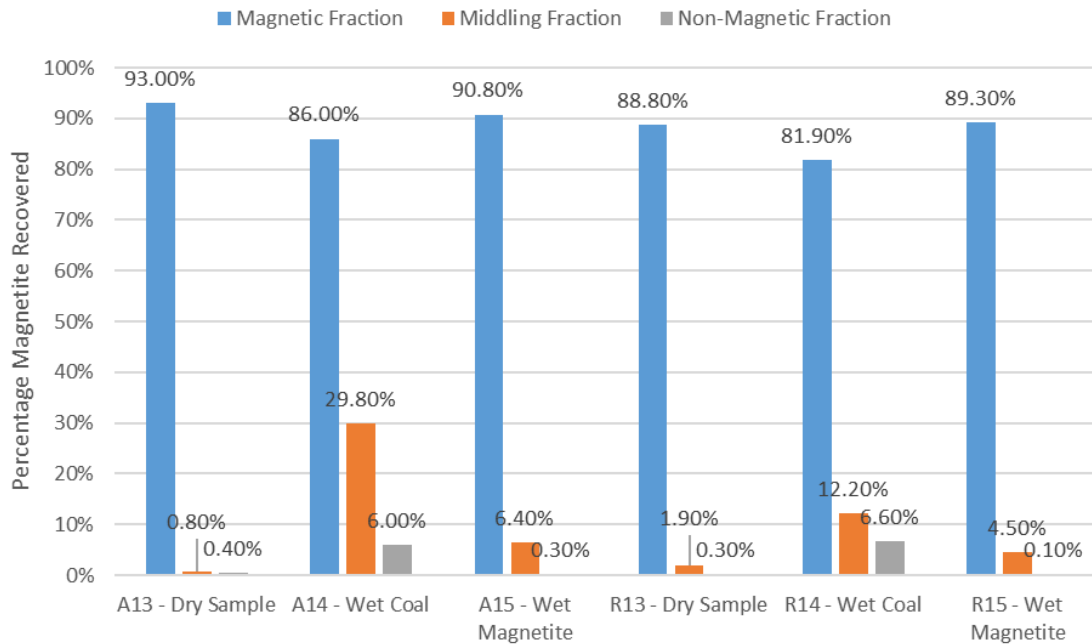


Figure 49: Magnetite recovered from the different magnetic fraction from the LIMS

Both wet coal samples (4.8% surface moisture for A14 and 2.8% surface moisture for R14) had the highest magnetite content in the middling sample (Figure 49). A14 had the highest percentage magnetite (29.8%), followed by R14 (12.2%). The wet magnetite samples had higher-than-expected magnetite recovery to the middlings, with 6.4% for sample A15 (magnetite surface moisture > 1%) and 4.5% for sample R15 (magnetite surface moisture > 1%). The recovery of magnetite in the middlings of the wet coal samples was expected to be similar to that of the dry and wet magnetite samples. This could be due to the nodules that formed during screening of the samples.

In the non-magnetic fractions shown in Figure 49, the highest magnetite recovery was achieved for the wet coal samples, which contained 6.0% magnetite in A14 and 6.6% magnetite in R14. These samples also gave the lowest recovery of non-magnetic components. The middling and non-magnetic fractions contained small amounts of magnetite that added to the overall loss of magnetite.

4.3.3. Magnetite losses per tonne

Further calculations were undertaken to extrapolate the data and calculate the loss of magnetite per tonne for each of the samples described in Section 4.3.1. The loss of magnetite in the middlings and non-magnetic fractions were combined. The original mass of the coal was converted to tonnes, the amount of magnetite needed was calculated, and the loss of magnetite (as a percentage) was used to calculate the loss per tonne of coal.

The total losses of magnetite per tonne of coal are shown in Table 8. According to the results, the lowest losses occurred for the dry samples: 13.02 kg/t (A13) and 14.10 kg/t (R13). The wet magnetite samples also showed smaller losses: 17.95 kg/t (A15) and 19.23 kg/t (R15). The largest losses occurred for the wet coal samples: 89.63 kg/t for A14 and 60.28 kg/t for R14. The data in Figure 50 confirm that the highest loss of magnetite occurred for the wet coal samples and the lowest losses occurred for the dry coal and wet magnetite samples.

Table 8: Magnetite losses

| Sample ID | Total magnetite losses (%) | Loss of magnetite (kg/t) |
|---------------------|----------------------------|--------------------------|
| A13 - Dry sample | 7 | 13.02 |
| A14 - Wet coal | 38 | 89.63 |
| A15 - Wet magnetite | 10 | 17.95 |
| R13 - Dry sample | 8 | 14.10 |
| R14 - Wet coal | 26 | 60.28 |
| R15 - Wet magnetite | 10 | 19.23 |

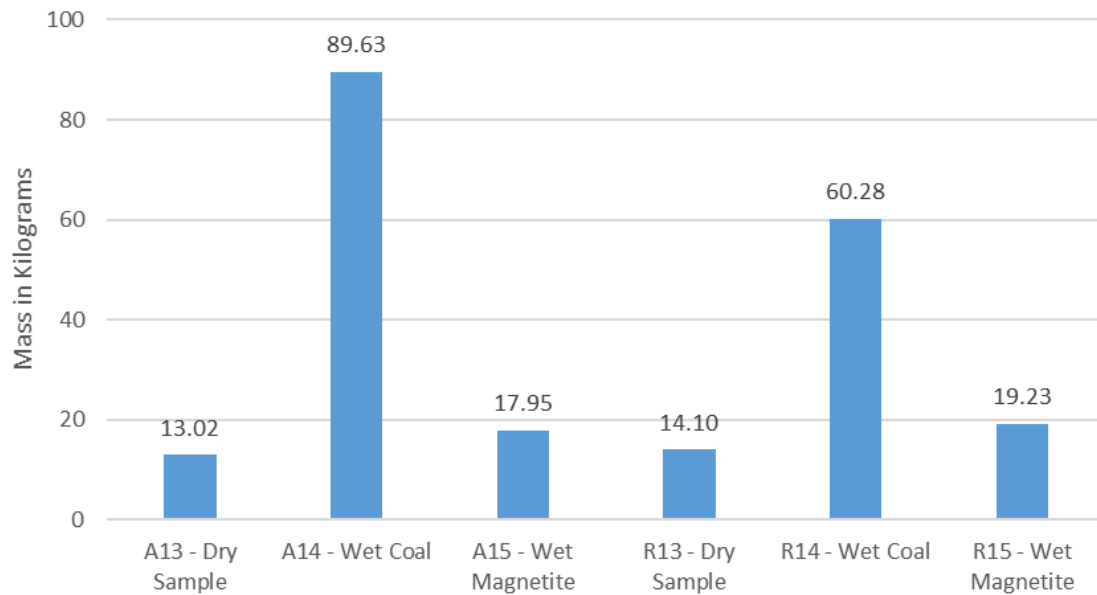


Figure 50: Loss of magnetite per tonne of coal

4.3.4. Nodule formation in magnetite

Nodules of magnetite formed during screening of the A14 and R14 samples (Figure 51). Three nodules were selected and opened. Two of the nodules only contained magnetite; the third also contained coal. The magnetite attached to the coal surface and formed magnetite agglomerates. Additional photographs of the wet coal are presented in Appendix 4.

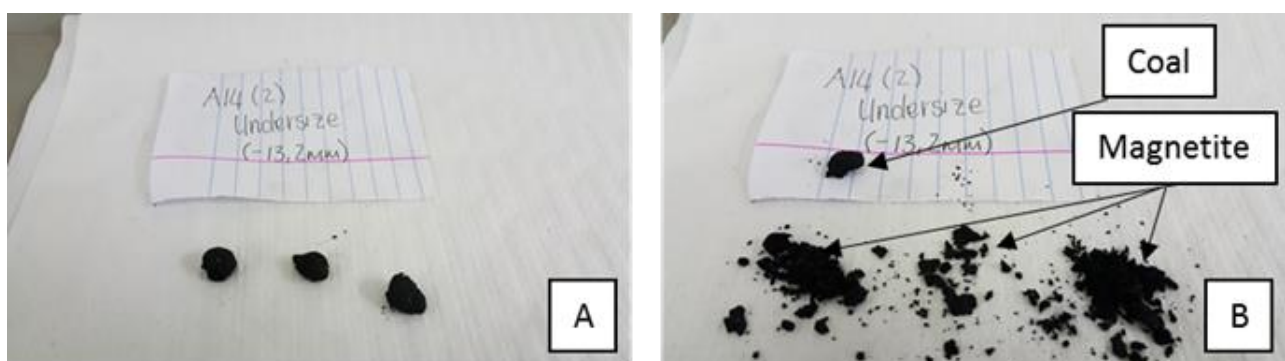


Figure 51: Nodules formed during screening of the wet coal samples

4.4. Phase 2: Effects of different screens on recovery of magnetite and high-titanium magnetite from the medium

In the Phase 2 test work, NDC coal was employed with magnetite and high-titanium magnetite. The tests were repeated once (×1), five times (×5), and ten times (×10) per screen, as shown in the summary in Section 3.4.1. A 3 mm screen was first used with a laboratory sieve shaker, as described in Section 3.4.3. The tests were repeated with a 13.2 mm laboratory sieve and a 3 mm high-frequency sieve shaker. The Bohou process makes use of a high-frequency screen to recover magnetite. The undersize samples were then split using a magnetic separator and magna chute, as described in Section 3.4.4. Recovery of the magnetic, middling, and non-magnetic fractions is discussed below. The tabulated data for this section can be found in Appendix 5.

4.4.1. Recovery of magnetite and high-titanium magnetite in the magnetic fraction

After the samples were split with the magnetic separator, they were washed in a magna chute. The recovery was calculated as shown in Equation 4:

$$\text{Magnetite recovery} = \frac{\text{Magnetite mass recovered (g)}}{\text{Initial mass of magnetite in feed (g)}} \times 100 \quad (4)$$

4.4.1.1. 3 mm screen

Figure 52 (summarized in Table 11 in Appendix 5) shows that the best recovery (99.96%) was obtained from the undersize of the dry sample that was passed through the screen five times. The second-highest recovery (99.49%) was obtained from the ×10 wet magnetite sample. The lowest recoveries were recorded for the wet coal samples: the ×5 wet coal sample had the lowest recovery of 3.30% and the ×10 sample had a recovery of 5.90%. The ×1 wet coal sample showed a recovery of 45.38%. The wet coal samples also showed the highest magnetite losses: 54.62%, 96.70%, and 94.10% for the ×1, ×5, and ×10 samples, respectively.

The same test sequence was repeated with the high-titanium magnetite: the results are shown in Figure 52 (summarized in Table 12 in Appendix 5). The ×10 wet

magnetite sample gave the highest recovery of 99.49%, followed by the x1 dry sample with a recovery of 99.45%. The lowest recoveries were recorded for the x5 (21.02%) and x1 (24.74%) wet coals.

The highest losses occurred in the wet coal samples, as for the magnetite. The highest loss of 78.98% occurred for x5 wet coal sample, followed by the x1 (72.26%) and x10 (62.46%) samples.

Data from Table 11 and Table 12 in Appendix 5 are combined in Figure 52. The greatest difference between magnetite and high-titanium magnetite was seen for the wet coal samples. The highest recovery of magnetite was measured for the x1 wet coal sample; the highest recoveries for the high-titanium magnetite samples were for the x5 and x10 wet coal samples. These results confirmed that the coal moisture content had a significant effect on the magnetite loss.

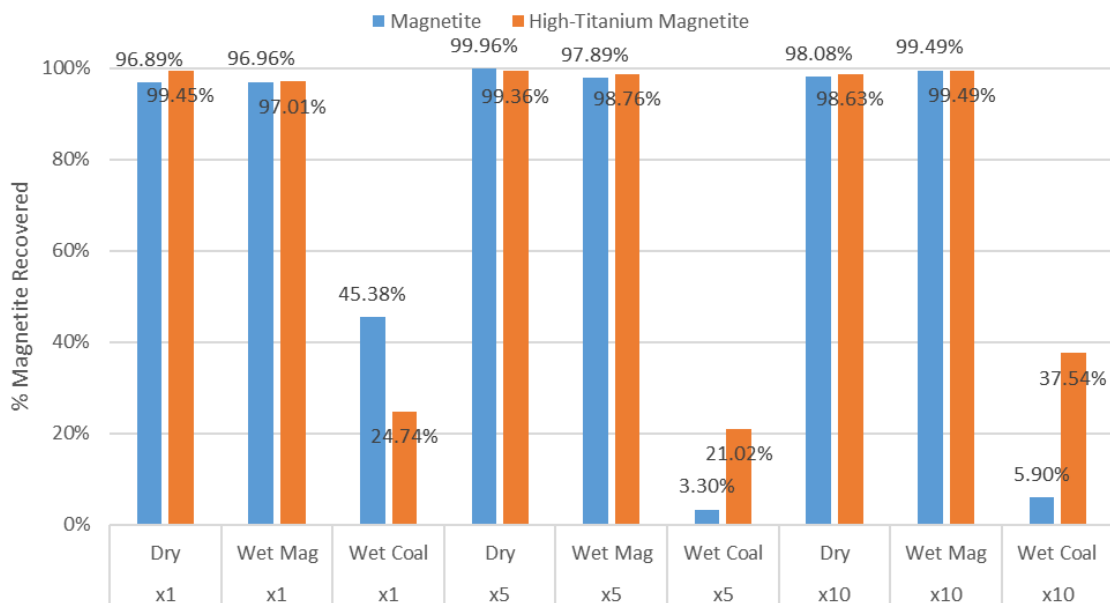


Figure 52: Recovery of magnetite and high-titanium magnetite using 3 mm screen

4.4.1.2. 13.2 mm screen

Figure 53, compiled from the data in Table 13 (Appendix 5), shows that the highest recoveries were obtained for the x10 (100%) and x5 (98.69%) wet magnetite samples. The lowest recoveries were recorded for the x5 (34.76%) and x10 (41.95%) wet coal

samples. The highest losses were obtained for the x5 (65.24%), x10 (58.05%), and x1 (55.12%) wet coal samples.

Recovery of the high-titanium magnetite with the 13.2 mm screen is shown in Figure 53, compiled from the data in Table 14 in Appendix 5. The highest recovery of 99.80% was for the x10 dry sample; the x1 dry sample gave 99.32% recovery. The lowest recovery was reported for the x5 (43.25%) and x1 (51.32%) wet coal samples. The highest losses occurred in the wet coal samples, with values of 56.75%, 48.68%, and 46.27% for the x5, x1, and x10 samples, respectively.

The recoveries of magnetite and high-titanium magnetite are shown in Figure 53. The values are similar to each other compared with data for the 3 mm screen. The highest losses occurred with the wet coal samples. High-titanium magnetite gave better results than magnetite for the wet coal samples. This could be due to a difference in surface properties of the two media.

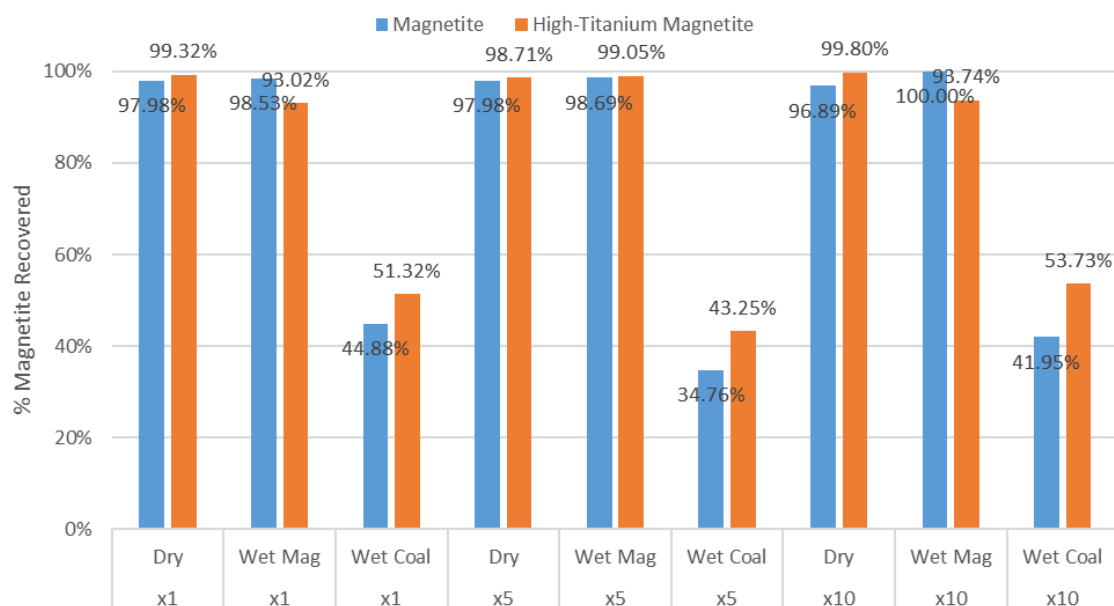


Figure 53: Recovery of magnetite and high-titanium magnetite using 13.2 mm screen

4.4.1.3. 3 mm high-frequency screen

The test work was repeated using a high-frequency screen with a 3 mm sieve. The results obtained for the magnetite recovery are shown in Table 15 in Appendix 5. The highest recovery was obtained from the x1 wet magnetite sample (96.18%) and the

lowest from the x1 wet coal sample (74.27%). The high-titanium magnetite results are shown in Table 16 in Appendix 5. The best results were obtained from the x5 wet magnetite (99.76%); the poorest recovery of 60.34% was obtained from the x1 wet coal sample.

The data from Table 15 and Table 16 in Appendix 5 are shown in Figure 54. The greatest losses occurred for the x1 wet coal sample. As the screening was repeated, the coal became drier and better results were achieved with the x5 wet coal samples.

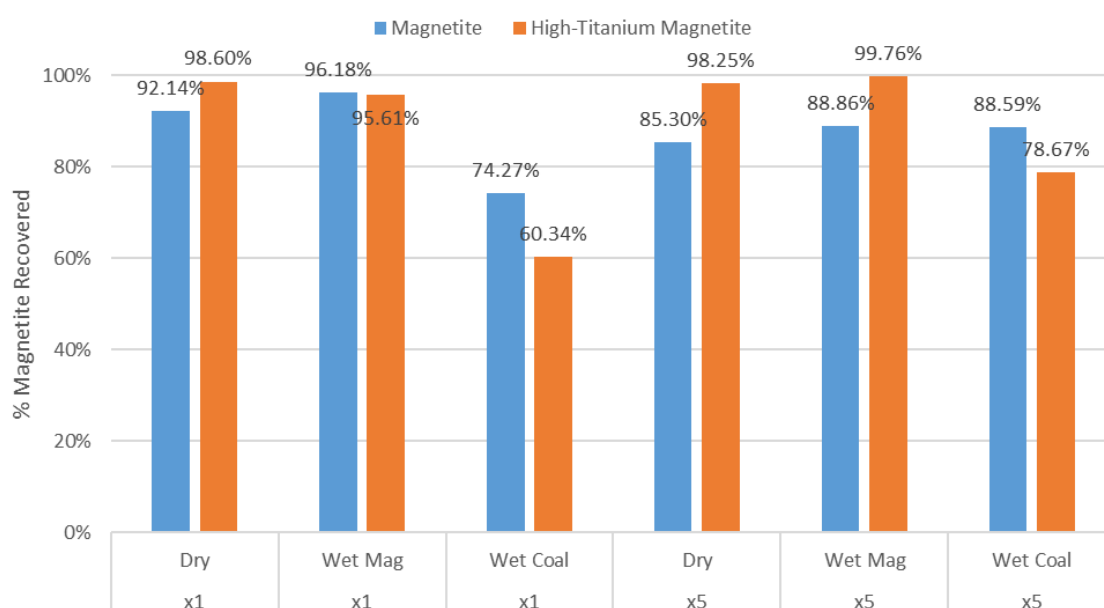


Figure 54: Recovery of magnetite and high-titanium magnetite using 3 mm high-frequency screen

4.4.1.4. Influence of moisture content on magnetic recovery in the magnetic fraction

The relationship between the recovery of magnetite and the surface moisture of the wet magnetite samples is shown in Figure 55. The surface moisture content varied between 3.9% and 4.4%, and the recovery of magnetite ranged between 88% and 100%. A lower surface moisture correlated with a higher recovery of magnetite. The lowest recovery was reported when using the high-frequency screen. This sample also had the highest surface moisture content.

The recovery of magnetite as a function of the surface moisture in the coal samples is plotted in Figure 56. The surface moisture varied between 3.5% and 5.5%, with magnetite recovery as low as 3% and as high as 88%. The high-frequency screen

gave the highest recovery when compared with samples of similar surface moisture content. The surface moisture of the coal was the most significant factor when compared with surface moisture of the magnetite. Wet coal mixed with dry magnetite caused the magnetite to stick to the coal; when wet magnetite was mixed with dry coal, high recoveries were still achieved.

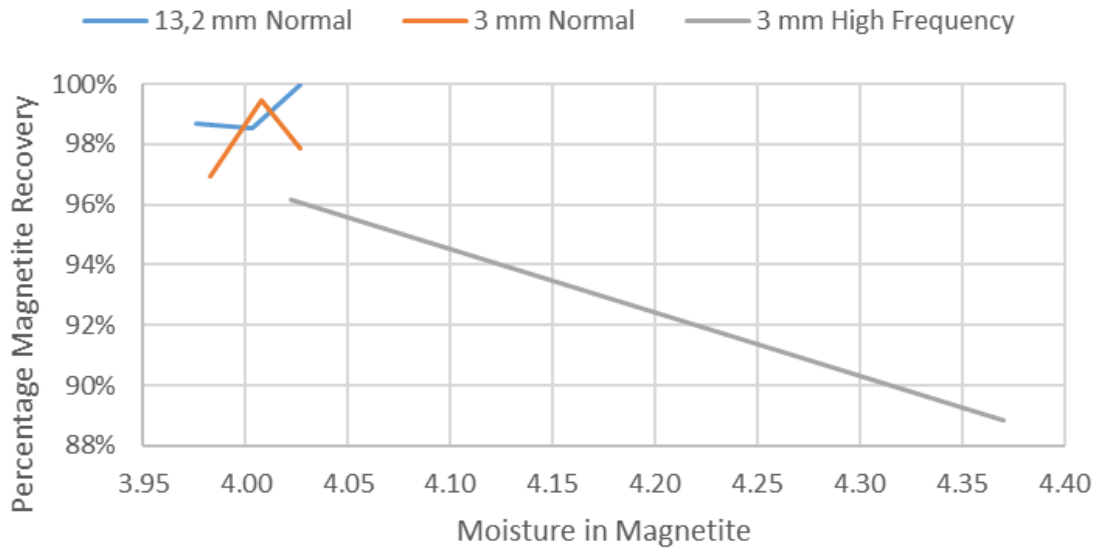


Figure 55: Magnetite recovery as a function of surface moisture of the magnetite

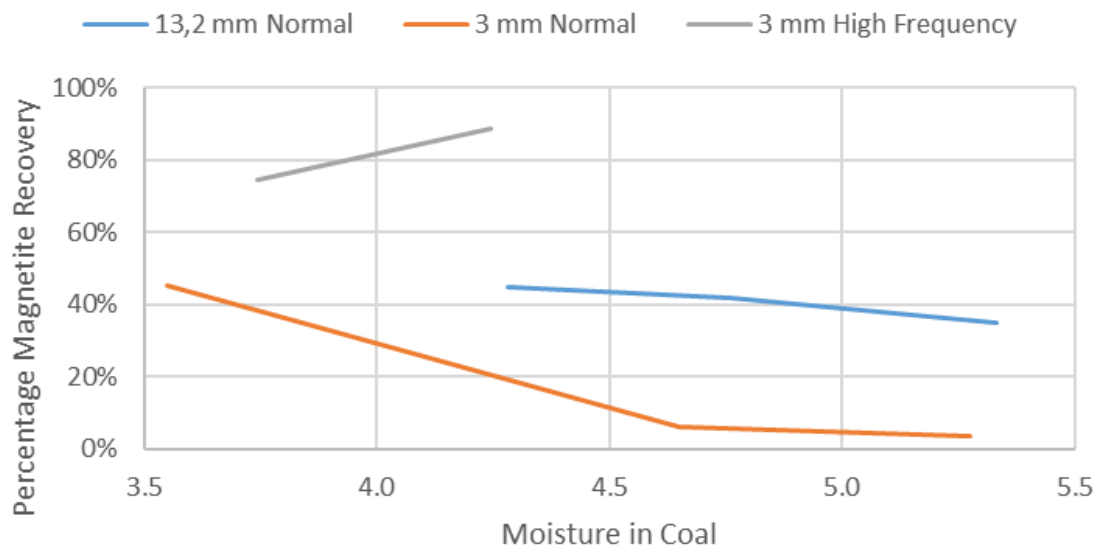


Figure 56: Magnetite recovery as a function of surface moisture of the coal

The effect of surface moisture of the high-titanium magnetite on its recovery is represented in Figure 57. The high-titanium media had higher recovery than the magnetite media. The surface moisture of the high-titanium magnetite was 3.9% to 4.2%, which was slightly less than the value of 4.4% of the magnetite samples, but the recovery was higher, falling between 92% and 100%.

The dependence of recovery of high-titanium magnetite on surface moisture of the coal sample is indicated in Figure 58. The highest recovery was measured for the sample with the highest surface moisture (6.6%) that was screened with the high-frequency screen. The coal samples dried while being screened by the high-frequency screen, which could have reduced the surface moisture and thereby increased the recovery. The surface moistures of the coal samples ranged from 4.6% to 6.6%; recovery of the high-titanium magnetite ranged from 21% to 78%.

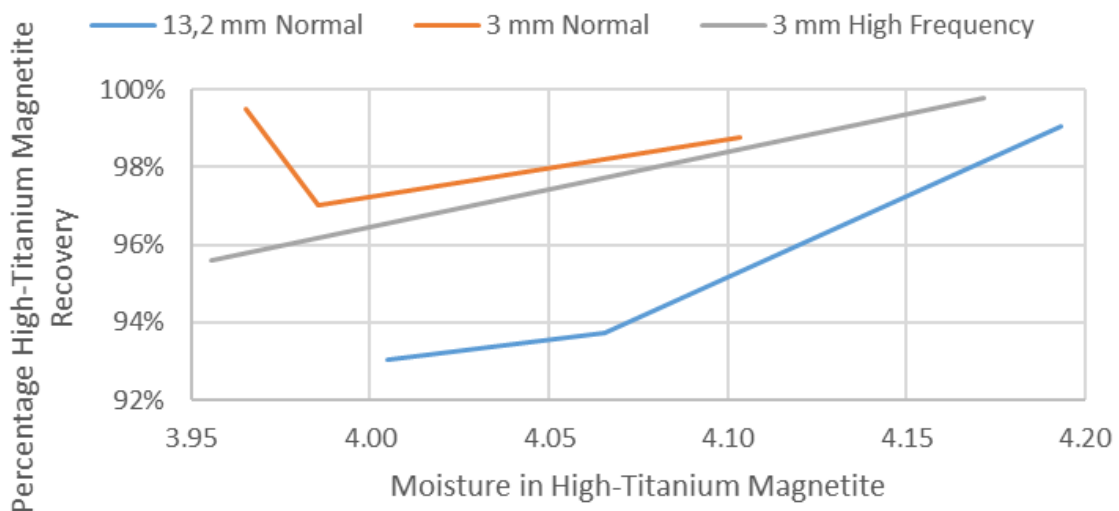


Figure 57: High-titanium magnetite recovery as a function of surface moisture of the high-titanium magnetite

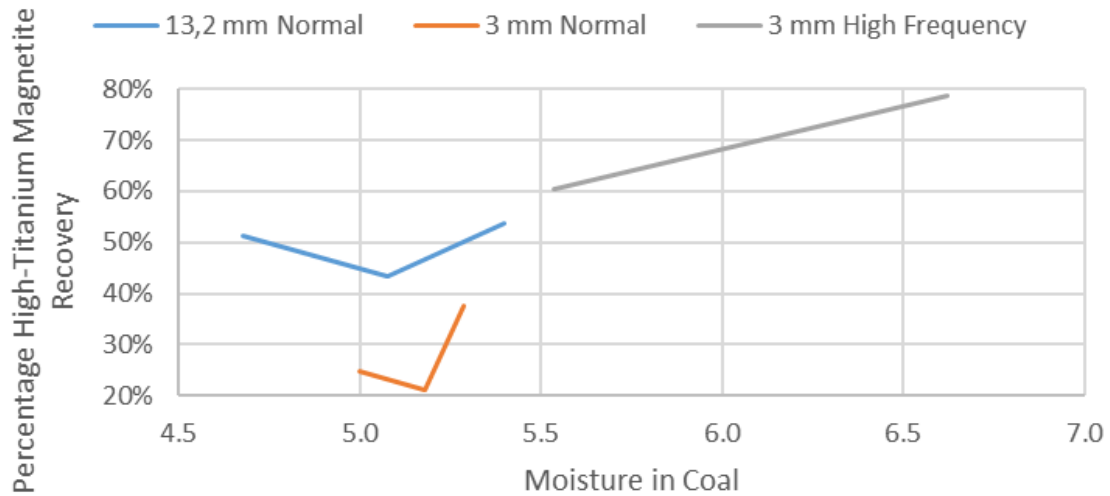


Figure 58: High-titanium magnetite recovery as a function of the surface moisture of the coal

The above results demonstrate that the surface moisture of the coal plays a large role in the losses of magnetite and high-titanium magnetite. Losses for the wet coal samples were higher than those of the wet magnetite samples. The magnetite performed slightly better than the high-titanium magnetite for the wet coal samples, with both media giving the highest recovery with the 3 mm high-frequency screen.

4.4.2. Recovery of magnetite in the magnetic, middling, and non-magnetic fractions

After the samples were washed in the magna chute, the masses of the magnetite and high-titanium magnetite were compared with their original feed masses. The magnetite recoveries to the undersize of all three screens of the magnetic and non-magnetic fractions are shown in Table 17 in Appendix 5. There were low quantities of magnetite in the non-magnetic fraction. The largest sample masses in the non-magnetics were obtained with the 13.2 mm screen, because this allowed for more coal in the undersize. Almost all of the samples had a small percentage of magnetite loss to the non-magnetic fraction. The magnetic fraction also included some non-magnetic material.

The same tests were repeated with the high-titanium magnetite: the results are shown in Table 18 in Appendix 5. Some losses occurred to the non-magnetic fraction and non-magnetic material was found in the magnetic fraction.

The data from Table 17 and Table 18 in Appendix 5 for the 3 mm screen are shown in Figure 59. The high-titanium magnetite yielded better results for the wet coal samples. The dry and wet samples gave similar results for the magnetite and high-titanium magnetite.

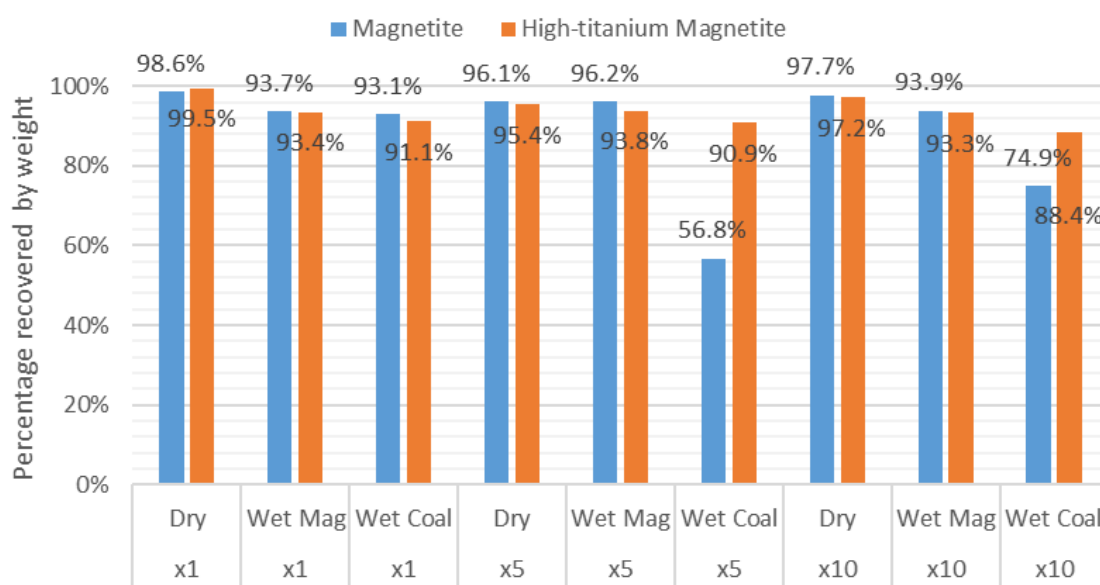


Figure 59: Percentages of magnetite and high-titanium magnetite deporting to the magnetic fraction (3 mm screen)

The results of Table 17 and Table 18 in Appendix 5 for the 13.2 mm screen are shown in Figure 60. High-titanium magnetite out-performed magnetite in the dry samples, so the samples contained less non-magnetic material. The high-titanium magnetite also out-performed the magnetite sample in the wet coal samples. Magnetite performed better for the wet medium samples.

Figure 61 summarises the results from the high-frequency screen. There were less non-magnetic particles in the magnetic samples recovered.

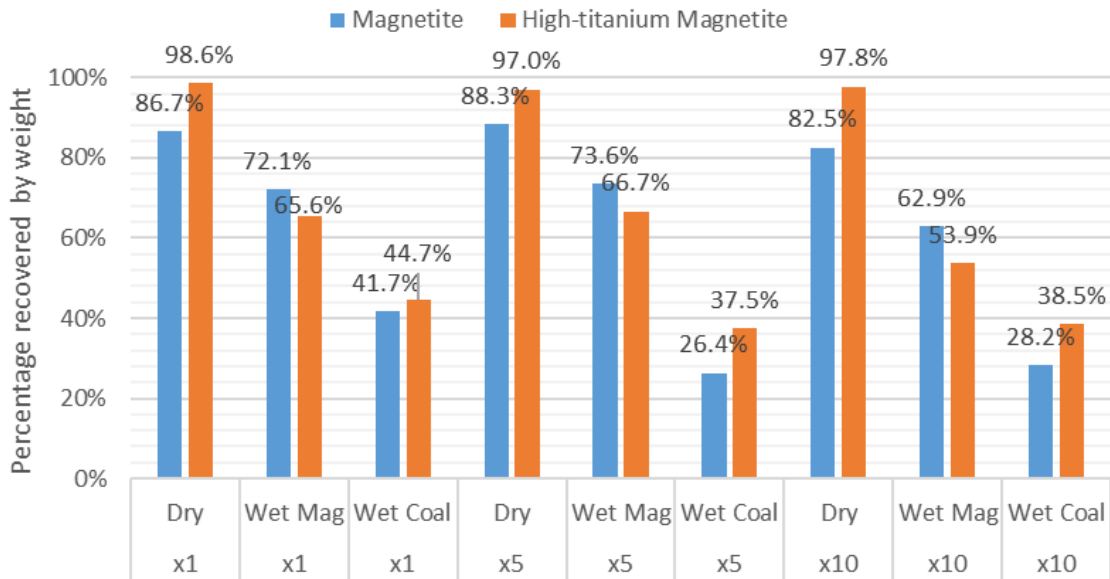


Figure 60: Percentage of magnetite and high-titanium magnetite deporting to the magnetic fraction (13.2 mm screen)

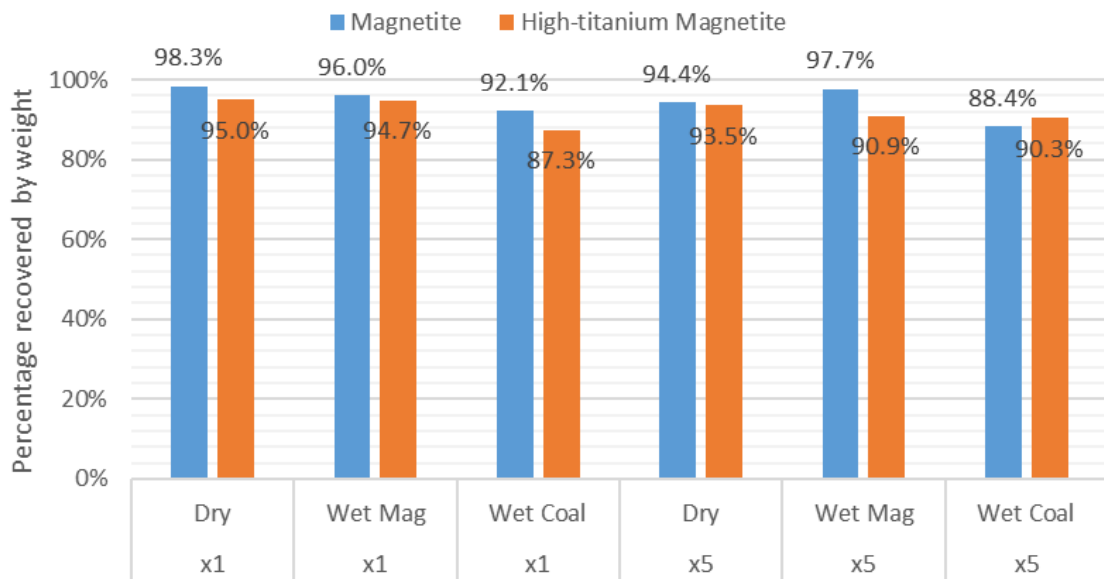


Figure 61: Percentage of magnetite and high-titanium magnetite deporting to the magnetic fraction (3 mm high-frequency screen)

The recovery of magnetite in the magnetic fraction as a function of the surface moisture content of the magnetite is indicated in Figure 62. The magnetite had a surface moisture between 3.9% and 4.4%; recoveries between 62% and 97.6% were reported. The 13.2 mm screen gave the lowest recovery, of between 62% and 73.6%

magnetite. The 3 mm and 3 mm high-frequency screens gave the highest recoveries of between 93.6% and 97.6% magnetite.

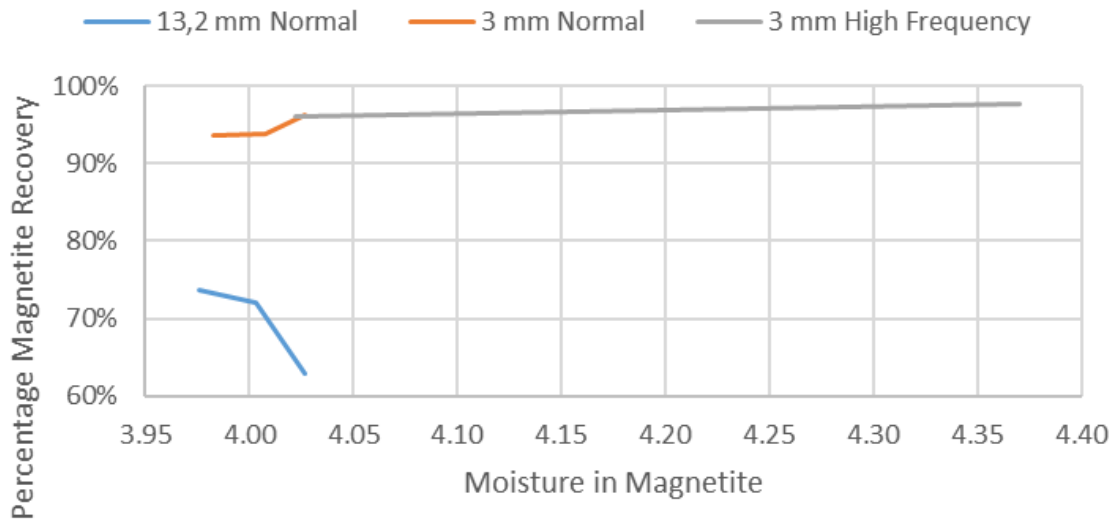


Figure 62: Effect of magnetite surface moisture on recovery of magnetite in the magnetic fraction

The effect of surface moisture of coal on the recovery of magnetite to the magnetic fraction is displayed in Figure 63. The surface moisture of the coal was between 3.7% and 5.3%. The 13.2 mm screen performed the most poorly of the three screens, giving recoveries between 26% and 41.7%. The 3 mm screen gave recoveries between 56% and 93%, and the high-frequency screen had the highest recovery, between 88% and 92%.

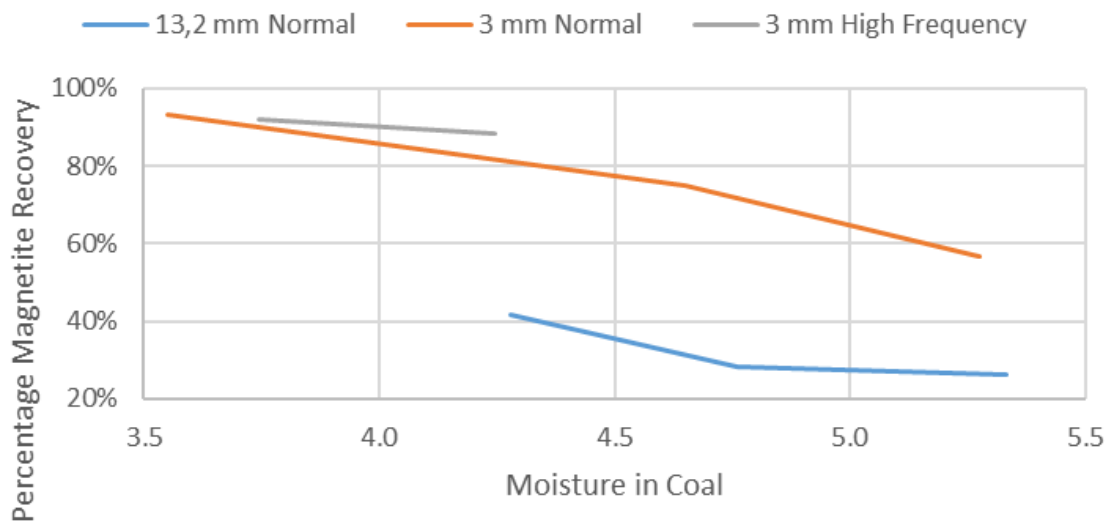


Figure 63: Coal surface moisture in comparison to recovery of magnetite in the magnetic fraction

The relationship between surface moisture and the recovery of high-titanium magnetite in the magnetic fraction is shown in Figure 64. The 3 mm screen samples had a surface moisture content of between 3.9% and 4.1%, whereas that of the high-frequency screen samples was between 3.9% and 4.17%. The 13.2 mm screen performed most poorly, giving a recovery between 53% and 66.6% and surface moisture contents between 4% and 4.19%. The 3 mm and 3 mm high-frequency screens gave recoveries above 90%.

The recovery of high-titanium magnetite in comparison with coal surface moisture is displayed in Figure 65. The surface moisture contents of the coal samples ranged from 4.7% to 6.6%. Both the 3 mm and 3 mm high-frequency screens gave recoveries above 88%, whereas the 13.2 mm screen had a recovery between 37% and 44.7%.

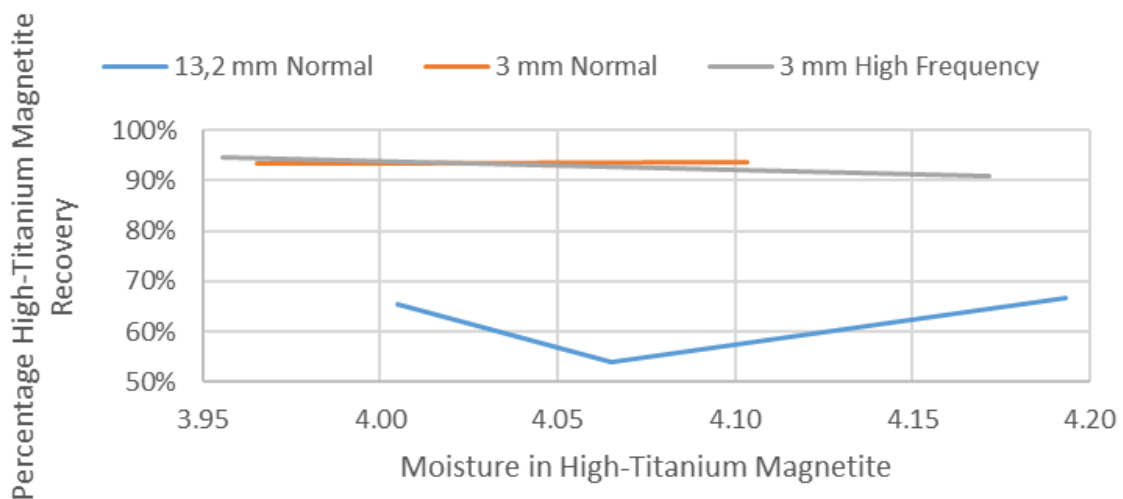


Figure 64: High-titanium magnetite surface moisture in comparison to recovery of high-titanium magnetite in the magnetic fraction

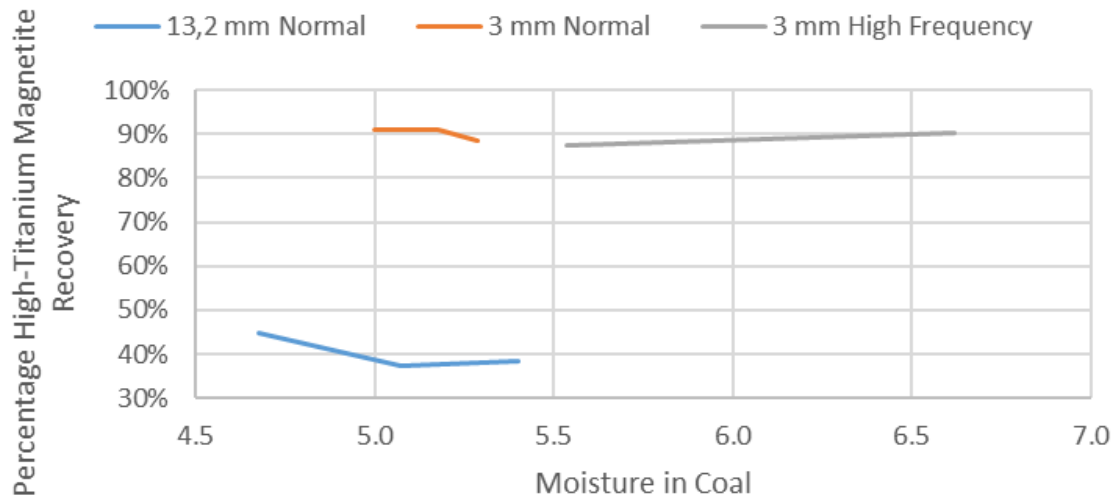


Figure 65: Coal surface moisture in comparison to recovery of high-titanium magnetite in the magnetic fraction

These results again confirmed that the surface moisture of coal played a significant role in the losses of both magnetite and high-titanium magnetite. Both media had relatively high recovery on the 3 mm and 3 mm high-frequency screens. Poor recovery was measured for the 13.2 mm screen for both the wet coal and wet magnetite samples.

4.4.3. Magnetite losses per tonne

Calculations were undertaken to extrapolate the data and calculate the loss of magnetite per tonne of coal for each of the samples discussed in Section 4.4.1. The losses of magnetite in the middlings and non-magnetic fractions were added. The media losses were calculated per tonne of coal. The results are summarized in Table 19 in Appendix 5 and shown in Figure 66 to Figure 68.

The highest losses for all three screens were measured for the wet coal samples. The highest losses of magnetite was recorded for the x5 (232.4 kg/t) and x10 (229.8 kg/t) wet coal samples with the 3 mm screen. The highest losses of high-titanium magnetite were found for the x1 (184.35 kg/t) and x5 (191.55 kg/t) wet coal samples using the 3 mm screen.

The lowest losses of magnetite were measured for the x5 dry (3 mm screen) and x10 wet (13.2 mm screen) magnetite samples, of 0.1 kg/t and 0.2 kg/t, respectively. The lowest losses of 0.49 kg/t of high-titanium magnetite occurred for the 13.2 mm x10 dry sample, and of 0.56 kg/t for the 3 mm high-frequency screen x5 wet sample.

The loss of magnetite per tonne of coal for the -13.2 mm size fraction is shown in Figure 66. The highest of magnetite losses occurred for the wet coal samples. The lowest losses were measured for the dry samples and the wet magnetite samples.

Losses on the -3 mm screen are shown in Figure 67. The highest losses occurred for the wet coal samples, as seen for the -13.2 mm size fraction. The high-titanium magnetite performed better than the magnetite in repetition of the tests.

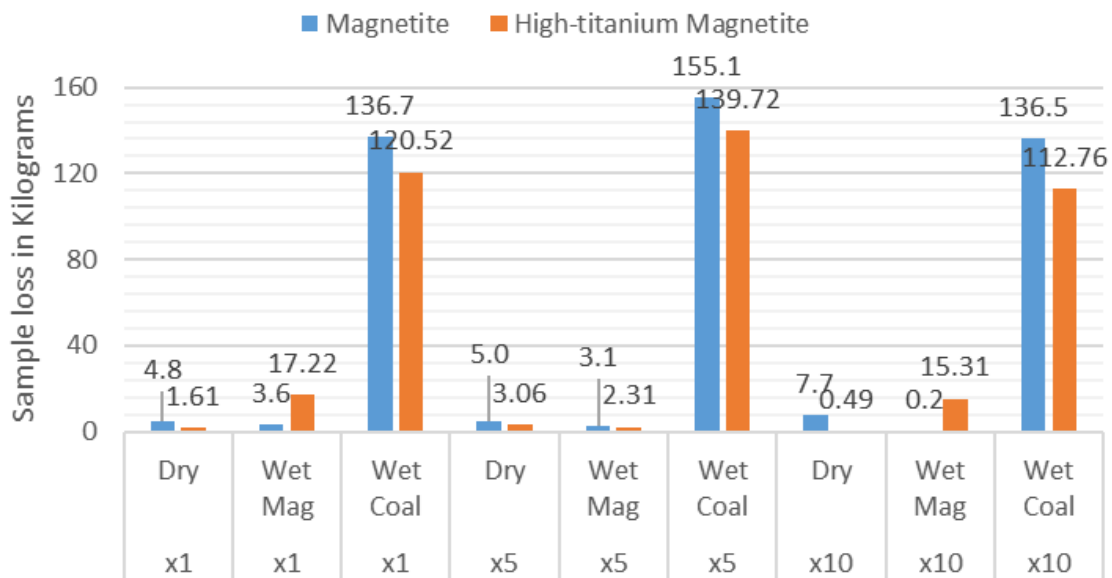


Figure 66: Loss of magnetite samples per tonne of coal for -13.2 mm screen

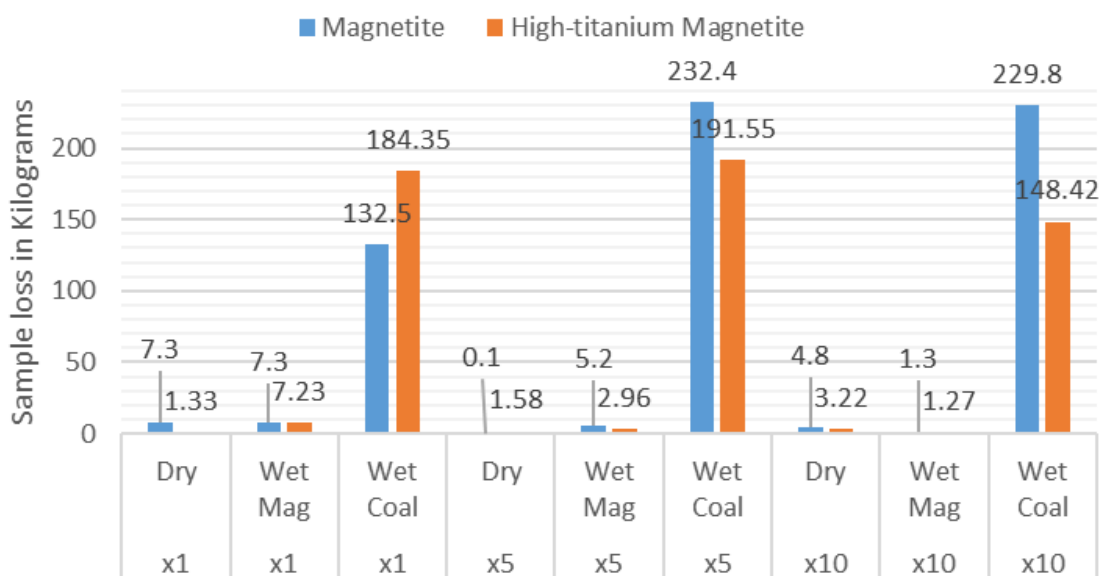


Figure 67: Loss of magnetite per tonne of coal for -3 mm screen

The high-frequency screen yielded the lowest loss for the wet coal samples (Figure 68). Although the losses were still significant, they were less than when using the other two screens. The high-frequency screen had higher losses for the dry samples and the wet magnetite samples. The surface moisture of the coal was a significant factor influencing the loss of magnetite.

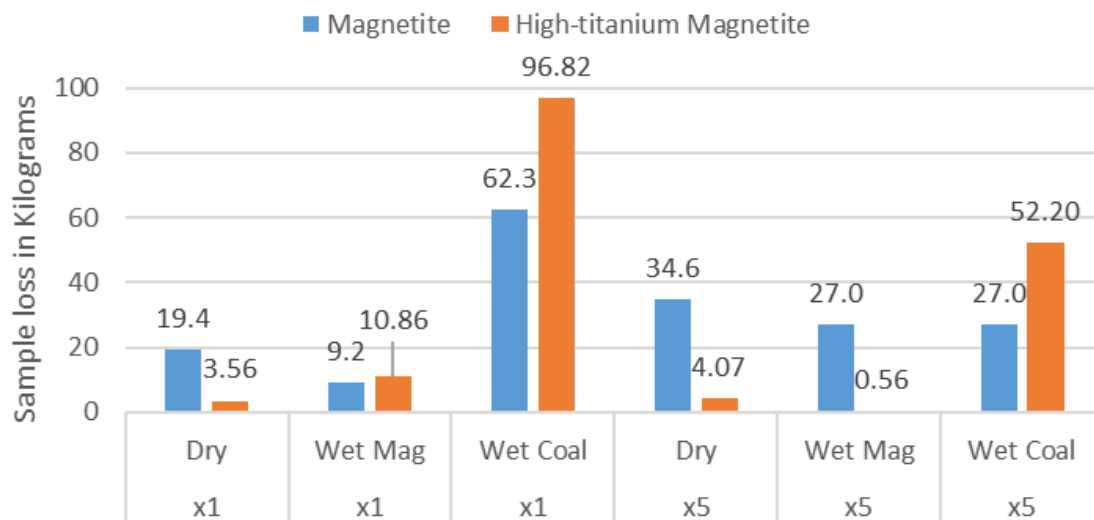


Figure 68: Loss of magnetite per tonne of coal for –3 mm high-frequency screen

The highest media losses were recorded for the wet coal samples, as summarised in Figure 69. The highest loss of magnetite was recorded with the 3 mm laboratory screen; the lowest magnetite loss occurred with the high-frequency screen.

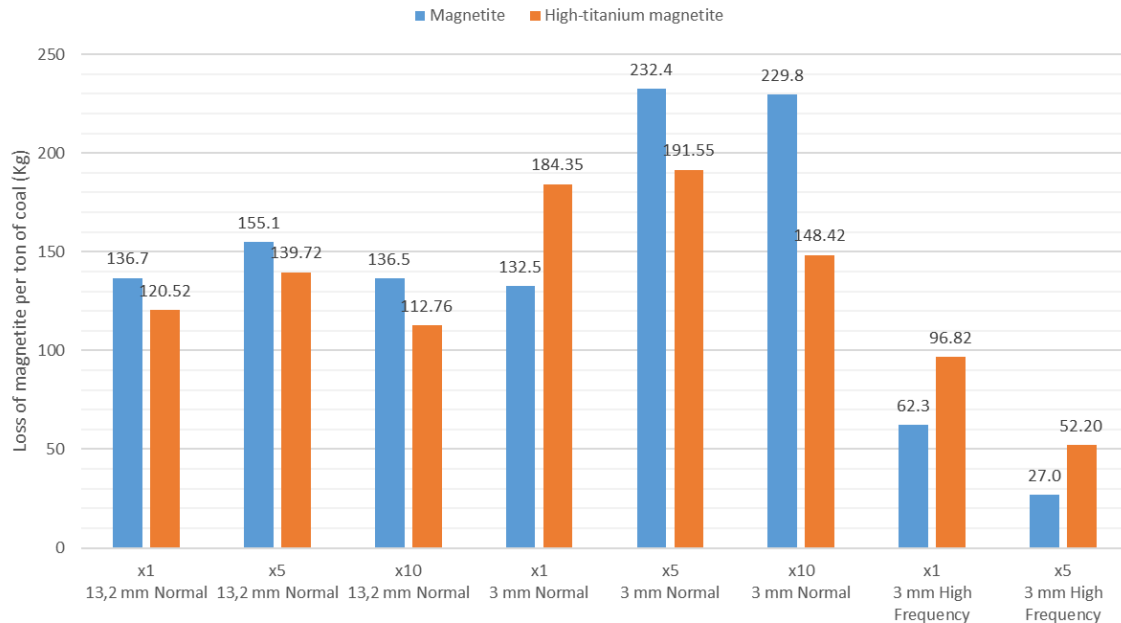


Figure 69: Loss of magnetite in wet coal samples

The highest losses per tonne occurred with the high-frequency screen (Figure 70). The losses ranged from 9.2 to 27 kg/t, with a magnetite surface moisture of between 4% and 4.37%. The lowest magnetite losses, of between 0.1 and 7.3 kg/t, occurred for the 3 mm and 13.2 mm screened samples, with the surface moisture ranging between 3.9% and 4.03%.

The magnetite loss compared with the surface moisture of the coal sample is displayed in Figure 71. This shows a different trend. The 3 mm screen had the highest magnetite losses, between 132.5 and 232.4 kg/t, and a surface moisture range between 3.5% and 5.3%. The 13.2 mm screen performed poorly, giving a loss between 136.5 and 155.1 kg of magnetite per tonne and a coal surface moisture between 4.3% and 5.3%. The high-frequency screen had the lowest magnetite losses of 27 to 62.3 kg/t and surface moisture of 3.7% to 4.2%.

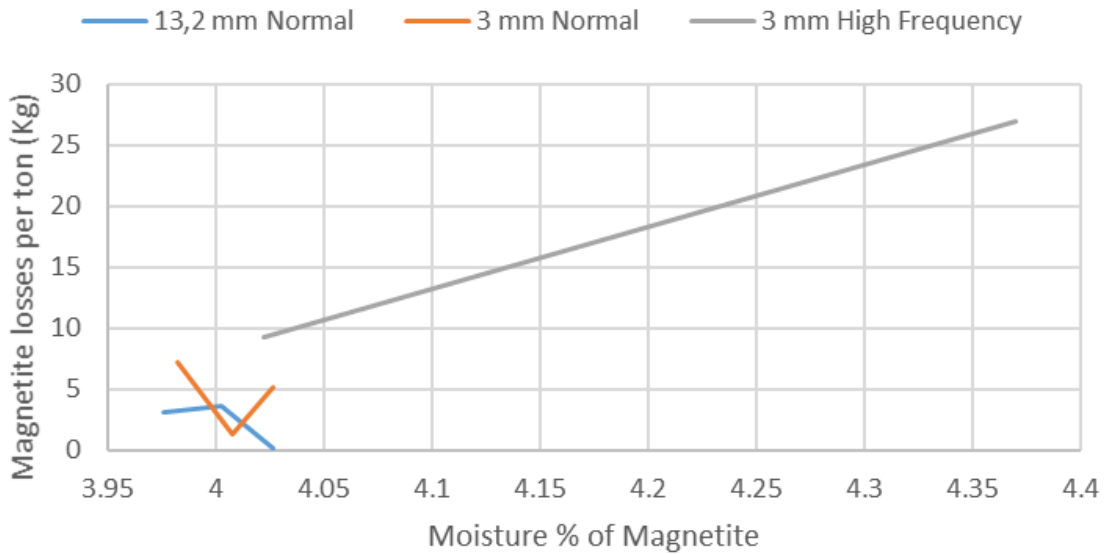


Figure 70: Loss of magnetite per tonne of coal as a function of moisture of the magnetite

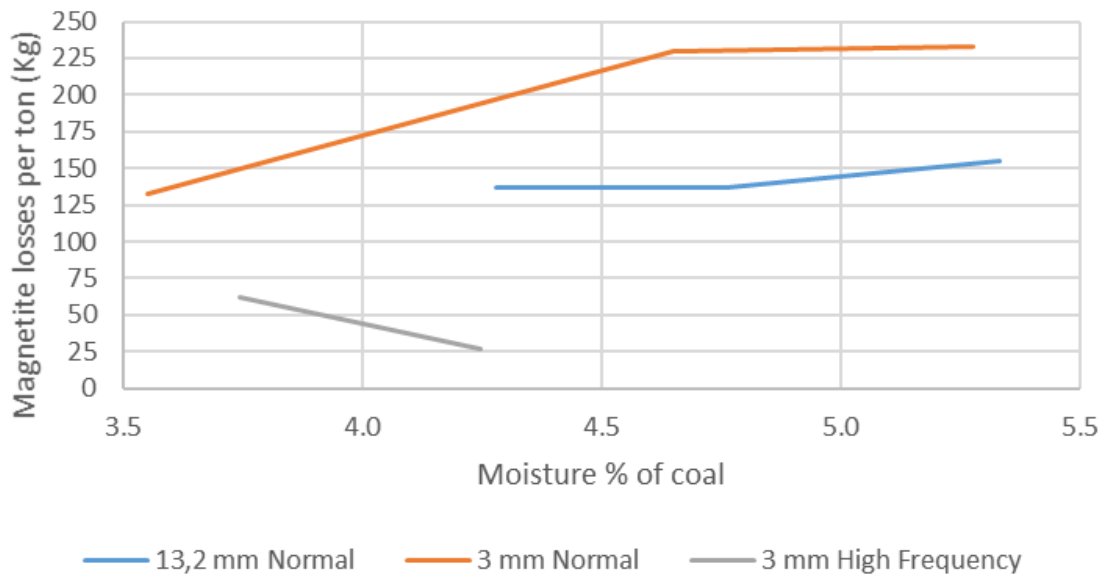


Figure 71: Loss of magnetite per tonne of coal as a function of moisture of the coal

In Figure 72, the loss of the high-titanium magnetite is compared with its surface moisture. The 13.2 mm screen gave the highest losses of between 2.31 and 17.22 kg/t and surface moisture between 4% and 4.19%. The high-frequency screen gave high-titanium magnetite losses in the range of 0.56 to 10.86 kg/t and surface moisture between 3.96% and 4.17%. The 3 mm screen gave high-titanium magnetite losses from 1.27 to 7.23 kg/t and surface moisture between 3.9% and 4.1%.

The effect of coal surface moisture on high-titanium magnetite losses is displayed in Figure 73. The highest losses were found for the 3 mm screen: 148–191.55 kg/t and surface moisture of the coal samples between 5% and 5.3%. Poor recovery was also found for the 13.2 mm screen, with losses between 112 and 139.7 kg/t, and surface moisture between 4% and 4.19%. The lowest losses were measured for the high-frequency screen samples, of 52 to 96.8 kg/t, and a surface moisture between 5.5% and 6.6%.

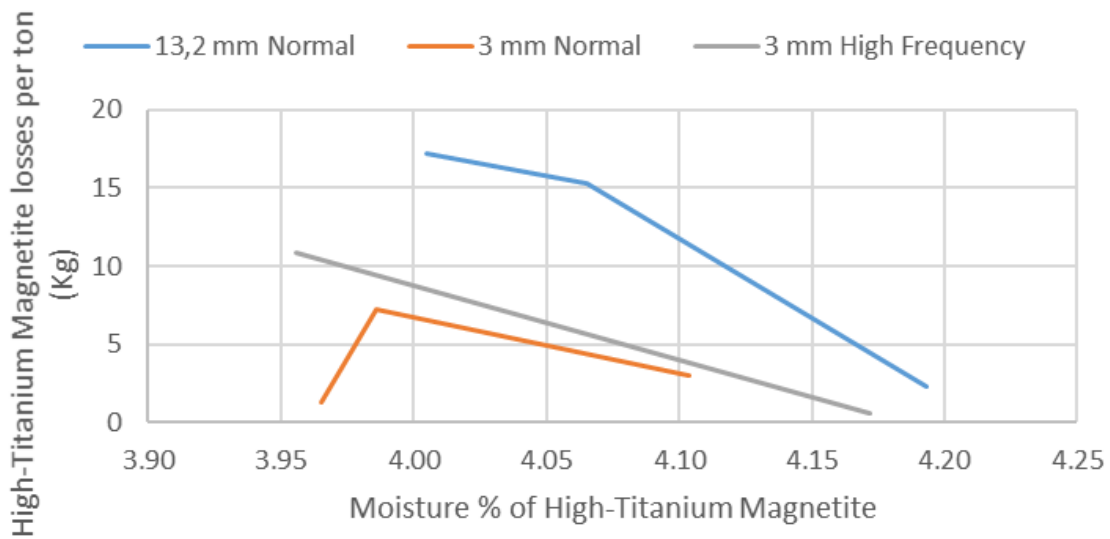


Figure 72: Loss of high-titanium magnetite per tonne as a function of surface moisture of the high-titanium magnetite

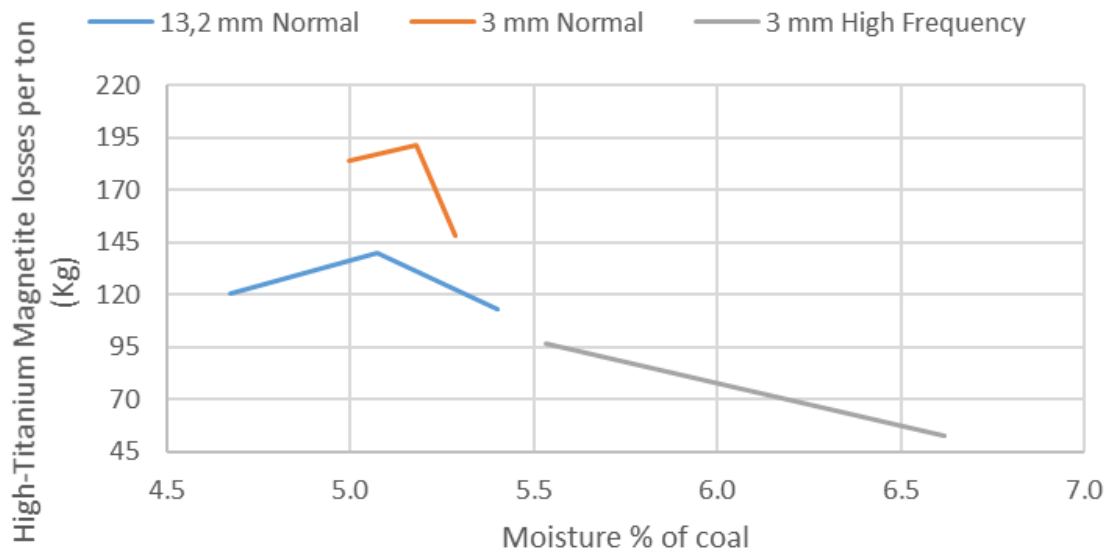


Figure 73: Loss of high-titanium magnetite per tonne as a function of surface moisture of the coal

4.4.4. Summary of the effect of moisture on media loss

Table 20 in Appendix 5 indicates the surface moistures of the magnetite and coal, and the corresponding magnetite sample loss per tonne of coal. The wet coal samples gave the highest magnetite losses.

A comparison of magnetite loss and its surface moisture is shown in Figure 74. The highest losses were obtained for the high-titanium magnetite samples. The highest moisture of 4.37% was measured for the x5 wet magnetite sample from the high-frequency screen. This sample also had the highest loss of magnetite (27.0%) which could be a possible outlier.

Losses of magnetite as a function of the surface moisture content of the coal are shown in Figure 75. The highest magnetite loss was observed for the magnetite sample, but the highest moisture content was observed with the high-titanium magnetite samples. The x5 high-titanium magnetite sample had the highest moisture content of the coal samples, with the second-lowest media loss.

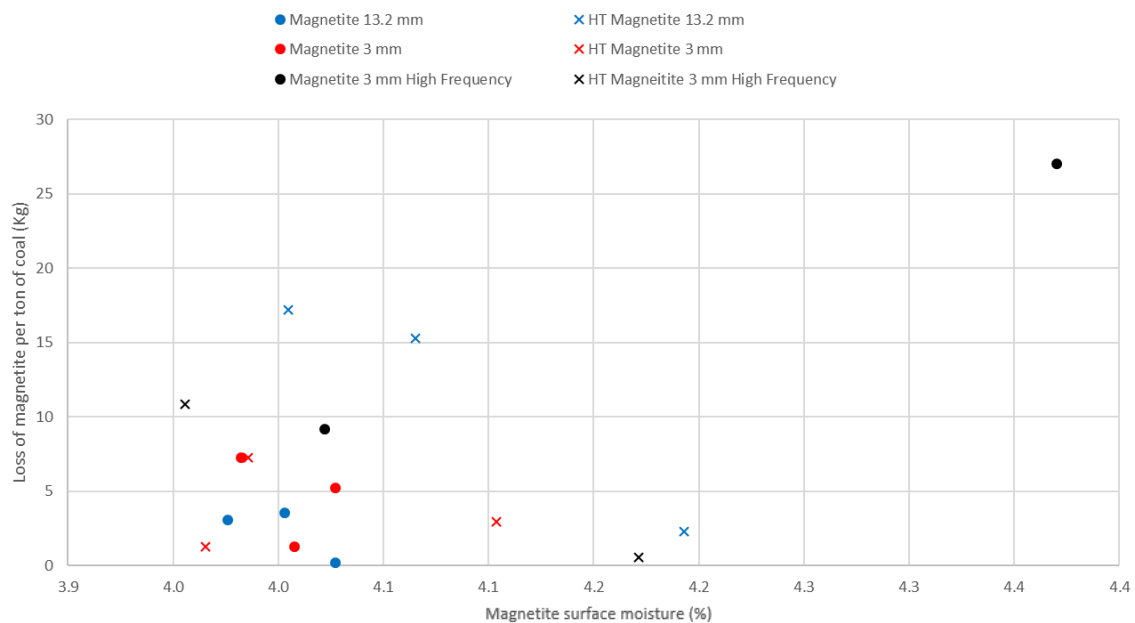


Figure 74: Loss of magnetite as a function of surface moisture of magnetite

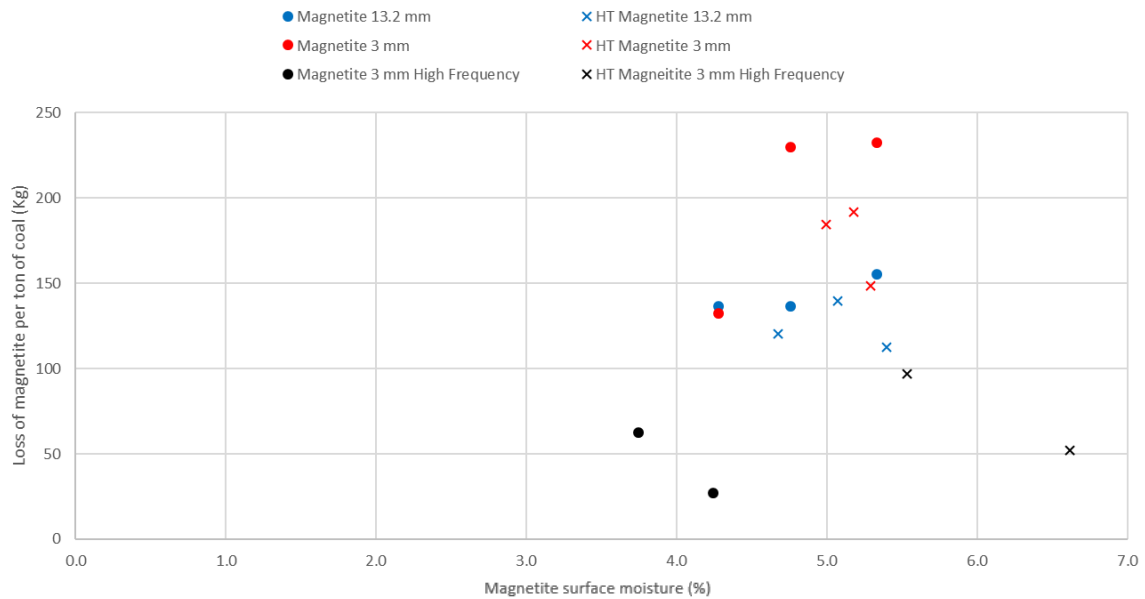


Figure 75: Loss of magnetite as a function of surface moisture of coal

A PSD test was run on the coal and magnetite samples to determine if the size range was similar to that of the materials used in the Bohou process. Although there is a difference in PSD results, the samples were similar enough to use for the test work. The mineralogical results indicated that the coal samples had a relatively low inert moisture, with the highest being the ROM sample (2.39%). It was also found that the coal samples contained kaolinite (a clay). The XRD results indicated that both the magnetite and high-titanium magnetite samples contained a mixture of magnetite and ilmenite. Figure 43 and Figure 44 show that the high-titanium magnetite sample contained more ilmenite than the magnetite sample.

In Phase 1, the dry samples (dry coal and magnetite) gave the highest recoveries of magnetite, with 93% recovered from the A13 sample and 92% recovered from the R13 sample. The highest losses were observed in the wet coal samples, with losses of 62% (A14) and 74% (R14).

A14 (wet coal) had a higher-than-expected magnetite percentage in the middlings. The high magnetite content may be due to nodules forming during screening. These nodules are made up of fine magnetite and coal particles that stick together.

The highest losses per tonne were found in the wet coal samples (A14 and R14). The A14 sample had a calculated loss of 89.63 kg/t and the R14 sample had a loss of 60.28 kg per tonne. The lowest losses were observed in the dry samples (dry coal and dry magnetite), with A13 having a loss of 13.02 kg per tonne and R13 having a loss of 14.10 kg per tonne.

In Phase 2, the performance of magnetite was compared with that of high-titanium magnetite. Three different screens were used. The high-titanium magnetite performed better with the 3 mm screen and the 3 mm high frequency screen. Both the magnetite and high-titanium magnetite performed similarly with the 13.2 mm screen. The high-titanium medium performed better with the wet coal samples than magnetite.

The highest losses were observed in the wet coal samples of both magnetite and high-titanium magnetite. The losses for the 13.2 mm screen were 155.1 kg per tonne for magnetite and 139.72 kg per tonne for high-titanium magnetite. The 3 mm screen showed losses of 232.4 kg per tonne magnetite and 191.55 kg per tonne high-titanium magnetite. The high frequency 3 mm screen gave losses of 62.3 kg per tonne magnetite and 96.8 kg per tonne high-titanium magnetite. Overall, the highest losses were found in the wet coal samples.

5. Conclusions

The objective of this study was to investigate the recovery of magnetite in the dry beneficiation of coal. The study has provided crucial information on selected factors that influence the magnetic recovery.

Magnetite is found in the PIC, with an estimation of resources that can be mined until 2040. Magnetite is used in the Bohou process, so it was selected as a medium for the study. High-titanium magnetite was collected from Namaqua Sands to compare its performance with that of magnetite from the PIC. QEMSCAN and SEM images showed that the magnetite particles had jagged edges, with clay adhering to the edges. The high-titanium magnetite particles were more rounded.

Coal samples were collected from Greenside Colliery in Witbank and New Denmark Colliery close to Secunda. The Greenside coal was used for Phase 1 of the test work and the New Denmark coal was used for Phase 2 of the investigation. The coal samples were screened at a size of 13.2 mm.

Magnetite was shown to be hydrophilic, with a contact angle that was unmeasurable. The PSD of magnetic sample showed 80% of the material passing 110 μm , which is finer than the equivalent values of 150 μm for the Shenhua magnetite and 200 μm for the high-titanium magnetite. Magnetite, clay, and coal were mixed and studied under the microscope. The clay attached to both the magnetite and coal.

From the initial study in Phase 1, it was determined that moisture plays an important role in the recovery of magnetite in dry beneficiation. The coal and magnetite samples were dried to remove the surface moisture and the coal screened to remove the 13.2 mm undersize. The coal and magnetite were mixed with water to add surface moisture to the samples. The samples were split into three categories: dry coal and magnetite; wet coal and dry magnetite; and dry coal and wet magnetite. The samples were screened once ($\times 1$), five times ($\times 5$), or ten times ($\times 10$) to determine any magnetite recovery changes with use. After the samples were screened at 13.2 mm, it was observed that the magnetite formed nodules. These comprised wet magnetite; in some cases, the nodules also contained small particles of coal.

The Phase 1 results showed that coal with a surface moisture above 1.4% resulted in large magnetite losses. This is problematic because the typical ROM coal surface moisture is much larger than this value (>5%). The dry coal and magnetite samples gave magnetite losses of less than 8%; the dry coal–wet magnetite samples gave a loss of less than 10%. The wet coal–dry magnetite systems gave magnetite losses exceeding 26%. Surface moisture of the coal had a strong impact on the magnetic loss than surface moisture of the magnetite.

In Phase 2, the study examined magnetite and high-titanium magnetite as media, as well as the use of three different screens (13.2 mm, 3 mm, and 3 mm high-frequency screens). The samples were prepared in the same manner as in Phase 1, with three categories: a dry coal and media; wet coal and dry media; and dry coal and wet media. A similar screening procedure was followed. The highest media losses occurred for the wet coal samples, as reported in the Phase 1 results. The lowest media recoveries (3.30% magnetite and 21.05% high-titanium magnetite) were obtained for the wet coal samples and the 13.2 mm screen. Losses for the wet coal samples were higher than for the wet media samples. Magnetite performed slightly better (74.27% recovery) than the high-titanium magnetite (60.34% recovery) for the wet coal samples, with the highest recoveries achieved with the 3 mm high-frequency screen.

The 3 mm screen gave the highest recovery for the dry samples and for the wet magnetite samples, although the high-frequency screen performed better for the wet coal samples. Overall recoveries from the high-frequency screen for the dry and wet magnetite samples were lower than for the conventional screens.

The high-frequency screen dried the coal samples more than the conventional screens, which could have had an effect on the media recoveries of the wet coal samples. The surface moisture of coal was recorded as a major contribution to the losses of magnetite and high-titanium magnetite in this test work.

In conclusion, this work has shown that magnetite can only be successfully recovered in the dry beneficiation of coal when the surface moisture is controlled to be less than 7% and by using a high-frequency screen.

6. Recommendations

It is advised that future testing be undertaken to investigate how to control the surface moisture on coal to avoid media losses.

Test work should be run on industrialized scale, because all test work in this study used small laboratory screens and a small high-frequency screen.

Coal samples with higher clay content should also be investigated to determine the effect of clay over time on the media losses.

Additional test work should be done on the degrading of the magnetite during the re-using of the magnetite.

Bibliography

- Akbari, H., Zhang, B., Sayeh, M., Mohanty, M., & Rahimi, S. (2012). *Application of Neural Network for Modeling the Coal Cleaning Performance of the FGX Dry Separator*. Colorado: Society for Mining Metallurgy and Exploration, Inc. (SME).
- Alexander, P. (2007). Women and coal mining in India and South Africa, c1900-1940. *African Studies*, 66(2-3), 201-222.
- Ambrós, W. M., Cazacliu, B. G., & Sampaio, C. H. (2016). Wall effects on particle separation in air jigs. *Powder Technology*, 301, 369-378.
- Ambrós, W. M., Sampaio, C. H., Cazacliu, B. G., Miltzarek, G. L., & Miranda, L. R. (2017). Usage of air jiggling for multi-component separation of construction and demolition waste. *Waste Management*, 60, 75-83.
- Asthana, H., & Sarkar, S. (1969). Coal cleaning in fluidized bed. *Chemical Ages of India*, 20, 792-796.
- ASTM D2234/D2234M-16. (2016). *Standard Practice for Collection of a Gross Sample of Coal*. West Conshohocken, PA: ASTM International.
- ASTM D3286. (1996). *Standard Test Method for Gross Calorific Value of Coal and Coke by the Isoperibol Bomb Calorimeter*. West Conshohocken, PA: ASTM International.
- ASTM D3302/D3302M-17. (2017). *Standard Test Method for Total Moisture in Coal*. West Conshohocken, PA: ASTM International.
- ASTM D4749-87. (2012). *Standard Test Method for Performing the Sieve Analysis of Coal and Designating Coal Size*. West Conshohocken, PA: ASTM International.
- ASTM D5142. (2009). *Standard Test Methods for Proximate Analysis of the Analysis Sample of Coal and Coke by Instrumental Procedures*. West Conshohocken, PA: ASTM International.
- Basson, I., Lourens, P., Paetzold, H.-D., Thomas, S., Brazier, R., & Molabe, P. (2017). Structural analysis and 3D modelling of major mineralizing structures at the Phalaborwa copper deposit. *Ore Geology Reviews*, 83, 30-42.
- Baudoin, M.-A., Vogel, C., Nortje, K., & Naik, M. (2017). Living with drought in South Africa: lessons learnt from the recent El Niño drought period. *International journal of disaster risk reduction*, 23, 128-137.
- Borrok, D. M., Kelsner, S. E., Boer, R. H., & Essene, E. J. (1998). The Vergenoeg magnetite-fluorite deposit, South Africa; support for a hydrothermal model for massive iron oxide deposits. *Economic Geology*, 93(5), 564-586.
- Butcher, A., Helms, T., Gottlieb, P., Bateman, R., Ellis, S., & Johnson, N. (2000). *Advances in the quantification of gold deportment by QEMSCAN*. Paper presented at the Seventh Mill Operators Conference, Kalgoorlie, WA, The Australasian Institute of Mining and Metallurgy.

- Cadle, A., Cairncross, B., Christie, A., & Roberts, D. (1993). The Karoo Basin of South Africa: type basin for the coal-bearing deposits of southern Africa. *International Journal of Coal Geology*, 23(1-4), 117-157.
- Carelse, C. (2012). *Mineralogy and Provenance of the Namakwa Sands Heavy Mineral Satellite Deposits*. (Doctoral dissertation), Stellenbosch: Stellenbosch University.
- Catuneanu, O., Wopfner, H., Eriksson, P., Cairncross, B., Rubidge, B., Smith, R., & Hancox, P. (2005). The Karoo basins of south-central Africa. *Journal of African Earth Sciences*, 43(1-3), 211-253.
- Chagwedera, K., Bada, S., & Falcon, R. (2018). Evaluation of alternative solid media for coal beneficiation using an air dense-medium fluidized bed. *Journal of the Southern African Institute of Mining and Metallurgy*, 118(8), 883-890.
- Chen, Q., & Wei, L. (2003). Coal dry beneficiation technology in China: The state-of-the-art. *China Particuology*, 1(2), 52-56.
- Chen, Q., & Yang, Y. (2003). Development of dry beneficiation of coal in China. *Coal Preparation*, 23(1-2), 3-12.
- Clark, D., & Emerson, D. (1991). Notes on rock magnetization characteristics in applied geophysical studies. *Exploration Geophysics*, 22(3), 547-555.
- Coetzee, C. B., Toerien, D. K., & Groeneveld, D. (1957). *Ilmeniethoudende Sand Langs die Weskus in die Distrik Vanrhynsdorp*: Geologiese Opname, Departement Mynwese, Unie van Suid-Afrika.
- Coulter, T. (1957). *The history and development of coal washing in South Africa*. Retrieved from Pretoria:
- De Korte, G. (2013). *Dry processing versus dense medium processing for preparing thermal coal*. Paper presented at the 17th International Coal Preparation Congress, Istanbul, Turkey.
- de Korte, G. (2015). Processing low-grade coal to produce high-grade products. *Journal of the Southern African Institute of Mining and Metallurgy*, 115(7), 569-572.
- Dean, R. S., & Davis, C. W. (1941). *Magnetic separation of ores*: US Government Printing Office.
- Dey, U., Mishra, S., Dutta, S., & Tiwary, S. (1997). *Efficient Use of Magnetite in Coal Beneficiation Plants for Heavy Media Separation-A case study*. Paper presented at the Proceedings Prof-97.
- Douglas, E., & Walsh, T. (1966). New type of dry heavy medium gravity separator. *Transactions of the Institution of Mining and Metallurgy Section C*, 75, 226-232.
- Drzymala, J. (1994). Hydrophobicity and collectorless flotation of inorganic materials. *Advances in Colloid and Interface Science*, 50, 143-185.
- Drzymala, J. (2007). *Mineral Processing: Foundations of Theory and Practice of Minerallurgy*: University of Technology.

- Dwari, R., & Rao, K. H. (2007). Dry beneficiation of coal—a review. *Mineral Processing and Extractive Metallurgy Review*, 28(3), 177-234.
- Eberhard, A. (2011). The future of South African coal: Market, investment and policy challenges. *Program on energy and sustainable development*, 1-44.
- Elvers, B., & Ullmann, F. (1990). *Ullmann's encyclopedia of industrial chemistry* (Vol. A16). New Jersey, USA: VCH.
- Eriksson, S. (1989). Phalaborwa: a saga of magmatism, metasomatism and miscibility *Carbonatites: Genesis and Evolution* (pp. 221-254): Unwin Hyman, London.
- Fan, M., Chen, Q., Zhao, Y., & Luo, Z. (2001). Fine coal (6–1 mm) separation in magnetically stabilized fluidized beds. *International Journal of Mineral Processing*, 63(4), 225-232.
- Fraas, F. (1973). Alternating current matrix-type magnetic separator. *Bureau of Mines Report of Investigations*(7746).
- Fraser, T., & Yancey, H. (1925). Transactions of the American Institute of Mining and Metallurgical Engineers
- Goldstein, J. I., Newbury, D. E., Michael, J. R., Ritchie, N. W., Scott, J. H. J., & Joy, D. C. (2017). *Scanning Electron Microscopy and X-ray Microanalysis*: Springer.
- Götz, A. E., Ruckwied, K., & Wheeler, A. (2018). Marine flooding surfaces recorded in Permian black shales and coal deposits of the Main Karoo Basin (South Africa): Implications for basin dynamics and cross-basin correlation. *International Journal of Coal Geology*, 190, 178-190.
- Groves, D. I., & Vielreicher, N. M. (2001). The Phalaborwa (Palabora) carbonatite-hosted magnetite–copper sulfide deposit, South Africa: an end-member of the iron-oxide copper–gold–rare earth element deposit group? *Mineralium Deposita*, 36(2), 189-194. doi:10.1007/s001260050298
- Gupta, A., & Yan, D. S. (2016). *Mineral Processing Design and Operations: an Introduction*: Elsevier.
- Hancox, P. J., & Götz, A. E. (2014). South Africa's coalfields—A 2014 perspective. *International Journal of Coal Geology*, 132, 170-254.
- Hand, P. E., England, T., Michael, D.C., Falcon, L.M. & Yell, A.D. (2002). *Coal Preparation in South Africa*. Johannesburg: The South African Coal Processing Society.
- Harney, D. M., Merkle, R. K., & Von Gruenewaldt, G. (1990). Platinum-group element behavior in the lower part of the upper zone, eastern Bushveld Complex; implications for the formation of the main magnetite layer. *Economic Geology*, 85(8), 1777-1789.
- Howie, R., Zussman, J., & Deer, W. (1992). *An Introduction to the Rock-Forming Minerals*: Longman.
- Johnson, M., Anhaeuser, C., & Thomas, R. J. (2006). *The Geology of South Africa*. Johannesburg: Geological Society of South Africa.

- Kalenda, T. (2017). *Evaluation of ilmenite as a possible medium in a dry dense medium fluidized bed*. (Master of Science), University of Pretoria.
- Kalenda, T., North, B., & Naude, N. (2019). Evaluation of ilmenite as dense medium for dry coal fluidized bed beneficiation. *Mineral Processing and Extractive Metallurgy Review*, 40(5), 323-332.
- Kim, H. K., Amouzegar, M. A., & Ao, S.-I. (2015). *Transactions on Engineering Technologies: World Congress on Engineering and Computer Science 2014*. San Francisco, USA: Springer.
- Klein, C., Dutrow, B., Dana, J. D., & Klein, C. (2002). *Manual of mineral science*. New York: Wiley.
- Klemm, D., Henckel, J., Dehm, R., & Von Gruenewaldt, G. (1985). The geochemistry of titanomagnetite in magnetite layers and their host rocks of the eastern Bushveld Complex. *Economic Geology*, 80(4), 1075-1088.
- Klemm, D., Snelthage, R., Dehm, R., Henckel, J., & Schmidt-Thome, R. (1982). *The formation of chromite and titanomagnetite deposits within the Bushveld Igneous Complex*. Berlin, Heidelberg: Springer.
- Klug, H. P., & Alexander, L. E. (1974). X-ray diffraction procedures: for polycrystalline and amorphous materials. *X-Ray Diffraction Procedures: For Polycrystalline and Amorphous Materials, 2nd Edition.*, 992.
- Knowles, L. C. A. K., C. M. (1936). *The Economic Development Of The British Overseas Empire* (Vol. 3). London: George Routledge And Sons, Limited.
- Kramer, A., Gaulocher, S., Martins, M., & Leal Filho, L. (2012). Surface tension measurement for optimization of flotation control. *Procedia Engineering*, 46, 111-118.
- Kumar, D., & Kumar, D. (2018). *Sustainable Management of Coal Preparation*. Cambridge, England: Woodhead Publishing.
- Langner, D. J. (2016). *The Dry Beneficiation of Duff Coal in a Dense Medium Fluidised Bed*. (Masters of Chemical Engineering), North-West University (South Africa), Potchefstroom Campus.
- Le Roux, M., Campbell, Q., & Langner, D. (2016). Destoning of fine coal in a fluidized bed. *XVIII International Coal Preparation Congress*, 1125-1130.
- Lohn, P. (1971). Fluidized bed heavy medium separation-A modern dry separation procedure. *Aufbereitung Technik*, 3, 140-146.
- Luo, Z.-F., Zhu, J.-F., Fan, M.-M., Zhao, Y.-M., & Tao, X.-X. (2007). Low density dry coal beneficiation using an air dense medium fluidized bed. *Journal of China University of Mining and Technology*, 17(3), 306-309.
- Luo, Z., Fan, M., Zhao, Y., Tao, X., Chen, Q., & Chen, Z. (2008). Density-dependent separation of dry fine coal in a vibrated fluidized bed. *Powder Technology*, 187(2), 119-123.

- Lurie, J. (1977). *South African geology for Mining, Metallurgical, Hydrological and Civil Engineering*. Johannesburg: McGraw-Hill.
- Mayoral, M., Izquierdo, M., Andrés, J., & Rubio, B. (2001). Different approaches to proximate analysis by thermogravimetry analysis. *Thermochimica Acta*, 370(1-2), 91-97.
- McCarthy, T. (2013). *The Story of Earth & Life: a Southern African Perspective on a 4.6-Billion-Year Journey*. Cape Town, South Africa: Penguin Random House
- Mogodi, P. (2012). *Analysis of energy consumption, economics and management at New Denmark Colliery*. (Masters of Science), University of the Witwatersrand, Johannesburg.
- Mohanta, S., Rao, C., Daram, A., Chakraborty, S., & Meikap, B. (2013). Air dense medium fluidized bed for dry beneficiation of coal: Technological challenges for future. *Particulate Science and Technology*, 31(1), 16-27.
- Nefedov, R. A., Orlov, V. V., Medvedev, R. O., Sachkova, A. S., & Sachkov, V. I. (2018). Hydrometallurgical processing technology of titanomagnetite ores.
- Noble, A., & Luttrell, G. H. (2015). A review of state-of-the-art processing operations in coal preparation. *International Journal of Mining Science and Technology*, 25(4), 511-521.
- Norrgran, D., & Orlich, J. (1988). Fundamentals of high-intensity magnetic separation as applied to industrial minerals. *Minerals & Metallurgical Processing*, 5(1), 1-11.
- North, B. C., Engelbrecht, A. D., Oboirien Bilainu, O., De la Rey, J., & Mashinini, L. (2017). Fluidized bed dry dense medium coal beneficiation. *Industrial Fluidization South Africa*, 1, 1-7.
- Oberteuffer, J. (1974). Magnetic separation: A review of principles, devices, and applications. *IEEE Transactions on Magnetics*, 10(2), 223-238.
- Ootaki, T., & Wolken, J. (1973). Octahedral crystals in Phycomyces. II. *The Journal of cell biology*, 57(2), 278-288.
- Parker, M. R. (1977). The physics of magnetic separation. *Contemporary physics*, 18(3), 279-306.
- Peatfield, D. (2003). Coal and coal preparation in South Africa-A 2002 review. *Journal of the Southern African Institute of Mining and Metallurgy*, 103(6), 355-372.
- Peng, Z., Moghtaderi, B., & Doroodchi, E. (2017). A simple model for predicting solid concentration distribution in binary-solid liquid fluidized beds. *AIChE Journal*, 63(2), 469-484.
- Philander, C., & Rozendaal, A. (2015). Geology of the Cenozoic Namakwa Sands heavy mineral deposit, west coast of South Africa: A world-class resource of titanium and zircon. *Economic Geology*, 110(6), 1577-1623.
- Pinetown, K. L., Ward, C. R., & Van der Westhuizen, W. (2007). Quantitative evaluation of minerals in coal deposits in the Witbank and Highveld Coalfields, and the potential impact on acid mine drainage. *International Journal of Coal Geology*, 70(1-3), 166-183.

- Pinheiro, H., Pretorius, C., Boshoff, H., & Barker, O. (1999). A techno-economic and historical review of the South African coal industry in the 19th and 20th centuries and analyses of coal product samples of South African collieries 1998–1999. *SABS Bulletin*, 113, 97.
- Ratshomo, K. (2014). *South Africa's Iron Ore Industry Developments, 2004-2013*. Retrieved from www.dmr.gov.za
- Robben, C., De Korte, J., Wotruba, H., & Robben, M. (2014). Experiences in dry coarse coal separation using X-ray-transmission-based sorting. *International Journal of Coal Preparation and Utilization*, 34(3-4), 210-219.
- Robl, T., Oberlink, A., & Jones, R. (2017). *Coal Combustion Products (CCPs): Characteristics, Utilization and Beneficiation*. Cambridge, England: Woodhead Publishing.
- Sachkov, V. I., Nefedov, R. A., Orlov, V. V., Medvedev, R. O., & Sachkova, A. S. (2018). Hydrometallurgical processing technology of titanomagnetite ores. *Minerals*, 8(1), 2-12.
- Sanders, G. J. (2007). *The Principles of Coal Preparation* (Vol. 130): Australian Coal Preparation Society Dangar, New South Wales.
- Simpson, J., Hunter, S., & Aytug, T. (2015). Superhydrophobic materials and coatings: A review. *Reports on progress in physics. Physical Society (Great Britain)*, 78, 086501. doi:10.1088/0034-4885/78/8/086501
- Sinatra, F. L. (2010). *Understanding the interaction between blood flow and an applied magnetic field*. (Graduate Theses and Dissertation Graduate Theses and Dissertation), University of South Florida.
- Snyman, C., & Botha, W. (1993). Coal in south Africa. *Journal of African Earth Sciences (and the Middle East)*, 16(1-2), 171-180.
- Solovova, I., Ryabchikov, I., Kogarko, L., & Kononkova, N. (1998). Inclusions in minerals of the Palaborwa carbonatite complex, South Africa. *Geochemistry international*, 36(5), 377-388.
- Southwood, M., & Cairncross, B. (2017). The minerals of Palabora, Limpopo Province, South Africa. *Rocks & Minerals*, 92(5), 426-453.
- Speight, J. G. (2015). *Handbook of Coal Analysis*. Hoboken, New Jersey: John Wiley & Sons.
- Surmon, M. (2019). *Draft Consolidated Environmental Management Programme. Amended to include the Proposed expansion of Mining Right MRC117 and Smelter Retrofit Project (1650800-314566-4)*. Retrieved from Johannesburg, South Africa:
- Svoboda, J. (2004). *Magnetic Techniques for the Treatment of Materials*. Dordrecht: Springer Science & Business Media.
- Tang, K., Lv, X., Wu, S., Xuan, S., Huang, X., & Bai, C. (2018). Measurement for contact angle of iron ore particles and water. *ISIJ International*, 58(3), 379-400.

- Tiwary, R. (2001). Environmental impact of coal mining on water regime and its management. *Water, Air, and Soil Pollution*, 132(1-2), 185-199.
- Utembe, W., Faustman, E., Matatiele, P., & Gulumian, M. (2015). Hazards identified and the need for health risk assessment in the South African mining industry. *Human & experimental toxicology*, 34(12), 1212-1221.
- Van der Merwe, N. J., & Scully, R. T. (1971). The Phalaborwa story: Archaeological and ethnographic investigation of a South African iron age group. *World Archaeology*, 3(2), 178-196.
- van Vollenhoven, A. (2017). *A report on a cultural heritage impact assessment for the proposed relocation of 3 x 400kv power lines at the landau 3 colliery, close to Emalahleni, Mpumalanga Province* (AE01724V). Retrieved from Johannesburg, South Africa: <https://sahris.sahra.org.za/>
- Vielreicher, N. M., Groves, D. I., & Vielreicher, R. M. (2000). The Phalaborwa (Palabora) deposit and its potential connection to iron-oxide copper-gold deposits of Olympic Dam Type. *Hydrothermal Iron-Oxide Copper-Gold and Related Deposits. A Global Perspective*, 1, 321-329.
- Von Ketelhodt, L., & Bergmann, C. (2010). Dual energy X-ray transmission sorting of coal. *Journal of the Southern African Institute of Mining and Metallurgy*, 110(7), 371-378.
- Wei, L., Chen, Q., & Zhao, Y. (2003). Formation of double-density fluidized bed and application in dry coal beneficiation. *Coal Preparation*, 23(1-2), 21-32.
- Weinstein, R., & Snoby, R. (2007). Advances in dry jigging improves coal quality. *Mining Engineering*, 59(1), 29-34.
- Weintraub, M., Deurbrouck, A., & Thomas, R. (1979). *Dry-cleaning coal in a fluidized bed medium*. Retrieved from
- Whitten, D. (1972). *The Penguin Dictionary of Geology*. Harmondsworth, England: Brooks, JRV.
- Wills, B. A., & Finch, J. (2015). *Wills' Mineral Processing Technology: an Introduction to the Practical Aspects of Ore Treatment and Mineral Recovery*. Great Britain: Butterworth-Heinemann.
- Wilson, M., & Anhaeusser, C. (1998a). *The Mineral Resources of South Africa*. South Africa: Council for Geoscience.
- Wilson, M., & Anhaeusser, C. (1998b). *The mineral resources of South Africa*(Handbook 16).
- Zhang, B., Akbari, H., Yang, F., Mohanty, M., & Hirschi, J. (2011). Performance optimization of the FGX dry separator for cleaning high-sulfur coal. *International Journal of Coal Preparation and Utilization*, 31(3-4), 161-186.
- Zhenfu, L., & Qingru, C. (2001). Dry beneficiation technology of coal with an air dense-medium fluidized bed. *International Journal of Mineral Processing*, 63(3), 167-175.
- Zhu, Q. (2014). *Coal sampling and analysis standards* (CCC/235). Retrieved from London, United Kingdom:

Appendix 1

Calorific values of coal samples

| Name | Mass (g) | CV (MJ/Kg) | Method |
|----------|----------|------------|---------------|
| COAL ROM | 0.9664 | 18.1697 | ASTM D5865-12 |
| COAL AFE | 0.9655 | 14.2982 | ASTM D5865-12 |

X-ray diffraction analysis of ROM and AFE coal samples

| ROM 1 | | | ROM 2 | | | AVERAGE | | |
|-----------|-------|------------------|-----------|-------|------------------|-----------|-------|------------------|
| | mass% | 3 σ error | | mass% | 3 σ error | | mass% | 3 σ error |
| Calcite | 8.52 | 2.1 | Calcite | 2.23 | 1.17 | Calcite | 5.38 | 1.64 |
| Dolomite | 0 | 0 | Dolomite | 0 | 0 | Dolomite | 0 | 0 |
| Kaolinite | 66.98 | 2.7 | Kaolinite | 73.58 | 2.28 | Kaolinite | 70.28 | 2.49 |
| Quartz | 24.5 | 1.98 | Quartz | 24.2 | 2.13 | Quartz | 24.35 | 2.06 |

| AFE 1 | | | AFE 2 | | | AVERAGE | | |
|-----------|-------|------------------|-----------|-------|------------------|-----------|-------|------------------|
| | mass% | 3 σ error | | mass% | 3 σ error | | mass% | 3 σ error |
| Calcite | 10.66 | 1.38 | Calcite | 11.06 | 1.14 | Calcite | 10.86 | 1.26 |
| Dolomite | 9.53 | 1.41 | Dolomite | 13.98 | 1.5 | Dolomite | 12 | 1 |
| Kaolinite | 57.91 | 2.13 | Kaolinite | 48.2 | 1.92 | Kaolinite | 53.06 | 2.03 |
| Quartz | 21.9 | 1.83 | Quartz | 19.94 | 1.47 | Quartz | 20.92 | 1.65 |
| | | | Siderite | 6.82 | 1.11 | Siderite | 6.82 | 1.11 |



Appendix 2

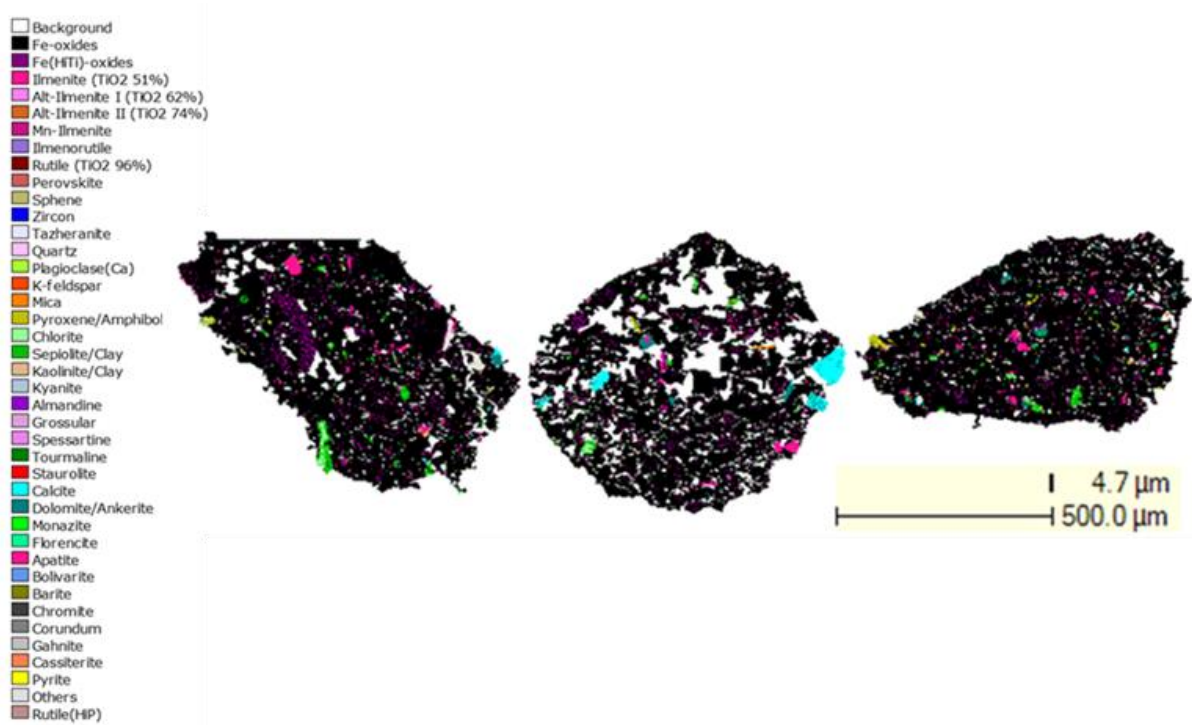


Figure 76: QEMSCAN image of magnetite

Appendix 3

Table 9: Total recovery of magnetite during initial test work.

| Sample ID | Original magnetite mass (g) | Magnetic fraction | | Middling fraction | | Non-magnetic fraction | | Total | | |
|---------------------|-----------------------------|-------------------------|-------------------------|-------------------------|-------------------------|-------------------------|-------------------------|------------------------|--------------------|--------------------|
| | | Recovered magnetite (g) | Recovered magnetite (%) | Recovered magnetite (g) | Recovered magnetite (%) | Recovered magnetite (g) | Recovered magnetite (%) | Magnetite recovery (%) | Magnetite loss (g) | Magnetite loss (%) |
| A13 - Dry sample | 372.99 | 346.01 | 92.96 | 0.14 | 0.04 | 0.73 | 0.20 | 93 | 26.11 | 7 |
| A14 - Wet coal | 373.38 | 229.51 | 86.02 | 1.25 | 0.47 | 1.54 | 0.58 | 62 | 141.08 | 38 |
| A15 - Wet magnetite | 372.89 | 335.93 | 90.79 | 0.47 | 0.13 | 0.32 | 0.09 | 90 | 36.17 | 10 |
| R13 - Dry sample | 373.78 | 345.02 | 88.83 | 0.34 | 0.09 | 0.32 | 0.08 | 92 | 28.10 | 8 |
| R14 - Wet coal | 373.27 | 273.93 | 81.92 | 1.11 | 0.33 | 1.67 | 0.50 | 74 | 96.56 | 26 |
| R15 - Wet magnetite | 372.93 | 333.73 | 89.30 | 0.4 | 0.11 | 0.08 | 0.02 | 90 | 38.72 | 10 |

Table 10: Recovery of magnetite in different fractions

| Sample ID | Magnetic fraction | | | Middling fraction | | | Non-magnetic fraction | | |
|---------------------|-------------------|-------------------------|-------------------------------------|-------------------|-------------------------|-------------------------------------|-----------------------|-------------------------|-------------------------------------|
| | Sample mass (g) | Recovered magnetite (g) | Contained magnetite in recovery (%) | Sample mass (g) | Recovered magnetite (g) | Contained magnetite in recovery (%) | Sample mass (g) | Recovered magnetite (g) | Contained magnetite in recovery (%) |
| A13 - Dry sample | 372.2 | 346.01 | 93.0 | 17.3 | 0.14 | 0.8 | 190.8 | 0.73 | 0.4 |
| A14 - Wet coal | 266.8 | 229.51 | 86.0 | 4.2 | 1.25 | 29.8 | 25.6 | 1.54 | 6.0 |
| A15 - Wet magnetite | 370 | 335.93 | 90.8 | 7.4 | 0.47 | 6.4 | 107.7 | 0.32 | 0.3 |
| R13 - Dry sample | 388.4 | 345.02 | 88.8 | 17.6 | 0.34 | 1.9 | 98.5 | 0.32 | 0.3 |
| R14 - Wet coal | 334.4 | 273.93 | 81.9 | 9.1 | 1.11 | 12.2 | 25.3 | 1.67 | 6.6 |
| R15 - Wet magnetite | 373.7 | 333.73 | 89.3 | 8.8 | 0.4 | 4.52 | 84.2 | 0.08 | 0.1 |

Appendix 4

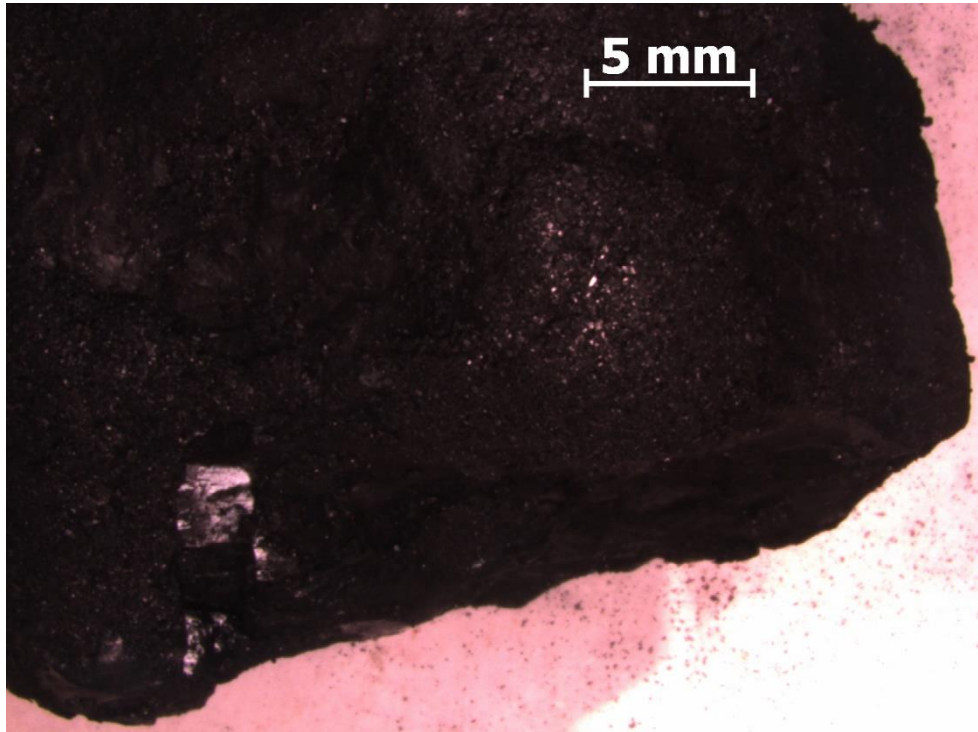


Figure 77: Microscope image of agnetite sticking to the surface moisture of coal

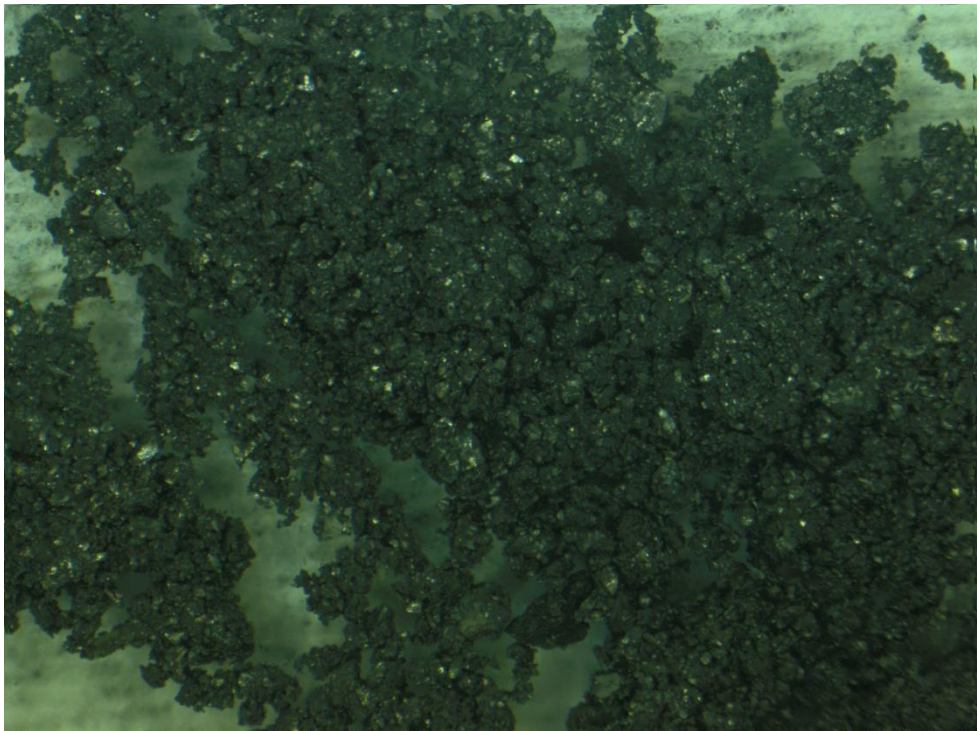


Figure 78: Clumps of magnetite and fine wet coal magnified at 1.25x



Appendix 5

Table 11: Magnetite recovery with 3 mm screen

| Repetitions | Method | Name | Original magnetite mass (g) | Magnetic fraction | | Non-magnetic fraction | | Total | | |
|-------------|----------|--------|-----------------------------|-------------------------|-------------------------|-------------------------|-------------------------|------------------------|--------------------|--------------------|
| | | | | Recovered magnetite (g) | Recovered magnetite (%) | Recovered magnetite (g) | Recovered magnetite (%) | Magnetite recovery (%) | Magnetite loss (g) | Magnetite loss (%) |
| ×1 | Dry | Bag 10 | 250.9 | 242.8 | 96.77 | 0.3 | 0.12 | 96.89 | 7.8 | 3.11 |
| ×1 | Wet mag | Bag 11 | 253.6 | 245.7 | 96.88 | 0.2 | 0.08 | 96.96 | 7.7 | 3.04 |
| ×1 | Wet coal | Bag 12 | 251.2 | 113.4 | 45.14 | 0.6 | 0.24 | 45.38 | 137.2 | 54.62 |
| ×5 | Dry | Bag 13 | 251 | 250.7 | 99.88 | 0.2 | 0.08 | 99.96 | 0.1 | 0.04 |
| ×5 | Wet mag | Bag 14 | 250.8 | 245.3 | 97.81 | 0.2 | 0.08 | 97.89 | 5.3 | 2.11 |
| ×5 | Wet coal | Bag 15 | 254.5 | 8.4 | 3.30 | 0 | 0.00 | 3.30 | 246.1 | 96.70 |
| ×10 | Dry | Bag 16 | 254.6 | 249.5 | 98.00 | 0.2 | 0.08 | 98.08 | 4.9 | 1.92 |
| ×10 | Wet mag | Bag 17 | 254.5 | 252.5 | 99.21 | 0.7 | 0.28 | 99.49 | 1.3 | 0.51 |
| ×10 | Wet coal | Bag 18 | 252.7 | 14.9 | 5.90 | 0 | 0.00 | 5.90 | 237.8 | 94.10 |

Table 12: High-titanium magnetite recovery with 3 mm screen

| Repetitions | Method | Name | Original magnetite mass (g) | Magnetic fraction | | Non-magnetic fraction | | Total | | |
|-------------|----------|--------|-----------------------------|----------------------------|----------------------------|----------------------------|----------------------------|---------------------------|-----------------------|-----------------------|
| | | | | Recovered HT magnetite (g) | Recovered HT magnetite (%) | Recovered HT magnetite (g) | Recovered HT magnetite (%) | HT magnetite recovery (%) | HT Magnetite loss (g) | HT magnetite loss (%) |
| ×1 | Dry | Bag 37 | 256.3 | 251.3 | 98.05 | 3.6 | 1.40 | 99.45 | 1.4 | 0.55 |
| ×1 | Wet mag | Bag 38 | 250.9 | 241.6 | 96.29 | 1.8 | 0.72 | 97.01 | 7.5 | 2.99 |
| ×1 | Wet coal | Bag 39 | 255.1 | 62.4 | 24.46 | 0.7 | 0.27 | 24.74 | 192 | 75.26 |
| ×5 | Dry | Bag 40 | 251.5 | 248.9 | 98.97 | 1 | 0.40 | 99.36 | 1.6 | 0.64 |
| ×5 | Wet mag | Bag 41 | 251 | 247.8 | 98.73 | 0.1 | 0.04 | 98.76 | 3.1 | 1.24 |
| ×5 | Wet coal | Bag 42 | 255.5 | 53.7 | 21.02 | 0 | 0.00 | 21.02 | 201.8 | 78.98 |
| ×10 | Dry | Bag 43 | 255.7 | 251.5 | 98.36 | 0.7 | 0.27 | 98.63 | 3.5 | 1.37 |
| ×10 | Wet mag | Bag 44 | 254.7 | 252.7 | 99.21 | 0.7 | 0.27 | 99.49 | 1.3 | 0.51 |
| ×10 | Wet coal | Bag 45 | 253.3 | 94.9 | 37.47 | 0.2 | 0.08 | 37.54 | 158.2 | 62.46 |



Table 13: Magnetite recovery with 13.2 mm screen

| Repetitions | Method | Name | Original magnetite mass (g) | Magnetic fraction | | Non-magnetic fraction | | Total | | |
|-------------|----------|-------|-----------------------------|-------------------------|-------------------------|-------------------------|-------------------------|------------------------|--------------------|--------------------|
| | | | | Recovered magnetite (g) | Recovered magnetite (%) | Recovered magnetite (g) | Recovered magnetite (%) | Magnetite recovery (%) | Magnetite loss (g) | Magnetite loss (%) |
| ×1 | Dry | Bag 1 | 252.5 | 246.6 | 97.66 | 0.8 | 0.32 | 97.98 | 5.1 | 2.02 |
| ×1 | Wet mag | Bag 2 | 252.3 | 247.2 | 97.98 | 1.4 | 0.55 | 98.53 | 3.7 | 1.47 |
| ×1 | Wet coal | Bag 3 | 250.9 | 111.6 | 44.48 | 1 | 0.40 | 44.88 | 138.3 | 55.12 |
| ×5 | Dry | Bag 4 | 252.9 | 247.2 | 97.75 | 0.6 | 0.24 | 97.98 | 5.1 | 2.02 |
| ×5 | Wet mag | Bag 5 | 251.5 | 245.5 | 97.61 | 2.7 | 1.07 | 98.69 | 3.3 | 1.31 |
| ×5 | Wet coal | Bag 6 | 251.7 | 87.5 | 34.76 | 0 | 0.00 | 34.76 | 164.2 | 65.24 |
| ×10 | Dry | Bag 7 | 254.2 | 245.8 | 96.70 | 0.5 | 0.20 | 96.89 | 7.9 | 3.11 |
| ×10 | Wet mag | Bag 8 | 250.8 | 250.1 | 99.72 | 0.7 | 0.28 | 100.00 | 0.00 | 0.00 |
| ×10 | Wet coal | Bag 9 | 251.5 | 105.2 | 41.83 | 0.3 | 0.12 | 41.95% | 146 | 58.05 |

Table 14: Recovery of high-titanium magnetite with 13.2 mm screen

| Repetitions | Method | Name | Original magnetite mass (g) | Magnetic fraction | | Non-magnetic fraction | | Total | | |
|-------------|----------|--------|-----------------------------|----------------------------|----------------------------|----------------------------|----------------------------|---------------------------|-----------------------|-----------------------|
| | | | | Recovered HT magnetite (g) | Recovered HT magnetite (%) | Recovered HT magnetite (g) | Recovered HT magnetite (%) | HT magnetite recovery (%) | HT Magnetite Loss (g) | HT magnetite loss (%) |
| ×1 | Dry | Bag 28 | 250.9 | 245.6 | 97.89 | 3.6 | 1.43 | 99.32 | 1.7 | 0.68 |
| ×1 | Wet mag | Bag 29 | 252.2 | 231.8 | 91.91 | 2.8 | 1.11 | 93.02 | 17.6 | 6.98 |
| ×1 | Wet coal | Bag 30 | 250.6 | 126.8 | 50.60 | 1.8 | 0.72 | 51.32 | 122 | 48.68 |
| ×5 | Dry | Bag 31 | 255.2 | 248.9 | 97.53 | 3 | 1.18 | 98.71 | 3.3 | 1.29 |
| ×5 | Wet mag | Bag 32 | 252.8 | 244.4 | 96.68 | 6 | 2.37 | 99.05 | 2.4 | 0.95 |
| ×5 | Wet coal | Bag 33 | 251.1 | 108.6 | 43.25 | 0 | 0.00 | 43.25 | 142.5 | 56.75 |
| ×10 | Dry | Bag 34 | 255.7 | 253.3 | 99.06 | 1.9 | 0.74 | 99.80 | 0.5 | 0.20 |
| ×10 | Wet mag | Bag 35 | 250.9 | 232.1 | 92.51 | 3.1 | 1.24 | 93.74 | 15.7 | 6.26 |
| ×10 | Wet coal | Bag 36 | 253.5 | 135 | 53.25 | 1.2 | 0.47 | 53.73 | 117.3 | 46.27 |

Table 15: Magnetite recovery with 3 mm high-frequency screen

| Repetitions | Method | Name | Original magnetite mass (g) | Magnetic fraction | | Non-magnetic fraction | | Total | | |
|-------------|----------|--------|-----------------------------|-------------------------|-------------------------|-------------------------|-------------------------|------------------------|--------------------|--------------------|
| | | | | Recovered magnetite (g) | Recovered magnetite (%) | Recovered magnetite (g) | Recovered magnetite (%) | Magnetite recovery (%) | Magnetite loss (g) | Magnetite loss (%) |
| x1 | Dry | Bag 19 | 251.8 | 231.7 | 92.02 | 0.3 | 0.12 | 92.14 | 19.8 | 7.86 |
| x1 | Wet mag | Bag 20 | 251.1 | 240.6 | 95.82 | 0.9 | 0.36 | 96.18 | 9.6 | 3.82 |
| x1 | Wet coal | Bag 21 | 253.8 | 188.5 | 74.27 | 0 | 0.00 | 74.27 | 65.3 | 25.73 |
| x5 | Dry | Bag 22 | 253.1 | 215.9 | 85.30 | 0 | 0.00 | 85.30 | 37.2 | 14.70 |
| x5 | Wet mag | Bag 23 | 254 | 225.4 | 88.74 | 0.3 | 0.12 | 88.86 | 28.3 | 11.14 |
| x5 | Wet coal | Bag 24 | 253.3 | 224.2 | 88.5% | 0.2 | 0.08 | 88.59 | 28.9 | 11.41 |

Table 16: High-titanium magnetite recovery with 3 mm high-frequency screen

| Repetitions | Method | Name | Original magnetite mass (g) | Magnetic fraction | | Non-magnetic fraction | | Total | | |
|-------------|----------|--------|-----------------------------|----------------------------|----------------------------|----------------------------|----------------------------|---------------------------|-----------------------|-----------------------|
| | | | | Recovered HT magnetite (g) | Recovered HT magnetite (%) | Recovered HT magnetite (g) | Recovered HT magnetite (%) | HT magnetite recovery (%) | HT magnetite loss (g) | HT magnetite loss (%) |
| ×1 | Dry | Bag 46 | 257 | 252.6 | 98.29 | 0.8 | 0.31 | 98.60 | 3.6 | 1.40 |
| ×1 | Wet mag | Bag 47 | 252.8 | 241.2 | 95.41 | 0.5 | 0.20 | 95.61 | 11.1 | 4.39 |
| ×1 | Wet coal | Bag 48 | 250.9 | 151.2 | 60.26 | 0.2 | 0.08 | 60.34 | 99.5 | 39.66 |
| ×5 | Dry | Bag 49 | 251.2 | 245.7 | 97.81 | 1.1 | 0.44 | 98.25 | 4.4 | 1.75 |
| ×5 | Wet mag | Bag 50 | 254.1 | 252.9 | 99.53 | 0.6 | 0.24 | 99.76 | 0.6 | 0.24 |
| ×5 | Wet coal | Bag 51 | 254.6 | 199.6 | 78.40 | 0.7 | 0.27 | 78.67 | 54.3 | 21.33 |

Table 17: Recovery of magnetite in different fractions

| Screen | Repetitions | Method | Name | Magnetic fraction | | | Non-magnetic fraction | | |
|---------------------|-------------|----------|--------|-------------------|-------------------------|---------------------------|-----------------------|-------------------------|---------------------------|
| | | | | Sample mass (g) | Recovered magnetite (g) | Magnetite in recovery (%) | Sample mass (g) | Recovered magnetite (g) | Magnetite in recovery (%) |
| 13.2 mm | x1 | Dry | Bag 1 | 284.4 | 246.6 | 86.7 | 240.2 | 0.8 | 0.3 |
| | x1 | Wet Mag | Bag 2 | 342.8 | 247.2 | 72.1 | 101.1 | 1.4 | 1.4 |
| | x1 | Wet Coal | Bag 3 | 267.4 | 111.6 | 41.7 | 5.8 | 1 | 17.2 |
| | x5 | Dry | Bag 4 | 279.8 | 247.2 | 88.3 | 232.4 | 0.6 | 0.3 |
| | x5 | Wet Mag | Bag 5 | 333.4 | 245.5 | 73.6 | 207.4 | 2.7 | 1.3 |
| | x5 | Wet Coal | Bag 6 | 331.8 | 87.5 | 26.4 | 0.2 | 0 | 0.0 |
| | x10 | Dry | Bag 7 | 297.9 | 245.8 | 82.5 | 265.5 | 0.5 | 0.2 |
| | x10 | Wet Mag | Bag 8 | 397.9 | 250.1 | 62.9 | 27.9 | 0.9 | 3.2 |
| | x10 | Wet Coal | Bag 9 | 373.5 | 105.2 | 28.2 | 0.6 | 0.3 | 50.0 |
| 3 mm | x1 | Dry | Bag 10 | 246.2 | 242.8 | 98.6 | 0.4 | 0.3 | 75.0 |
| | x1 | Wet Mag | Bag 11 | 262.3 | 245.7 | 93.7 | 0.5 | 0.2 | 40.0 |
| | x1 | Wet Coal | Bag 12 | 121.8 | 113.4 | 93.1 | 0.8 | 0.6 | 75.0 |
| | x5 | Dry | Bag 13 | 260.9 | 250.7 | 96.1 | 1.6 | 0.2 | 12.5 |
| | x5 | Wet Mag | Bag 14 | 255.1 | 245.3 | 96.2 | 0.3 | 0.2 | 66.7 |
| | x5 | Wet Coal | Bag 15 | 14.8 | 8.4 | 56.8 | 0.2 | 0 | 0.0 |
| | x10 | Dry | Bag 16 | 255.3 | 249.5 | 97.7 | 0.6 | 0.2 | 33.3 |
| | x10 | Wet Mag | Bag 17 | 269 | 252.5 | 93.9 | 1.8 | 0.7 | 38.9 |
| | x10 | Wet Coal | Bag 18 | 19.9 | 14.9 | 74.9 | 0.1 | 0 | 0.0 |
| 3 mm high-frequency | x1 | Dry | Bag 19 | 235.6 | 231.7 | 98.3 | 0.5 | 0.3 | 60.0 |
| | x1 | Wet Mag | Bag 20 | 250.7 | 240.6 | 96.0 | 2.1 | 0.9 | 42.9 |
| | x1 | Wet Coal | Bag 21 | 204.6 | 188.5 | 92.1 | 0.2 | 0 | 0.0 |
| | x5 | Dry | Bag 22 | 228.8 | 215.9 | 94.4 | 2.7 | 0 | 0.0 |
| | x5 | Wet Mag | Bag 23 | 230.8 | 225.4 | 97.7 | 0.7 | 0.3 | 42.9 |
| | x5 | Wet Coal | Bag 24 | 253.6 | 224.2 | 88.4 | 3.3 | 0.2 | 6.1 |

Table 18: Recovery of high-titanium magnetite in different fractions

| Screen | Repetitions | Method | Name | Magnetic fraction | | | Non-magnetic fraction | | |
|---------------------|-------------|----------|--------|-------------------|----------------------------|------------------------------|-----------------------|----------------------------|------------------------------|
| | | | | Sample mass (g) | Recovered HT magnetite (g) | HT magnetite in recovery (%) | Sample mass (g) | Recovered HT magnetite (g) | HT magnetite in recovery (%) |
| 13.2 mm | ×1 | Dry | Bag 28 | 249.1 | 245.6 | 98.6 | 229.8 | 3.6 | 1.6 |
| | ×1 | Wet mag | Bag 29 | 353.6 | 231.8 | 65.6 | 101 | 2.8 | 2.8 |
| | ×1 | Wet coal | Bag 30 | 283.5 | 126.8 | 44.7 | 9.3 | 1.8 | 19.4 |
| | ×5 | Dry | Bag 31 | 256.5 | 248.9 | 97.0 | 225.7 | 3 | 1.3 |
| | ×5 | Wet mag | Bag 32 | 366.6 | 244.4 | 66.7 | 101.3 | 6 | 5.9 |
| | ×5 | Wet coal | Bag 33 | 289.6 | 108.6 | 37.5 | 3.9 | 0 | 0.0 |
| | ×10 | Dry | Bag 34 | 259.1 | 253.3 | 97.8 | 241.7 | 1.9 | 0.8 |
| | ×10 | Wet mag | Bag 35 | 430.9 | 232.1 | 53.9 | 38.7 | 3.1 | 8.0 |
| | ×10 | Wet coal | Bag 36 | 350.4 | 135 | 38.5 | 21.1 | 1.2 | 5.7 |
| 3 mm | ×1 | Dry | Bag 37 | 252.5 | 251.3 | 99.5 | 3.9 | 3.6 | 92.3 |
| | ×1 | Wet mag | Bag 38 | 258.6 | 241.6 | 93.4 | 1.8 | 1.8 | 100.0 |
| | ×1 | Wet coal | Bag 39 | 68.5 | 62.4 | 91.1 | 0.6 | 0.6 | 100.0 |
| | ×5 | Dry | Bag 40 | 261 | 248.9 | 95.4 | 3.7 | 1 | 27.0 |
| | ×5 | Wet mag | Bag 41 | 264.2 | 247.8 | 93.8 | 0.5 | 0.1 | 20.0 |
| | ×5 | Wet coal | Bag 42 | 59.1 | 53.7 | 90.9 | 3.8 | 0 | 0.0 |
| | ×10 | Dry | Bag 43 | 258.8 | 251.5 | 97.2 | 4 | 0.7 | 17.5 |
| | ×10 | Wet mag | Bag 44 | 270.8 | 252.7 | 93.3 | 0.6 | 0.6 | 100.0 |
| | ×10 | Wet coal | Bag 45 | 107.3 | 94.9 | 88.4 | 4.1 | 0.2 | 4.9 |
| 3 mm high-frequency | ×1 | Dry | Bag 46 | 265.9 | 252.6 | 95.0 | 1.1 | 0.8 | 72.7 |
| | ×1 | Wet mag | Bag 47 | 254.8 | 241.2 | 94.7 | 2 | 0.5 | 25.0 |
| | ×1 | Wet coal | Bag 48 | 173.2 | 151.2 | 87.3 | 0.3 | 0.2 | 66.7 |
| | ×5 | Dry | Bag 49 | 262.9 | 245.7 | 93.5 | 2.8 | 1.1 | 39.3 |
| | ×5 | Wet mag | Bag 50 | 278.2 | 252.9 | 90.9 | 3.9 | 0.6 | 15.4 |
| | ×5 | Wet coal | Bag 51 | 221.1 | 199.6 | 90.3 | 6.7 | 0.7 | 10.4 |

Table 19: Magnetite and high-titanium magnetite losses per ton

| Screen | Repetitions | Method | Magnetite | | | High-titanium magnetite | | |
|---------------------|-------------|----------|--------------------|--------------------|-----------------------|-------------------------|--------------------|-----------------------|
| | | | Magnetite mass (g) | Magnetite loss (g) | Magnetite loss (kg/t) | Magnetite mass (g) | Magnetite loss (g) | Magnetite loss (kg/t) |
| 13.2 mm | ×1 | Dry | 252.5 | 5.1 | 4.8 | 250.9 | 1.7 | 1.61 |
| | ×1 | Wet mag | 252.3 | 3.7 | 3.6 | 252.2 | 17.6 | 17.22 |
| | ×1 | Wet coal | 250.9 | 138.3 | 136.7 | 250.6 | 122 | 120.52 |
| | ×5 | Dry | 252.9 | 5.1 | 5.0 | 255.2 | 3.3 | 3.06 |
| | ×5 | Wet mag | 251.5 | 3.3 | 3.1 | 252.8 | 2.4 | 2.31 |
| | ×5 | Wet coal | 251.7 | 164.2 | 155.1 | 251.1 | 142.5 | 139.72 |
| | ×10 | Dry | 254.2 | 7.9 | 7.7 | 255.7 | 0.5 | 0.49 |
| | ×10 | Wet mag | 250.8 | 0.2 | 0.2 | 250.9 | 15.7 | 15.31 |
| | ×10 | Wet coal | 251.5 | 146 | 136.5 | 253.5 | 117.3 | 112.76 |
| 3 mm | ×1 | Dry | 250.9 | 7.8 | 7.3 | 256.3 | 1.4 | 1.33 |
| | ×1 | Wet mag | 253.6 | 7.7 | 7.3 | 250.9 | 7.5 | 7.23 |
| | ×1 | Wet coal | 251.2 | 137.2 | 132.5 | 255.1 | 192 | 184.35 |
| | ×5 | Dry | 251 | 0.1 | 0.1 | 251.5 | 1.6 | 1.58 |
| | ×5 | Wet mag | 250.8 | 5.3 | 5.2 | 251 | 3.1 | 2.96 |
| | ×5 | Wet coal | 254.5 | 246.1 | 232.4 | 255.5 | 201.8 | 191.55 |
| | ×10 | Dry | 254.6 | 4.9 | 4.8 | 255.7 | 3.5 | 3.22 |
| | ×10 | Wet mag | 254.5 | 1.3 | 1.3 | 254.7 | 1.3 | 1.27 |
| | ×10 | Wet coal | 252.7 | 237.8 | 229.8 | 253.3 | 158.2 | 148.42 |
| 3 mm high-frequency | ×1 | Dry | 251.8 | 19.8 | 19.4 | 257 | 3.6 | 3.56 |
| | ×1 | Wet mag | 251.1 | 9.6 | 9.2 | 252.8 | 11.1 | 10.86 |
| | ×1 | Wet coal | 253.8 | 65.3 | 62.3 | 250.9 | 99.5 | 96.82 |
| | ×5 | Dry | 253.1 | 37.2 | 34.6 | 251.2 | 4.4 | 4.07 |
| | ×5 | Wet mag | 254 | 28.3 | 27.0 | 254.1 | 0.6 | 0.56 |
| | ×5 | Wet coal | 253.3 | 28.9 | 27.0 | 254.6 | 54.3 | 52.20 |

Table 20: Comparison of moisture content and loss of magnetite

| Screen | Repetitions | Method | Magnetite | | | High-titanium magnetite | | |
|---------------------|-------------|----------|------------------------|-------------------|-----------------------|-------------------------|-------------------|-----------------------|
| | | | Magnetite moisture (%) | Coal moisture (%) | Magnetite loss (kg/t) | Magnetite moisture (%) | Coal moisture (%) | Magnetite loss (kg/t) |
| 13.2 mm | x1 | Dry | - | - | 4.8 | - | - | 1.61 |
| | x1 | Wet mag | 4.00 | - | 3.6 | 4.00 | - | 17.22 |
| | x1 | Wet coal | - | 4.3 | 136.7 | - | 4.7 | 120.5 |
| | x5 | Dry | - | - | 5.0 | - | - | 3.06 |
| | x5 | Wet mag | 3.98 | - | 3.1 | 4.19 | - | 2.31 |
| | x5 | Wet coal | - | 5.3 | 155.1 | - | 5.1 | 139.7 |
| | x10 | Dry | - | - | 7.7 | - | - | 0.49 |
| | x10 | Wet mag | 4.03 | - | 0.2 | 4.07 | - | 15.31 |
| | x10 | Wet coal | - | 4.8 | 136.5 | - | 5.4 | 112.8 |
| 3 mm | x1 | Dry | - | - | 7.3 | - | - | 1.33 |
| | x1 | Wet mag | 3.98 | - | 7.3 | 3.99 | - | 7.23 |
| | x1 | Wet coal | - | 3.5 | 132.5 | - | 5.0 | 184.4 |
| | x5 | Dry | - | - | 0.1 | - | - | 1.58 |
| | x5 | Wet mag | 4.03 | - | 5.2 | 4.10 | - | 2.96 |
| | x5 | Wet coal | - | 5.3 | 232.4 | - | 5.2 | 191.6 |
| | x10 | Dry | - | - | 4.8 | - | - | 3.22 |
| | x10 | Wet mag | 4.01 | - | 1.3 | 3.97 | - | 1.27 |
| | x10 | Wet coal | - | 4.6 | 229.8 | - | 5.3 | 148.4 |
| 3 mm high-frequency | x1 | Dry | - | - | 19.4 | - | - | 3.56 |
| | x1 | Wet mag | 4.02 | - | 9.2 | 3.96 | - | 10.86 |
| | x1 | Wet coal | - | 3.7 | 62.3 | - | 5.5 | 96.82 |
| | x5 | Dry | - | - | 34.6 | - | - | 4.07 |
| | x5 | Wet mag | 4.37 | - | 27.0 | 4.17 | - | 0.56 |
| | x5 | Wet coal | - | 4.2 | 27.0 | - | 6.6 | 52.20 |